THESIS WORK

Master of Science in Energy Technology

Karlsruhe Institute of Technology

SELECTION OF IDEAL TEST PLATFORMS FOR METHODICAL REAL DRIVING EMISSIONS DEVELOPMENT USE CASES

Johannes Rupfle

Tutor
Prof. Dr. sc. techn. Thomas Koch (KIT)

Examiners
Maximilian Dietrich, M.Sc. (BMW Group)
Alexander Heinz, M.Sc (KIT)
Prof. Dr. Ing. Martin Gabi (KIT) / Dr.Ing. Cecilia Smoglie (ITBA)

Munich
11/06/2019

Non-disclosure notice

Non-disclosure notice

The Academic Work contains confidential information that is subject to secrecy. Therefore, the Academic Work must not be duplicated or published without prior written approval of BMW AG. This requirement of approval terminates on: 11.06.2022

Declaration of Originality and Good Scientific Practice

I confirm that this assignment is my own work and that I have not sought or used inadmissible help of third parties to produce this work and that I have clearly referenced all sources used in the work. I have fully referenced and used inverted commas for all text directly or indirectly quoted from a source.

I have considered the rules for safeguarding good scientific practice of the Karlsruhe Institute of Technology (KIT) in the current version.

Place, Date Signature

Abstract

The present thesis elaborates essential requirements for the test environment in the context of Real Driving Emissions (RDE). Within the scope of the work, a comprehensive literature research to current methodical approaches in the RDE development is carried out and the results are compared. To compare the derived requirements with the existing hardware, software and simulation methods, a tool is created that both maps the current status and evaluates a target status and thus provides an overview of the capabilities of the test environment. For selected use cases of RDE development, concrete development needs are identified and solution approaches are proposed. In the results section, different driver controllers are compared with each other and essential objectives are discussed. In the results part, different driver controllers are compared with each other and essential objectives are discussed, engine operating conditions and deviations to the real vehicle are pointed out, important road load parameters are identified, characteristics of the test bench conditioning systems are discussed and the performance requirements on the electrical machine for different test bench set-ups are analyzed.

La presente tesis elabora los requisitos esenciales para el área de pruebas en el contexto de RDE. En el curso del trabajo se realiza una búsqueda literaria extensiva de los enfoques metódicos actuales en el desarrollo de RDE y se comparan los resultados. Para la comparación de los requisitos con el hardware, el software y los métodos de simulación existentes, se crea una herramienta que representa el estado actual y evalúa el estado de la planificación y, por lo tanto, proporciona una visión general de las capacidades del entorno de prueba. Para casos de uso seleccionados del desarrollo se muestran detalles concretos y se recomiendan métodos de solución. En la sección de resultados se comparan los diferentes controladores de los conductores y se discuten los objetivos esenciales, se muestran las condiciones de operación del motor y las desviaciones desde el vehículo real, se identifican los parámetros importantes de la carga en la carretera, se discuten las características de los sistemas de acondicionamiento de los bancos de pruebas y se analizan los requisitos de rendimiento de la máquina eléctrica para las diferentes superestructuras de los bancos de pruebas.

Contents

1 Introduction

Due to increasing discrepancies in fuel consumption and emissions between type approval results and real world data [75] [39] as well as societal pressure, in September 2017 the New European Driving Cycle (NEDC) type approval cycle used until then was replaced by the new and more realistic Worldwide Harmonized Light Vehicles Test Cycle (WLTC). Simultaneously, the measurement of RDE was introduced.
A road trip is performed under specified boundary conditions. The extension of the type approval by this module represents a major challenge for emission calibration engineers due to the large number of possible trips under various conditions regarding temperature, climate conditions and altitude, but also driving dynamics.

In order to adequately meet these new challenges and still efficiently transfer significant development efforts to the test environment, it is necessary to revise the development methods as well as the test environment hardware and software. The aim of this work is to identify the relevant parameters for RDE development and thus to enable the selection of a test platform for specific use cases. Furthermore, discrepancies that have been identified are to be used to identify further development needs.

In spite of the already completed introduction and the successful compliance with the requirements of the type approval, there is still a need for further development regarding the treatment of the development tasks. The identification of the key aspects here has an essential importance. The implementation of Hardware in the Loop (HiL) applications is to be mentioned here as a big and challenging task, but also a very valuable instrument.
HiL applications are able to map realistic driving situations with varying degrees of virtualization in the test environment. For example, realistic driving scenarios can be run by automated driver controllers to supplement or completely replace trips with real vehicles.

Within the scope of the work, the RDE relevant pollutants and their formation mechanisms are explained in more detail and an overview of the current emissions legislation, which is still partly subject to changes, is given. Short preparation times and short-term changes are at the expense of the manufacturers and therefore require agile and flexible development.

A methodology for identifying further development needs and for the selection of the optimal test platform for the respective RDE relevant use case is presented in chaper 3. In the further

course, an intensive literature research is carried out to supplement the BMW-internal development scope with regard to RDE and to give an overview of the development tasks to be performed and the resulting challenges.

In order to create a comparison of the requirements for the test environment and the performance data of the test facility resulting from the RDE boundary conditions, a matching tool was developed as part of this work. The test benches were considered both categorised and test bench-specific. In several iteration loops and with the assistance of collected use cases, relevant parameters for RDE development are identified in the work. The tool utilizes a simple and user-friendly input to identify the core problems and to maintain the big picture.

The test environment and the test vehicles are explained in more detail. Selected derived results are illustrated by experiments and are further discussed in chapter 5.
Key elements regarding the relocation of RDE development activities to the test environment are, for example, the development of a realistic automated driver controller and the realistic simulation of temperature conditions of the engine.
In addition, new performance demands on the electrical machine lead to changed demands and an increased need for powerful machines as well as machines with low mass moments of inertia to be able to reproduce real vehicle behaviour.
Another important aspect is the realistic mapping of the driving resistances of various development tasks. These include the simple consideration of rolling, air and acceleration resistances for performing driving cycles as well as the modelling of inclination and cornering resistances for the reproduction of real driving situations or for HiL applications.

2 State of the Art

2.1 Origins and Effects of Regulated Contaminants

In recent years, regulated pollutant emissions have been reduced overall. The following chart (2.1) shows the shares of total emissions of the relevant EU6 regulated emissions by sector in 1995 and 2016.

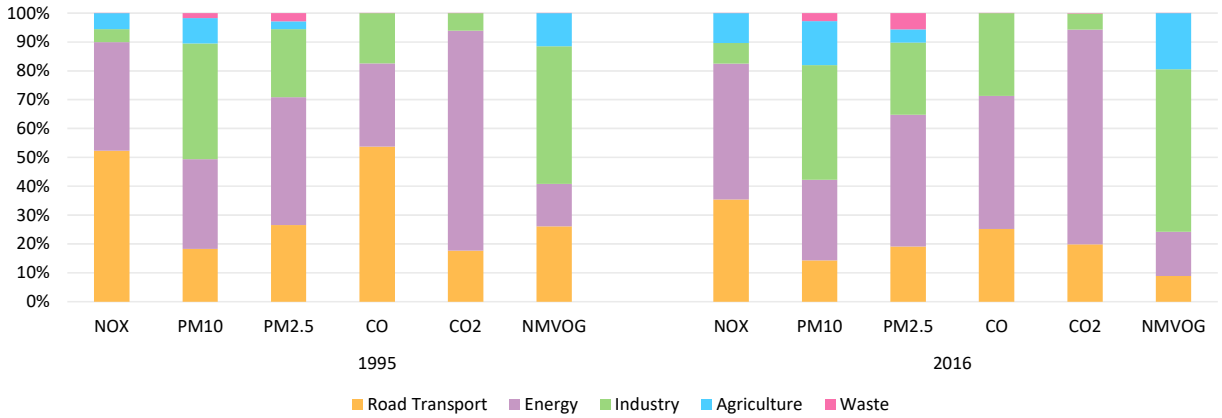

Figure 2.1: National emission trend for the German atmospheric emission reporting [45]

The total emissions are divided into the five sectors of energy, transport, industry, agriculture and waste. The graphic demonstrates that the road transport shares of all pollutants except carbon dioxide (CO_2) emissions have been lowered over the shown period of 21 years. In fact no increase of the total CO_2 emission level has occurred. The total amount of CO_2 emissions decreased by 5 % from about 166.5 Mt in the year 1995 to 158.5 Mt in the year 2016. The slight increase of the road transport share is caused by a significant reduction of 17 % and 20 % of the total CO_2 emissions of the sectors energy and industry, respectively and the increased traffic volume over the respective time. CO_2 removals caused by land use, land use change and forestry are not considered in the percentages, but in the total amount of emitted CO_2.

It is clearly visible that the total carbon monoxide (CO) emissions decreased by about 44 % while the share of the transport sector dropped by 28 % percent which results in a total CO emission reduction of 79 %. This reduction is mainly caused by the overall application of three-way catalytic converters in the early 1990s and by an increasing combustion efficiency. [94] [14] Like CO_2, CO is a color- and odourless gas but with high toxicity. Its toxic effect originates from its stronger bound to the haemoglobin of the red blood cells in comparison with oxygen,

so that oxygen deficiency can occur. Due to the aforementioned high reduction due to constant improvements, CO is not seen as a limiting factor in RDE development, because the limit values are comparatively easy to comply with.

According to the chart, overall non-methane volatile organic compounds (NMVOC) have been reduced a 48 % between the years 1995 and 2016. The share of the road transport emissions of 26 % by 1995 was reduced by about 17 % to 9 % in the year 2016. Methane (CH4) is excluded from the total hydrocarbons (THC) because of its special position. It is one of the most important greenhouse gases and its origins can be found in animal farming, landfills and in natural sources. [62]

Nitrogen oxide (NO_x) emissions are among the most important regulated contaminants of the current legislation which will be discussed later in this thesis. In the shown period of time, the total amount of NO_x emissions was reduced by about 44 % while it was reduced in the road transport sector by about 62 %. In the agricultural and the industrial sector, the shares of NO_x emissions increased by 5 % and 3 % respectively. In fact, even the absolute value in the agricultural sector shows a slight increase of about 6000 t. This is a result of the strong increase of agricultural activities [103].

Furthermore, particulate matter (PM) represents a very critical air pollutant [47] [4]. Its total emitted mass decreased by about 42 % as well as the emissions of particulate matter PM10 and PM2.5 (a number attached to the back refers to the aerodynamic diameter in µm) in the road transport sector decreased about 38 % and 49 % respectively. Overall, the share of road traffic emissions has also dropped by 4 % and 7 % respectively.

Secondary emissions are less important in the context of RDE emission development and are therefore mentioned only marginally.

For the present case of methodical RDE emission control, the most important pollutants are discussed in more detail in section 2.1.1 and 2.1.2.

2.1.1 Nitrogen Oxides

The principal nitrogen oxides formed during engine combustion are nitrogen monoxide (NO) and nitrogen dioxide (NO_2) and nitrogen tetroxide (N_2O_4). NO is a colorless and highly toxic gas which converts to NO_2 under standard conditions. NO_2 is a red-brown and highly corrosive gas with a pungent odor and forms an equilibrium mixture with NO. N_2O_4 converts to NO_2 at higher temperatures and reverts to N_2O_4 at lower temperatures. [49]

In higher concentrations nitrogen oxides cause respiratory irritations and inflammations. Nitrogen oxides, combined with volatile organic compounds in an adequate mixing ratio, favour the formation of photochemical ozone which leads to the so called summer smog. Furthermore, nitrogen oxides are an important precursor in the formation of nitric acid. Together with sulphuric acid, which is produced by sulphur oxide and steam, it is responsible for acid rain and its effects, such as damage to buildings and the harmful influence on flora and fauna. [104] [49] [92]
A distinction is made between three main mechanisms of nitric oxide formation in internal combustion engines.

There is the main mechanism related to combustion engines of thermal-NO_x formation in the burnt gas. First described by Zeldovich in 1946 [111] and later extended by Lavoie [65] in 1970, the enhanced Zeldovich mechanism consists of three elementary reactions.

$$O + N_2 \longrightarrow NO + N \tag{2.1}$$

$$N + O_2 \longrightarrow NO + O \tag{2.2}$$

$$N + OH \longrightarrow NO + H \tag{2.3}$$

Due to the stable molecular nitrogen (N_2) triple bond, reaction 2.1 has a high activation energy and only takes place sufficiently quickly at high temperatures. Therefore, the temperature is the limiting factor and the reason why this mechanism is named thermal-NO_x. In addition, the time component still has an important role as well.
Figure 2.2 shows the nitric oxide formation in four ethylene-air flames as a function of reaction time. It is clearly visible that the mixture ratio influences the flame temperature, which correlates directly with the NO_x formation (cf. characterization of N_2 triple bond). A slightly lean mixture, in this case corresponding to an air-fuel ratio of $\lambda = 1.05$, favours the formation of NO_x due to the presence of oxygen. However, if the air-fuel ratio increases further, the reduction of the combustion temperature predominates and NO_x emissions are reduced.
The x-axis shows the time dependence. The higher the residence time, the higher the NO_x concentration [78]. This leads to a coherence between the engine speed and the formation of NO_x. Summed up, it can be said, that the formation of NO_x is highly temperature dependent, and is also dependent on oxygen concentration and residence time, which can be confirmed by looking at an engine characteristics map. With an identical indicated mean pressure, the NO_x concentration is expected to decrease by increasing the engine speed at the same time. However,

the NO_x concentration is expected to increase by growing indicated mean effective pressures due to the rising temperature.

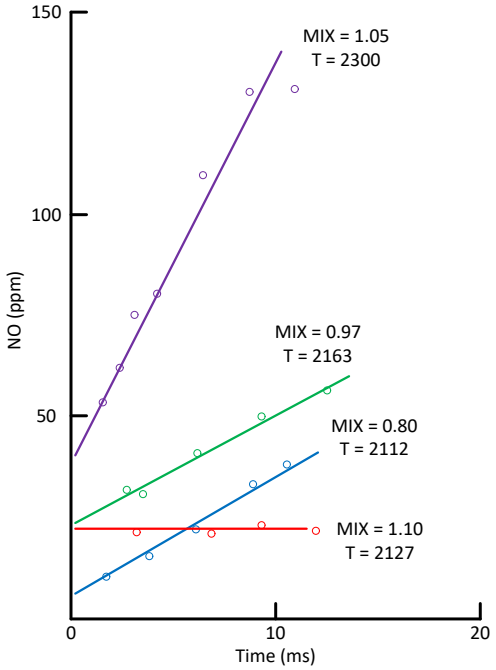

Figure 2.2: NO in four ethylene-air flames as a function of reaction time. Reaction time is the sampling distance, from burner surface to probe tip, divided by the calculated velocity of the hot products. Mixture strength and flame temperature are noted on each curve. [37]

Prompt-NO_x is formed in the flame front itself. This process is linked to the formation of the methylidyne (CH) radical, which can react in many different ways. This mechanism was first described by Fenimore in 1972 [37]. Further research in 2008 comes to the conclusion that cyanonitrene (NCN) is formed as an intermediate product in the flame front. The formed NCN can react with different species to form hydrogen cyanide (HCN^-), cyanide (CN), isocyanate (-NCO) and NO. As can be seen from the different reaction paths described above, there is still a considerable need for research into the individual reaction rates of prompt-NO formation. [99] [46]

Furthermore, the third mechanism of fuel-NO_x is of secondary importance due to the negligible nitrogen content in the fuel. This mechanism has a higher influence when coal or heavy fuel oil is used. [69]

2.1.2 Particulate Matter

Particulate matter has both harmful effects on the climate and on public health. In the upper atmosphere, particulate matter changes the radiation budget and cloud formation. In the lower atmosphere, it modifies the visibility, biogeochemical cycles and decreases the human health. In

developed countries, PM show a slight decrease, while in some countries such as Bangladesh, the PM level increased by about 31.4 % between the years 1991 and 2011. [76] Iran, for example, is one of the Middle East countries that faces serious environmental problems due to the rapid growth of its urban population, industries, desert dust and deserts in its neighborhood, all being major sources of PM [7].

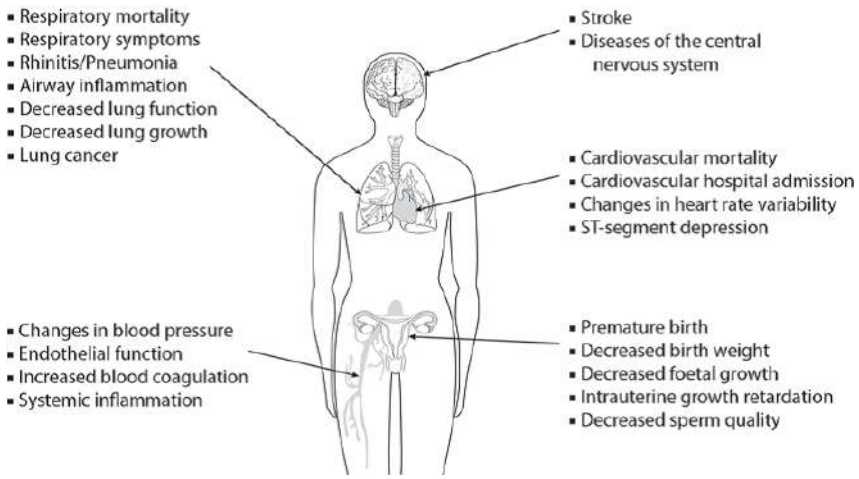

Figure 2.3: Organs of the human body that can be affected by air pollution [83]

Various long- and short-term studies on mortality and PM have been summarized in a number of reviews. Figure 2.3 illustrates the potential health effects. It is indicated that PM could decrease heart rate variability which may correlate with cardiac morbidity [7]. PM passes the barriers deeply into the pulmonary alveoli where it causes respiratory problems such as oxidative stress and may enter the circulation where it correlates with neuroinflammation in the central nervous system. It is also associated with preterm births and decreased birth weight, as well as with increased risk of diabetes due to insulin resistance along with aggravation of the metabolic imbalance. [89] [7] [18]

Karagulian [60] distinguishes between six categories of main sources of particulate matter: traffic, industry, domestic fuel burning, natural sources including soil dust and sea-salt and unspecified sources of pollution of human origin.
Traffic is a source category with a high percentage of the global amount of emitted PM. In addition to the primary PM emissions from exhaust, it includes secondary emissions like the emission of gaseous PM precursors, wear of brake linings, clutch, tires and road material as well as re-suspended dust particles.
Industry as a second main category primarily includes the emission from oil and coal burning, but also from petrochemical, metallurgic, ceramic and pharmaceutical industry.
Domestic fuel burning includes wood, coal, gas and oil firing for cooking and heating and is a mayor influencing source in central Europe, where wood and coal are used for heating. The

smog of London of 1952, for example, was partially due to domestic firing. In this context, Bell [13] estimates about 12.000 excess deaths of acute and persisting effects between December 1952 and February 1953.
Soil dust and sea salt are included in natural sources of PM. A challenging task is to separate the re-suspension from fields or bare soils from road-dust emitted and re-suspended by traffic.
The sixth category of unspecified sources of human origin includes the particles of secondary origin. They are formed in the atmosphere by reacting with agricultural ammonia (NH_3) emission of sulfur dioxide (SO_2) emission from shipping, industrial activities and power generation. Inorganic nitrate aerosols are based on NH_3 and NO_x. Due to the residence time of three to nine days, they are associated with a long range transport. Secondary organic aerosols can be emitted directly, formed in the air by reacting with other substances or formed with assistance of volatile organic compounds (VOC) [82].

Particulate matter is mainly classified into PM10, PM2.5 and PM0.1 which refers to the respective aerodynamic diameter of 10 µm, 2.5 µm as well as 0.1µm. The PM10 ratio varies between the different sources of PM. Natural sources show a higher contribution in PM10 while PM emissions from combustion processes are more important in PM2.5 and below due to an analysis of Kleeman et. al. [63]

2.2 Legal Framework

The protection of air quality and the reduction of greenhouse gas emissions are priority goals of the European Union (EU). For instance, regulation (EU) No 333/2014 [30], the EU has set limits of 95 gCO_2/km for car fleets to be achieved in 2020.

Due to the increasing traffic volume and the large number of other emission sources, more and more stringent regulations are required to comply with urban limit values. Increasing environmental awareness also has a positive impact on the introduction of more stringent emission limits. Section 2.2 deals with the evolution of global emission standards and gives an overview of the current European Euro 6/IV legislation.

2.2.1 Evolution of Emission Standards and Development Milestones

Due to California's special climatic conditions, the very first emission legislation "Clean Air Act" was introduced there in 1968 [61] [8]. In Japan, the first emission legislation was introduced at about the same time [107]. The first European regulations came into effect in 1970 [95]. Figure 2.4 shows a summary of the evolution of the legal regulations for passenger cars.

The European Economic Community (EEC) introduced the European emission standards in 1989 and launched the Euro 1 standard (91/441/EEC) in 1992 [101]. Its test procedure is performed using the NEDC (Fig. 2.5 a), which consists of four repetitions of the urban driving cycle (UDC) and the Extra Urban Driving Cycle (EUDC) [85]. Over the years, the emission limits were lowered and the test procedures changed.

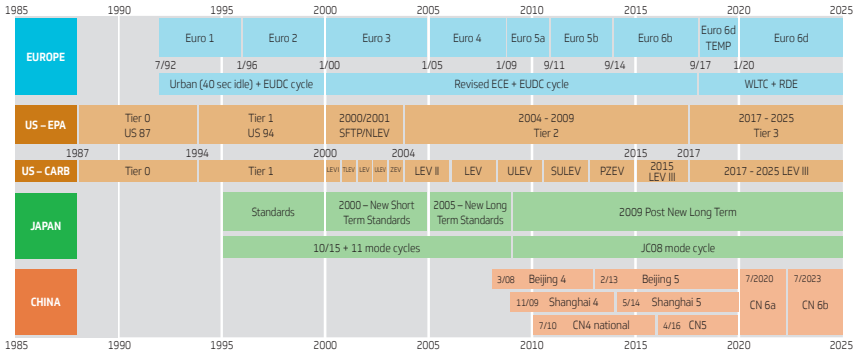

Figure 2.4: Evolution of the global emission legislation [21]

In 2013, the World Forum for Harmonization of Vehicle Regulations (WP.29) developed a new test cycle, which was introduced in 2017. The objectives of the Development under the Worldwide Harmonized Light Vehicles Test Procedure (WLTP) informal group were to develop a WLTC (Fig. 2.5 b) which represents typical driving characteristics around the world and to develop a gearshift procedure which simulates representative gearshift operation for light duty vehicles [105].
The resulting driving cycle is divided into four parts for low, medium, high, and extra-high speed. When compared to the NEDC, the average speed increased by about 12.9 km/h from 33.6 km/h to 46.5 km/h and the maximum speed was increased by about 11 km/h to a value of 131 km/h. The total duration was increased from 1180 s to 1800 s, which more than doubles the distance to 23.27 km due to the higher average speed. The maximum positive acceleration was raised from 1.04 m/s^2 to 1.67 m/s^2. Nevertheless, it should be noted that it is difficult for any type approval test to capture all emission-affecting factors.

Based on the results of Fontaras et al. [38], the shortfall between certified and actually emitted CO_2 emissions for an average European passenger car type approved on the basis of NEDC was estimated in the order of 27 % while the same figure drops to 13 % considering the boundaries and characteristics of the WLTC. This is equal to a ratio between WLTC and NEDC of 1.12. [66] RDE measurements have also been introduced to ensure that real driving emissions remain within defined limits even under varying environmental conditions and different driver influences. Further details regarding the development of the WLTC and trip requirements, boundary conditions, trip validity and emissions evaluation of RDE measurements are described in section 2.2.2.

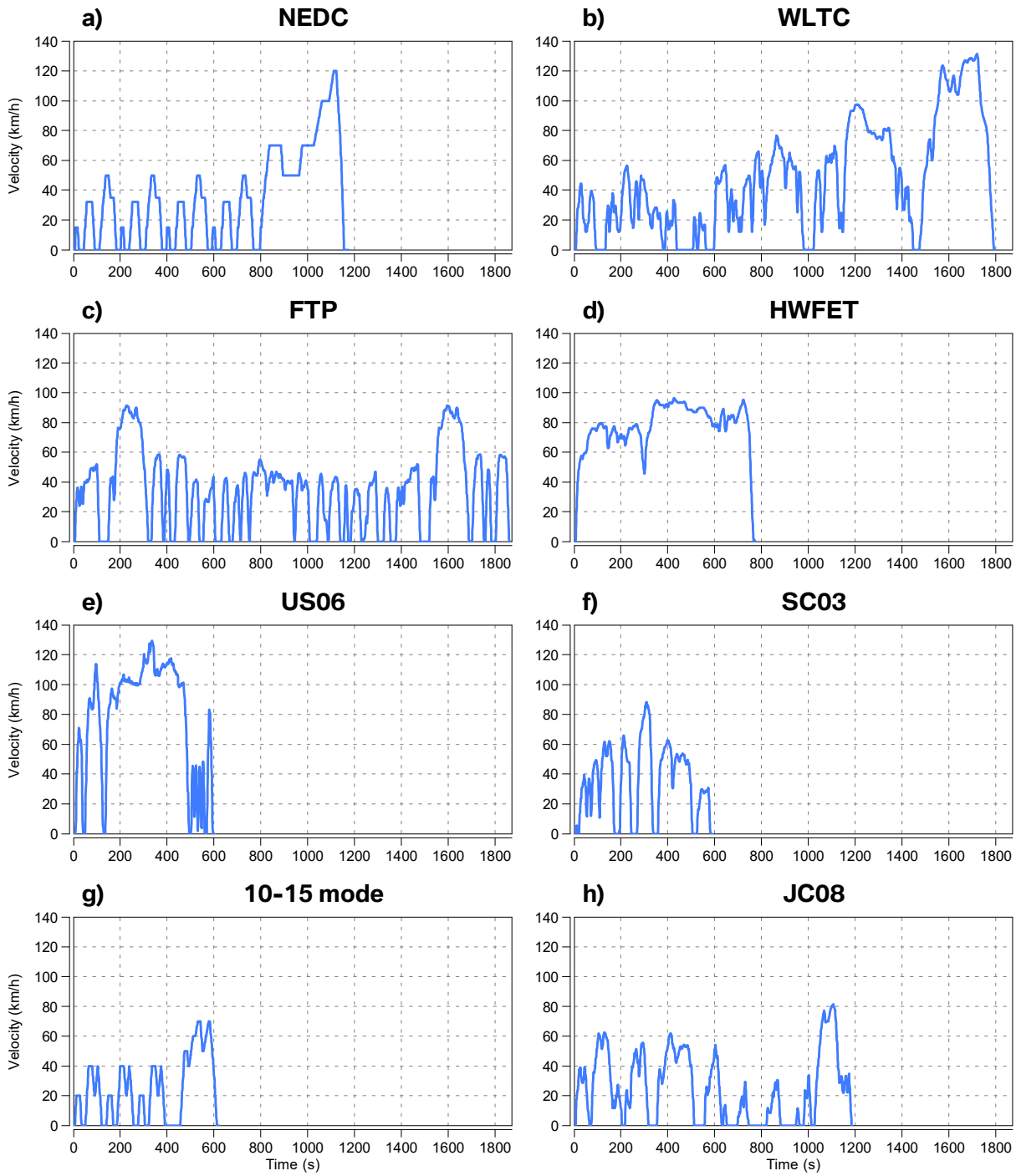

Figure 2.5: Overview of current global driving cycles [24] [105] [79]

The US equivalent Tier 0, which was introduced five years earlier than Euro 1, had stricter limit values and was further tightened with the phasing-in of Tier 1 in 1994. [27] Originally, consumption data were determined using two federally mandated tests. The Federal Test Procedure (FTP) (Fig. 2.5 c) and the Highway Fuel Economy Test (HWFET) (Fig. 2.5 d) that represent city and highway driving schedules, respectively. These cycles are characterized by an average speed of 34.2 km/h and 77.7 km/h. The maximum speed is about 96.4 km/h. The

city schedule is performed with cold engine and includes idling time of 18 %, while the highway schedule is performed with preconditioned engine and includes no idling time.

The Environmental Protection Agency (EPA) added three new Supplemental Federal Test Procedures (SFTPs) in 2006 to adapt the procedure to the current technical state and the demands like higher speeds, more aggressive driving behaviour, the use of air conditioning, and the effect of cold temperature. [80] [26] [90]

The Supplemental FTP Driving Schedule (US06) (Fig. 2.5 e) was added to represent a much more aggressive driving behaviour and higher operating speeds of up to 129 km/h. This cycle is characterized by a maximum acceleration of 3.78 m/s^2, more than twice the maximum value of the WLTC.

Furthermore, there is the speed correction driving schedule (SC03) (Fig. 2.5 f), which is performed at ambient conditions of 35 °C with the air conditioning system working. The cycle represents a 5.8 km route with a maximum speed of 88.2 km/h and a duration of 596 seconds. Compared with the WLTC, its dynamic is also significantly higher with a maximum acceleration of 2.28 m/s^2.

In fact, the last added cycle is a FTP performed at an ambient temperature of -7 °C with a cold start. The complete test procedure is also known as 5-cycle method. [80]

The Tier 3 and respectively the LEV III standards for California are currently being phased-in until 2022. According to the 4^{th} meeting of the RDE informal working group (IWG) in Tokyo, the EPA is currently developing an RDE procedure for the US [22]. The EPA is evaluating if the 4^{th} RDE package (further detailed in section 2.2.2) is appropriate for the US standards and how the emissions calculation compare with 40 C.F.R. §1065 2011. Furthermore, a validation tool is processed and initially compared with Microsoft Excel add-in for analyzing vehicle emissions data recorded with portable emissions measurement system (PEMS) (EMROAD), , which is only used for dynamics validation since the introduction of the 4^{th} RDE package. [25]

In Japan, the first schedule called 10-mode was used when emission standards for cars were first developed in 1973. It simulates urban driving with a maximum speed of 40 km/h. In 1993, the cycle has been modified by adding a 15-mode segment to a series of three 10-mode cycles. It simulated highway driving speed up to 70 km/h. (Fig. 2.5 g) Over the years, the NO_x limit has been lowered and a limit value for PM has been introduced. Due to the low speed profile of the 10-15 mode, Japan had the largest gap between official and real-world CO_2 emmissions [102]. A considerable step was made in the year 2005 by introducing the New Long Term emission standards and by replacing the existing type approval cacle 10-15 mode by the new JC08 (Fig.

2.5 h), which is longer, has higher average and maximum speed, and requires more aggresive acceleration to map a more realistic driving style [102]. In 2018, Japan introduced their new future regulations for passenger cars, which is comparable to the Euro 6 legislation. The type approval uses the WLTC. Japan also plans to introduce RDE for new type approvals in 2022. [74] [21]

China has largely adopted the European legislation lagging behind the equivalent EU standard by up to 10 years [54]. Up to the current China 5 standard, the Chinese legislation applies the NEDC as an instrument for type approval. With the adopted China 6 standard, which is planned to come into effect in July 2020 (China 6a) and July 2023 (China 6b), the WLTC will be applied for vehicle type approval.

As statet in the 172nd session of the WP.29, the Ministry of Industry and Information Technology (MIIT) simultaneously launched a program with the objective to develop the China Automotive Testing Cycle (CATC) for application in both fuel consumption and emission standards. [110] The China 6b standard targets to cut off Euro 6 emission limits of hydrocarbon (HC) by 50 %, as well as 40 % and 33 % for NO_x and PM respectively, and is adopted as a largely fuel-neutral standard. Therefore, for diesel and petrol engines the same limit values apply to the most part. Compared to the Euro 6 standard, this results in stricter CO limits for gasoline engines and stricter NO_x limits for diesel engines. The introduction of a nitrous oxide (N_2O) limit has also been decided.

Furthermore, a slightly modified version of the European RDE regulation will be implemented. The main differences are reflected in the conformity factor ($CF_{pollutant}$), which describes the not-to-exceed (NTE) limits of the respective pollutant. The permitted emissions are calculated by multiplying the Euro 6 emissions limits by the $CF_{pollutant}$. The $CF_{pollutant}$ is set to 2.1 for NO_x and particle number (PN) and is likely to be re-evaluated in July 2022. The China 6 RDE measurements also come with a further extended altitude range up to 2,400 m. The maximum speed during the motorway segment is set to 120 km/h (135 km/h for 3 % of motorway driving time) to adapt the regulation to the Chinese driving behaviour and existing speed limits. Cold starts are also excluded from the RDE procedure. [71] [32] [54]

2.2.2 Current Euro 6 Legislation

In 2007, the current framework for the approval of motor vehicles for the Euro 6/IV (2007/46/EC) [31] legislation was passed by the European Parliament and the Council of the European Union and was applied in 2014.
According to the regulation (EC) No 715/2007 of the European Parliament and of the Council of the European Union, recital 15, an update or replacement of the NEDC may be required to

"reflect changes in vehicle specification and driver behaviour". [32] The use of PEMS and a NTE regulatory concept should also be considered. [32]

Since 2017, the Euro 6 type approval consists of a two-part test procedure. In addition to the limit values that must be observed during the implemented WLTC, NTE emission limits for RDE must be complied with. Table 2.1 shows the limit values determined for Euro 5 and Euro 6, respectively. The limit values of diesel and gasoline vehicles are regulated separately. In case of diesel standards, the NO_x limits have been lowered significantly. The reduction from 0.18 g/km to 0.08 g/km means a drop of 56 %. This level is 84 % lower than the NO_x emission limit of the Euro 3 regulation, when the limits for NO_x were first implemented. The standards for PM and PN for diesel cars are the same as those from Euro 5. Nevertheless, there was a reduction of about 96 % from Euro 1 limits. [106]

At the first sight, the emission limits of gasoline engines are more or less the same. Due to the widespread implementation of gasoline direct injection (GDI) engines and the higher particulate emissions associated with them, a PN limit value was also introduced for gasoline engines. It was given a phase-in of three years with a limit value one order of magnitude less strictly than the limit of diesel engines to extend the period of developing new emission control techniques to meet the standards. Although the limit values appear to be unchanged, the impact of the new test cycle has intensified the pressure on car manufacturers and their suppliers. In order to comply with the current regulations, a number of additional efforts have to be made.

Tsiakmakis estimates a sales weighted average CO_2 ratio related to the introduction of the WLTC for conventional passenger cars for 2015 fleet composition to be 1.21. [97] A case study of the Joint Research Centre (JRC) from 2015 tested 21 Euro 4-6 gasoline and diesel vehicles with respect to the emission difference between NEDC and WLTC based type approval. The study reveals, that moving from NEDC to WLTC does not have much impact on NO_x and CO emissions neither from gasoline nor from diesel vehicles. However, the influence on NO_x of diesel vehicles and CO of low-powered gasoline vehicles appears to be very high.

In addition, Regulation No 715/2007 [32] requires Original Equipment Manufacturers (OEMs) to check in-service conformity (ISC) measures for a period of up to five years or 100 000 km, whichever is sooner. ISC conformity shall be checked, in particular, for tailpipe emissions as tested against emission limits and can be performed by non governmental organization (NGO). Durability testing for pollution control devices shall be checked for at least 160 000 km. [66] [109] [32] [64]

Table 2.1: Comparison of light-duty Euro 5 and Euro 6 vehicle emission standards [32]

Pollutant		Euro 5 Light-Duty		Euro 6 Light-Duty	
		Gasoline	Diesel	Gasoline	Diesel
CO	in g/km	1.0	0.5	1.0	0.5
HC	in g/km	0.1 [a]		0.1	
HC+NO_x	in g/km		0.23		0.17
NO_x	in g/km	0.06	0.18	0.06	0.08
PM	in g/km	0.005 [b]	0.005	0.005 [b]	0.005
PN	in 1/km		6.0×10^{11}	6.0×10^{11} [c]	6.0×10^{11}

[a] and 0.068 g/km for NMHC
[b] applicable only to DI engines, 0.0045 g/km using the PMP measurement procedure
[c] applicable only to DI engines, 6×10^{12} 1/km within the first three years of Euro 6 effective dates

WLTC Development

As described in section 2.2.1, the WLTC development was carried out by the WP.29 of the United Nations Economic Commission for Europe (UNECE) to represent typical driving characteristics around the world. The employment of a specific driving cycles always has its individual advantages as well as disadvantages. The former type approval cycle (NEDC), for example, consists of several steady-state test modes and is therefore easy to reproduce, but it does not reflect a real driving behaviour. The Japanese JC08 represents a real driving style more accurately, but only covers reduced speeds and not all possible driving situations. Due to this issue, the EPA adopted the above described 5-cycle-method in order to cover a wide range of driving situations. [105]

To develop a new cycle to meet global needs WP.29 collected in-use data from different regions of the world and combined them with suitable weighting factors to reflect the market shares. Over 765,000 km of data from the EU, India, Japan, Korea and the USA were recorded. The dataset consists of a wide range of vehicle categories, road types and driving conditions. The final result for Class 3 vehicles ($v_{max} > 120$ km/h), representing European passenger cars, is the WLTC CL3 version 5.3, consisting of a low, medium, high and extra-high speed phase. The speed thresholds of the phases are 60, 80, and 110 km/h, respectively. Each dataset of collected data split into regions was considered as it is shown in table 2.2.The EU is considered as a whole by individual weighting factors for each European country. Germany is considered as 12 % of the European dataset. The summed up driving hours for each phase are converted into a factor to determine each phase duration based on the total duration of 1800 s, which is a derivation of the duration of the Worldwide Harmonized Heavy Duty Cycle (WHDC). [105] [98]

The driving characteristics for each region are evaluated and unified for each phase of the cycle to build the world-wide database. Considered characteristics are average speed, relative positive acceleration (RPA), average short trips duration and average idle duration. The number

Table 2.2: Length of speed phases to determine cycle duration of WLTC [105]

		Low	Medium	High	Ex-High	Total
EU	in Mh	23 300.0	12 400.0	15 700.0	16 400.0	67 900.0
USA	in Mh	15 900.0	22 600.0	29 500.0	21 300.0	89 300.0
Japan	in Mh	11 100.0	6160.0	1160.0	328.0	18 800.0
Korea	in Mh	4050.0	1840.0	2090.0	443.0	8420.0
India	in Mh	15 600.0	8470.0	5640.0	64.2	29 800.0
World-wide	in Mh	70 000.0	51 500.0	54 200.0	38 500.0	214 000.0
Proportion		0.327	0.240	0.253	0.180	1.000
Cycle duration	in s	589	433	455	323	1800

of short trips and idle periods for each phase was determined according to the equations 2.4, rounded to an integer number (where i, I and ST refer to the respective phase, idling and short trip duration and number). A challenging task was to choose an adequate combination of short trips and idling periods. They have to fit the unified average characteristics and thereby have to match the calculated time duration.

Determination of short trips and idles number [105]:

$$\begin{aligned} N_{\mathrm{ST,i}} &= \frac{t_{\mathrm{i}} - \bar{t}_{\mathrm{I,i}}}{\bar{t}_{\mathrm{ST,i}} + \bar{t}_{\mathrm{I,i}}} \\ N_{\mathrm{I,i}} &= N_{\mathrm{ST,i}} + 1 \end{aligned} \tag{2.4}$$

In case of the low speed phase, furthermore, the first short trip and idling period of the day have to be determined as a representative of cold start conditions. Due to the high short trip duration of the extra-high speed phase in real world data compared to the defined duration in the WLTC, the short trip was developed with a modified methodology based on a combination of different segments defined as take-off, cruise and slow-down, extracted from real world data. Japan introduced the initial WLTC cycle speed profile in the 9$^{\mathrm{th}}$ a WLTP Sub-group on the Development of the Harmonized driving Cycle (DHC) meeting, which was revised several times in the validation phase until the final versions were adopted. [105]

The gearshift procedure development for vehicles with manual transmission followed various approaches. The engine speed distribution was calculated for selected vehicles and applied to the database. As a result of the consideration that the driving behaviour influences the shifting procedure much more than the technical characteristics of the gearbox, two new approaches were discussed: A vehicle speed based shifting table and a normalized engine speed based shifting table. Both have advantages and disadvantages, such as differences in the average engine

speed and driveability problems, which led to a final approach, that is based on the individual acceleration performance of a vehicle.

With a focus on prospective development strategies, the shift prescription is based on the test mass, full load power curve, driving resistance coefficients (F_0, F_1, F_2) and gear ratios in addition to the rated engine speed and the power to mass ratio.
The equations 2.5 to 2.9 are the main equations for gear selection and shift point determination for vehicles equipped with manual transmission. The precalculations are excluded to ensure a clear presentation. In chronological order, the required power (Equation 2.5) is calculated first, as a function of the driving resistance coefficients, the vehicle speed and a term consisting of a mass factor, the vehicle test mass, acceleration and vehicle speed. Then the engine speed for each gear i_{actual} is calculated for each second j (Equation 2.6) and limited to the possible gears regarding to the possible engine speed ($n_{\text{min\_drive}}$) using equation 2.7.

The required power is compared to the available power using equation 2.8, which contains a SM and an ASM. The possible gears are determined in the last step. (Equation 2.9)
The initial gear selection shall be checked and modified by determined correction steps in order to avoid too frequent gearshifts and to ensure driveability and practicality. [35] [105] [19]

Calculation of required power:

$$P_{\text{required,j}} = \frac{F_0 * v_{\text{j}} + F_1 * {v_{\text{j}}}^2 + F_2 * {v_{\text{j}}}^3}{3600} + \frac{kr * a_{\text{j}} * v_{\text{j}} * TM}{3600} \tag{2.5}$$

Determination of engine speeds:

$$n_{\text{i,j}} = ndv_{\text{i}} * v_{\text{j}} \tag{2.6}$$

Selection of possible gears with respect to engine speed:

$$\begin{aligned} n_{\text{min\_drive,i=1}} &= n_{\text{idle}} \\ n_{\text{min\_drive,i=2}} &= 1.15 * n_{\text{idle}} \\ n_{\text{min\_drive,i>2}} &= n_{\text{idle}} + 0.125 * (n_{\text{rated}} - n_{\text{idle}}) \\ n_{\text{max1}} &= n_{\text{95\_high}} \\ n_{\text{max2}} &= ndv_{\text{i}} * ng_{\text{max}} \end{aligned} \tag{2.7}$$

$$\begin{aligned} i \geq ng_{\text{vmax}}: &\qquad n_{\text{min\_drive}} \leq n_{\text{i,j}} \leq n_{\text{max1}} \\ i \geq ng_{\text{vmax}}: &\qquad n_{\text{min\_drive}} \leq n_{\text{i,j}} \leq n_{\text{max2}} \\ i = 1: &\qquad n_{\text{i,j}} < n_{\text{min\_drive}} \end{aligned}$$

Calculation of available power:

$$P_{\text{available,i,j}} = P_{\text{wot}} * (1 - (SM + ASM)) \tag{2.8}$$

Determination of possible gears to be used:

$$\begin{gathered} i_{\text{min}} < i_{\text{actual}} < i_{\text{max}} \\ \\ \text{1. Conditions of 2.7 are fulfilled} \\ \text{2. } n_{\text{gear}} > 2, \text{ if } P_{\text{available,i,j}} \geq P_{\text{required,j}} \end{gathered} \tag{2.9}$$

Real Driving Emissions (RDE)

The RDE legislation, introduced with the Euro 6 Regulation (EC) No 715/2007 [32], amended by (EC) No 692/2008 [33], was developed in four different packages. In the following, several major changes and supplements of the legal framework will be detailed.
The 1st package ((EU) 2016/427) [28] amended (EC) No 692/2008, Article 3 by adding paragraph 10, which forces the manufacturer to ensure emission conformity at an RDE test performed in accordance to Annex IIIA (Verifying Real Driving Emissions).
In the 2nd RDE package [29], Annex II amended Annex IIIA of Regulation (EC) No 692/2008 by defining the NTE values and setting a temporary $CF_{\text{pollutant}}$ for NO_x. Furthermore, Appendix 7b introduced the procedure to determine the cumulative positive elevation gain of a trip.
Appendix 5, point 1 and Appendix 6, point 3.5 of the 3rd RDE package ((EU) 2017/1151) [35] specify, that cold start emissions are to be recorded, but excluded from the emissions calculation of both evaluation methods moving average window (MAW) and Power Binning.

In January 2019, the 4th RDE package ((EU) 2018/1832) [19] was applied. Important changes are applied in Annex III, which amends Annex IIIA of (EU) 2017/1151. The NO_x margin of the $CF_{\text{pollutant}}$ was set to 0.43 instead of 0.50 and Appendix 5 was replaced, so that the MAW method becomes the only method to determine the validity of an RDE test.

In contrast to WLTC type approval, the RDE type approval is characterized by a large number of possible route profiles with various driving characteristics and varying environmental influences. Figure 2.6 shows the steps to validate an RDE trip and to calculate the final emissions result.

The Urban, Rural and Motorway sections must each have a minimum length of 16 km and a percentile distribution of 34%, 33% and 33% respectively with a tolerance of ± 5%. The allowed

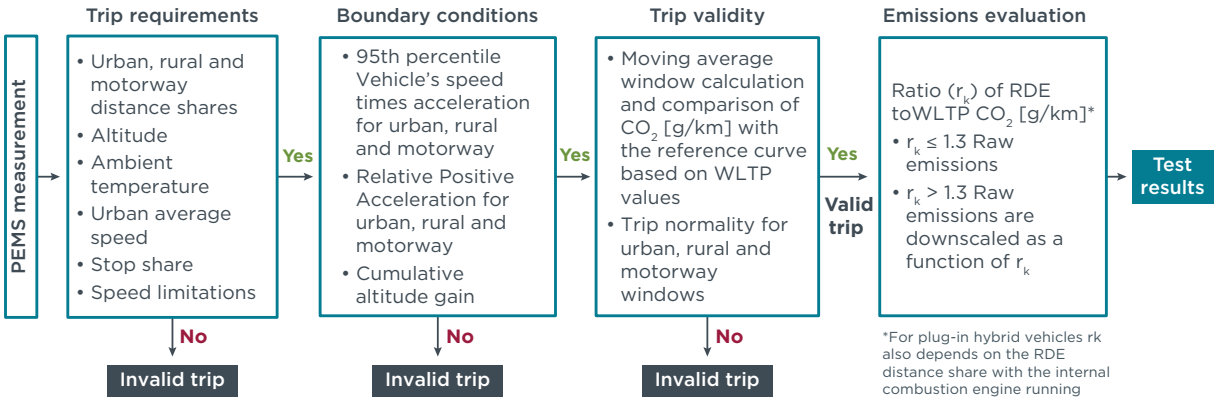

Figure 2.6: Steps of an RDE test validity procedure and emission calculations from January 2020. [55]

test altitude is limited to 1300 m. Ambient temperature can vary between −7 °C and 35 °C. The urban average speed has to be between 15 km/h and 40 km/h and the urban stop share shall be 6 % to 30 %.
The speed phases urban, rural and motorway cover speed ranges under 60 km/h, between 60 km/h and 90 km/h and respectively higher than 90 km/h. The motorway phase has to cover a speed range of up to 110 km/h with at least 5 min above 100 km/h and a speed limit of 145 km/h which can be exceeded by +15 km/h for not more than 3 % of motorway driving time. [19] [55] [6] [5]

Furthermore, the 95$^{\text{th}}$ percentile of $v_{\text{k}} * a_{\text{pos,k}}$ (vehicle speed multiplied by the positive acceleration at each sample k) shall not exceed the limits given by the equations 2.10 and the RPA, calculated like it is given in the equations 2.11, shall be below the limits also given in the equations 2.11.

Limit values of the 95$^{\text{th}}$ percentile of $v_{\text{k}} * a_{\text{pos,k}}$.

$$\begin{aligned} \bar{v}_{\text{k}} \leq 74.6 km/h: &\quad (v_{\text{k}} * a_{\text{pos,k}})_{95} \leq 0.1360 * \bar{v}_{\text{k}} + 14.440 \\ \bar{v}_{\text{k}} > 74.6 km/h: &\quad (v_{\text{k}} * a_{\text{pos,k}})_{95} \leq 0.0742 * \bar{v}_{\text{k}} + 18.966 \end{aligned} \tag{2.10}$$

Calculation and limit values of RPA

$$\begin{aligned} RPA_{\text{k}} = &\quad \sum\nolimits_j (\Delta t * (v_{\text{k}} * a_{\text{pos,k}})_{\text{j}} / \sum\nolimits_i (v_{\text{i}} * \Delta t) \\ \bar{v}_{\text{k}} \leq 94.05 km/h: &\quad RPA_{\text{k}} > -0.0016 * \bar{v}_{\text{k}} + 0.1755 \\ \bar{v}_{\text{k}} > 94.05 km/h: &\quad RPA_{\text{k}} > 0.025 \end{aligned} \tag{2.11}$$

To calculate the positive cumulative elevation gain of a total trip, all positive, interpolated and smoothed road grades are integrated and based on a distance of 100 km. The cumulative elevation gain shall not exceed 1200 m/100km for the total trip and in addition for the urban share alone. The calculation is based on the Global Positioning System (GPS) altitude measurement

and is corrected by altitude data of a topographic map, when the altitude difference between the two datasets exceeds 40 m. The obtained altitude data shall be smoothed by a two-step procedure. [19] [55] [6] [5]

As figure 2.6 shows, a MAW calculation has to be done for trip validity. The calculation is based on the CO_2 characteristic curve of a vehicle which is given by the reference points (1-3) of the vehicle CO_2 characteristic curve P_1, P_2 and P_3 shown in figure 2.7 (a) and are defined by the average speeds and the specific CO_2 emissions of the low speed, high speed and extra high speed phases, respectively. The upper tolerance around the vehicle CO_2 characteristic curve is set to 45 % for urban driving and 40 % for rural and motorway driving, the lower tolerance to 20 % for the whole trip ($M_{CO_2,d,cc}$ and its calculated tolerance limits). A trip is valid when it comprises at least 50 % of the windows that are within the tolerances defined. The trip is divided into CO_2 mass based averaging windows expressed in a distance specific mass emission over the average vehicle speed. [19] [55] [6] [5]

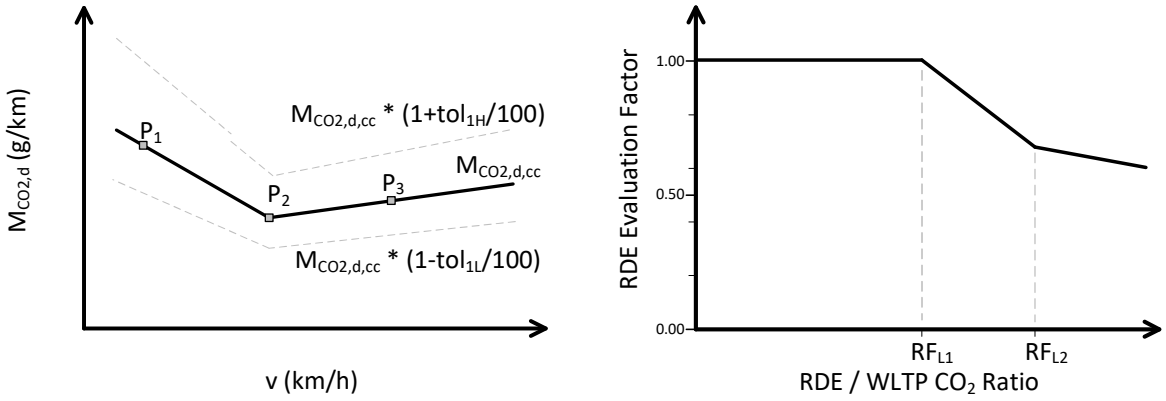

(a) Vehicle CO_2 characteristic curve and tolerances for internal combustion engine (ICE)

(b) Function to calculate the result evaluation factor

Figure 2.7: Trip normality and emissions calculation method [19]

With the adoption of the 4th RDE package, the final emission evaluation is no longer performed using the MAW based distance specific CO_2 emissions, but with the total amount of distance specific emitted CO_2 corrected by the result evaluation factor RF_k (Figure 2.7 (b)) calculated for the whole RDE trip. The RF_k calculation is given by the equations 2.12. The final RF_k are set to 1.30 and 1.50, respectively. RF_k is determined by a sectionally defined function where r_k represents the ratio between the distance specific CO_2 emissions of RDE and the WLTC test run. The RF_k is defined by 1, a linear function with the parameters a_1 and b_1 and a reciprocal function, respectively. [19] [55] [6] [5]

Result evaluation factors calculation:

$$
\begin{aligned}
RF_{\mathrm{k}} &= \begin{cases} r_{\mathrm{k}} \leq RF_{\mathrm{L1}} & 1 \\ RF_{\mathrm{L1}} < r_{\mathrm{k}} \leq RF_{\mathrm{L2}} & a_1 r_{\mathrm{k}} + b_1 \\ r_{\mathrm{k}} > RF_{\mathrm{L2}} & \frac{1}{r_{\mathrm{k}}} \end{cases} \\
r_{\mathrm{k}} &= \frac{M_{\mathrm{CO_2,RDE,k}}}{M_{\mathrm{CO_2,WLTC,k}}} \\
a_1 &= \frac{RF_{\mathrm{L2}} - 1}{[RF_{\mathrm{L2}}(RF_{\mathrm{L1}} - RF_{\mathrm{L2}})]} \\
b_1 &= 1 - a_1 RF_{\mathrm{L1}}
\end{aligned}
\tag{2.12}
$$

After the emission results are calculated, they are compared with the emission limit values multiplied by a $\mathrm{CF_{pollutant}}$ to obtain the NTE limits for the RDE test run. The $\mathrm{CF_{pollutant}}$ itself was introduced with the 1st RDE package [28]. For $\mathrm{NO_x}$ emissions, a temporary $\mathrm{CF_{pollutant}}$ of 2.1 and a final $\mathrm{CF_{pollutant}}$ of 1 with an error margin of 0.5, taking into account the additional measurement uncertainties, was set in the 2nd RDE package [29]. With the 3rd RDE package [35] [34] the $\mathrm{CF_{pollutant}}$ values for PN was set to 1 with an error margin of 0.5. The 4th RDE package [19] corrected the error margin of $\mathrm{NO_x}$ to 0.43. A judgement of the General Court [20] of the 13 December 2018 annulled the $\mathrm{CF_{pollutant}}$ for $\mathrm{NO_x}$ emissions due to the fact that the Commission had no power to amend the limits for RDE type approval by applying correction coefficients. It further holds that even if it had to be accepted that technical constraints may justify a certain adjustment, a difference such as that stemming from the contested regulation means that it is impossible to know whether the Euro 6 standard is complied with during those tests. [41] The court annuls point 2 of Annex II to Commission Regulation (EU) 2016/646 [29] which defines the $\mathrm{CF_{pollutant}}$ for $\mathrm{NO_x}$ emissions. The court justifies maintaining the effects of the annulled provision in relation to the past and for a reasonable period of 12 months to enable the amendment of the relevant legislation. For vehicle manufacturers, this judgement means in a nutshell that, in the worst case, measurement inaccuracy in type approval is to the detriment of the manufacturer and must therefore be taken into account at the development phase. This effectively reduces the NTE limits for type approval to be carried out successfully and safely by twice the error margin.

3 Methodology and Data Acquisition

Since the introduction of the RDE legislation places completely new requirements on emission development, new demands also apply to the test field. This challenge can hardly be met with the established development approaches. From a conceptual point of view, this means that many test facilities are not capable of satisfying the new requirements brought by the RDE regulations. In order to maintain a highly efficient development environment, test bench hardware, software components, models and development methods must be adapted and developed further on an ongoing basis. Due to the wide variety of activities and the large number of test platforms that the BMW Group operates, it is a major task to maintain an overview of the current requirements of the specialist departments and the technical capabilities of the test field. In order to accomplish this task, a methodology must be developed which compares the capabilities of the test environment with the requirements derived from the new boundary conditions and thus determines the needs of the systems in a well-directed form to help understand the big picture.

3.1 Methodology Overview

With the aim of utilizing use cases as a key tool to derive test bay requirements, it is necessary on the one hand to define clear system boundaries and on the other hand to create a suitable development framework. The developed methodology used in this work is inspired by the idea of Dr. Ivar Jacobson of creating Use-Case 2.0 [59] to handle complex development environments. In principle, this method is applied extensively in software engineering, but can also be modified for use in other areas of development. Jacobson describes basic principles of successful application of use cases including keeping it simple by telling stories, understanding the big picture, focusing on value and adapting to meet the team's needs.

Figure 3.1 gives an overview of the included components of the methodical development approach that was developed as part of this work. The boundaries of the system to be improved and adapted containing hardware components, software tools, models and development methods are depicted on the right side. The left side describes the system of stakeholders. Stakeholders are all persons, groups and organizations with a justified interest to make demands. Stakeholders can be divided into two sub-groups: Stakeholders with a primary influence on the development methodology are on the right side (direct stakeholders) and those who influence the direct stakeholders are on the left side. The direct stakeholders can in turn be subdivided into emission developers, pre-development departments or test facility developers, i.e. all parties with a legit-

imate interest in influencing the system itself. On the other side, e.g. the legislator is setting the framework of type approval which influences the developers and results in the demands of those.

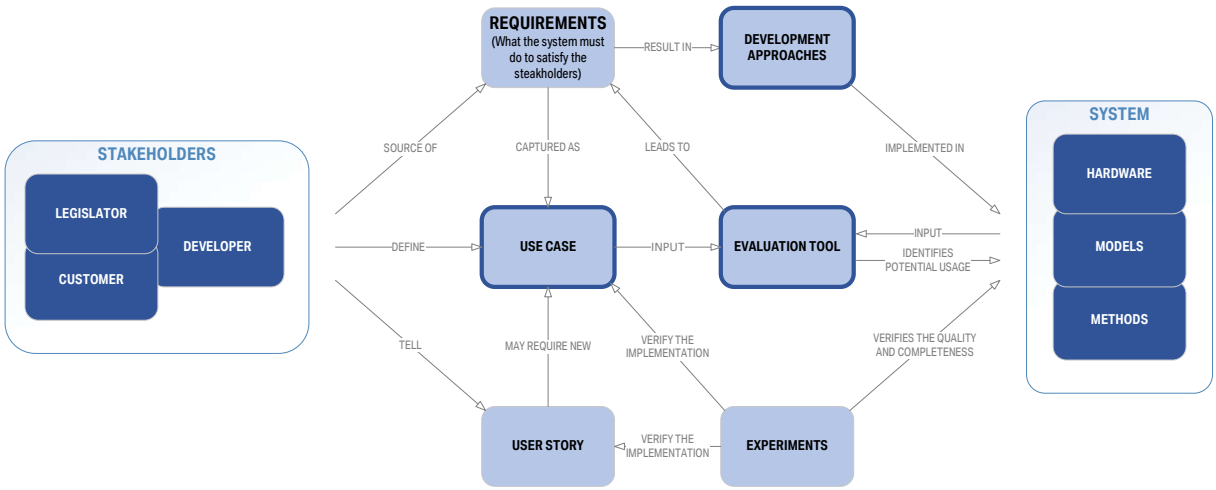

Figure 3.1: Methodology overview to meet RDE requirements

As part of the analysis, the internal specialist departments were asked about the development activities to be performed by them to define use cases with respect to RDE emission development. A use case is the way of using the system to achieve a particular goal. The totality of the use cases shows all the possible ways to utilize the system and besides indicates the value it provides. A use case is a development activity whose level of detail can vary substantially. It can therefore be a development concept but also a particular manoeuvre with predefined boundary conditions and initial states of the test carrier. With the help of user stories, a detour to formulate a use case was created. If the stakeholder is not in a condition to define a use case, an informal user story is used to express the fundamental intention of the stakeholder. A team of specialists can subsequently develop a use case based on the story.

In order to be able to link the requests in the form of use cases to the corresponding system, a selection tool, which is described in more detail in section 3.4, was developed as a main part of this research. On the one hand, the developed tool identifies the potential usage of the various subsystems, on the other hand, it leads to system requirements, which may result in a new development approach to further optimize the overall system.

The final essential part of the methodology are experiments which both verify the quality of the system and, possibly, uncover new weak points or vulnerabilities, as well as primarily aim to validate the complete implementation of the subsystems required for the respective use case.

In order to validate the methodology as a whole and to ensure that it depicts and links all parts correctly, both use cases from the literature and use cases from BMW's internal specialist departments were taken into account in the process.

3.2 Literature Review

In order to get an overview of the current development strategies and especially examined problems, relevant literature was analysed within the scope of this work and the aspects dealt with were considered and evaluated under BMW specific boundary conditions.
The Institute for Internal Combustion Engines and Powertrain Systems (VKM) of the TU Darmstadt is intensively engaged in the development of RDE specific methods. Therefore, the results of their work receive particular attention. Maschmeyer [67] presented three main use cases related to RDE emission development. In the proceedings of Bauer [9] and Hipp [50], they are further detailed. These are less detailed use cases that describe the principal development types and are therefore of essential relevance for the RDE development process. Each higher detailed use case can be represented by one of these cases, or can be seen as a modification or extension of one of those.

Use case 1 (UC1) describes a realistic reproduction and analysis of an existent vehicle measurement. The aim is to reflect the measured values of importance as accurately as possible. Mainly this use cases is characterized by the specification of the engine load and speed as controlled variables. The load input is appropriate for reproduction on the engine test bench and provides a high reproduction quality. However, it is not possible to change any parameter from the original measurement. One profile can only be used for one specific test configuration. This type of control is less suitable for operation with a powertrain test rig. At the powertrain test bench it is more appropriate to operate the experiments speed-based. Due to the intermediate gearbox, the engine speed cannot be specified directly, but results from the specified vehicle speed, road load parameters and the gear that is engaged.
Therefore, the aim of reproducing the exact engine conditions is more harder to achieve. The advantage of this control type can be seen in the possible variation of operating parameters, which, in fact can be seen as use case 2, defined by Maschmeyer, Bauer and Hipp [67] [9] [50].

The speed-based reconstruction of reference routes (UC2) targets a replacement of real vehicle on-road measurements by test bench measurements, characterized by a high reproduction quality. In its simplest form, this control type requires a simple longitudinal model of the vehicle dynamics and a speed profile as an input. It can be expanded by additional models like lateral dynamics, inclination input or tire slip. Basically, the velocity input is interpreted and translated to an engine load by a simulated driver. The driving character implemented in the simulation

has major influence on the results given by the test runs. Therefore, considerable effort has to be made to ensure a real world comparable driving character of the virtual driver.

The speed profiles can be generated by real world data, pre-simulations or combinations of events. In this case, the simulated driver's job is to reproduce the velocity input in a realistic way. There is no need to consider more impacts than those of the driver parameters. An extension could be to take into account the curve radius and let the driver adapt the velocity due to determined limits of lateral acceleration, which leads to the third use case.

In contrast to the afore mentioned use cases, the virtual integration (UC3) targets a route-based testing with a driver controller which adapts to the given boundary conditions under determined parametrisation of its characteristic values. A main task with respect to this use case is the effort caused by the additional degree of freedom brought in by the disappearance of the speed profile. The driver controller is now exclusively responsible for determining the characteristics of the measurement based on the boundary conditions given by the route profile combined with the dynamic limits, traffic and environmental influences and the parametrisation of the driver itself. The level of virtualization extends from Vehicle in the Loop (ViL) to Model in the Loop (MiL) approaches, depending on the target of the experiments and the stage of development.

Essentially, the main methods described by the VKM are presented in [50]. The idea of a most-relevant scenario, which is linked indirectly to the UC2, aims to isolate emission-critical manoeuvres and eliminate irrelevant aspects to ensure the successful completion of all possible certification cycles. In this context, historical effects, which represent a sequence of driving manoeuvres resulting in an overall increase of emissions, can also be of importance. In addition, the use of fleet data is mentioned in [93]. This can be interpreted as data input for the generation of a most relevant scenario for one specific powertrain as well as a whole vehicle generation.
A thermally real test bench environment is named as another important aspect. In other words, this complies a realistic vehicle temperature behaviour of the mediums on the one hand, but also an exact reproduction of measured medium temperatures on the other hand. An example of this might be the charge air temperature, which on the engine test bench is usually controlled by a water-cooled intercooler with a constant setpoint temperature. In the first stage, an improvement would be to enable vehicle-realistic charge air temperatures with the use of the vehicle's intercooler. A further improvement would be to enable a setpoint dependent charge air temperature. The same phenomena are also mentioned for other medium temperatures such as coolants or oil temperatures. [9] [50] [93] [67]

Friedmann et al. and Faubel et al. describe a methodical approach using neural networks to determine influences of vehicle and environmental parameters to vehicle's emissions behaviour with the aim of determining a 3-dimensional matrix linking the parameters with the resulting

emissions response [40] [36]. As an exemplary use case, Mink et al. lists an impact analysis on emissions with focus on particle raw emission behaviour [72]. With the application of online Design of Experiments (DoE) to determine optimal injection patterns, they targeted an optimisation of the injection pressure, leading to an improvement of the spray breakup and therefore the mixture formation in highly dynamic, representative RDE sequences. Friedmann et al. designed a modular structured tool-set to select a route variant based on route characteristics and the results of previous trips, according to the specific needs of the test to be performed. The resulting data can then be used as a characteristic footprint for emissions prediction. [40].

Comparable with the method presented by Gerstenberg et al. is dealing with an RDE robustness matrix consisting of the influences of the route, traffic situation and the driving style. [43] Gerstenberg et al. recommends the relocation of RDE development activities to Engine in the Loop (EiL) test environments in [42] and presents a comprehensive transmission simulation in [44].
A special aspect to be mentioned is the realistic torque intervention that is simulated on an engine test bench configuration. The torque intervention includes ignition angle variations as well as injection cutoff. The transmission control unit (TCU) software can be fully integrated, so that shifting points and shifitng procedures are identical to the vehicle behaviour. The residual bus simulation as an input to the virtual TCU also includes inclination signals that have a major influence on shift behaviour.

Summarizing the analysed literature, it can be concluded that integral virtualization related to RDE emission development is intended especially in earlier development stages. Due to the complexity of engine models, especially emission models, these cannot completely replace tests performed with engines. However, in order to reduce the number of road trips with PEMS measurement equipment and thus the resulting costs and the effort, the use of EiL test rigs is considered to be the preferred solution in the literature. Another point worth mentioning is the use of DoE and big data approaches for robustness analysis and emissions prediction based on an impact analysis including weighted influencing parameters. The data produced by the emissions prediction can additionally be used for emissions correction of varying results caused by deviating influencing factors.

3.3 Derivation of Representative Test Benches

In order to develop a tool that allows for the selection of the optimal test platform, it is useful to classify the test platforms into certain categories. The classified test benches can be differentiated more profoundly, so that an analysis of individual test benches is made possible while keeping an overall overview. In addition, a classification allows the user to focus directly on a preferred platform category and to compare it to alternative types. Figure 3.2 visualizes the

classification process of platforms made in this work. The classification may revised when new demands regarding RDE development occur.

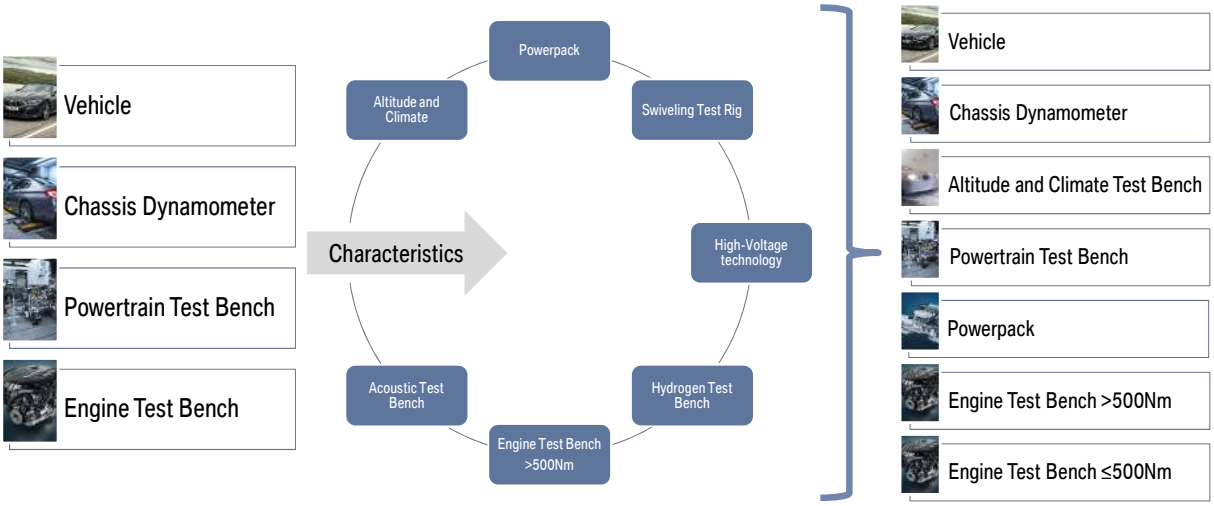

Figure 3.2: Derivation of representative Test Bench categories

On the left side, the basically available types of test benches are depicted. In order to allow a comparison with the real vehicle, it was added as a fourth category besides the classic chassis dynamometer, the powertrain test bench and the engine test bench. In the central part of the illustration, various characteristics of the test bench types are presented as examples. The list represents a few examples of features related to RDE development. They depend on one hand on the development target and on the other on the technical specifications of the test environment.

Altitude and climate test benches are a form of test benches which allows experiments under real environment conditions. In addition to the large scale regulatable temperatures of all media, they are characterized by the possibility to adjust the ambient pressure. This enables the reproduction of real conditions in an exact way. In the example of the BMW Group, the altitude and climate test benches are all equipped with vehicle transmissions and correspondingly dimensioned electrical machine.

The powerpack test bench is by definition a powertrain test bench but with just the real vehicle transmission without axle drives and with just one in-line mounted electrical machine.

Swiveling test rigs can be used, for example, for oil sump analysis by simulating lateral acceleration by tilting the engine.

Since hybridization has become increasingly important, high-voltage technology must also be considered to cover all technological possibilities.

Furthermore, alternative fuels such as hydrogen can be considered for development purposes.

Technical framework conditions, such as engine test benches with very high torque or test benches with acoustic measurement technology are also included in the selection process.

In order to make a selection of the appropriate categories, the development objective and also the development boundary conditions must be clearly defined. The following distinction was made on the basis of the currently prevailing boundary conditions and existing development priorities with regard to RDE emission development. The right side of figure 3.2 shows the elaborated test bench categories determined on the basis of the test bench types and their relevant characteristics in the context of RDE.

The vehicle with PEMS measurement equipment represents a direct reference and benchmark for the selected categories.

The chassis dynamometer is a central element in RDE development. Both generic cycles and type approval tests can be realistically displayed from the vehicle side. As the existing chassis dynamometers are basically very similar, no further differentiation is necessary in this respect. Only the performance data of the individual test benches are differentiated, as it is the case for all other test bench types, too.

Altitude and climate test benches are highly demanded for the reproduction and analysis of temperatures in the limit range. In many cases, it is sufficient to condition only the engine mediums within the RDE-valid temperature ranges. This possibility is also given by other test benches, therefore altitude and climate test benches are only available in limited quantities.
Within the scope of this work, only test benches with more than one electrical machine or with integrated axle drives in the test bench design are referred to as powertrain test benches. All other test rig setups with integrated vehicle transmissions are referred to as powerpack.

In addition, the torque class of the engine test benches is differentiated from a technical point of view. Here a practical limitation of 500 Nm has been established. With regard to the nominal engine torque, this separates the high-performance engines like the v-engines developed by the BMW Group from the low- to medium performance engines.

3.4 Development of a Tool for Optimal Test Platform Selection

Based on the considerations on test bench categorisation, criteria of importance for RDE development were elaborated. With assistance of the use cases and the development methods from

the literature and the specialist departments, a series of criteria has been collected that need to be analysed. In the beginning, an evaluation of the criteria was defined to evaluate the test bench types. At the same time, the evaluation indirectly convey the importance of the criteria. An attempt was made to evaluate the criteria by rating aspects to be considered.
Figure 3.3 illustrates the process of evaluation and the related problematics: On the left side, the criteria, divided into the six categories of ambient conditions, test unit conditions measurement, required features, control type and simulation, are listed. The evaluation takes part by rating the aspects shown in the central part of the figure. The first aspect determines whether the criterion is taken into account in this context. The second aspect rates the adjustability, accuracy or the realism, depending on the criteria to be evaluated. Furthermore, the reproducibility is assessed by the third aspect. Finally, the dynamism compared with the behaviour of the real vehicle is to be evaluated. Combined with the seven categories of test benches, this process results in a matrix of 1344 issues to be evaluated. This means, that when this is the basis for the selection tool to operate with, there are 192 issues for each use case to be evaluated, as well. In principle, it is not absolutely necessary to complete all points, but the usability is affected by the high complexity of the necessary input.

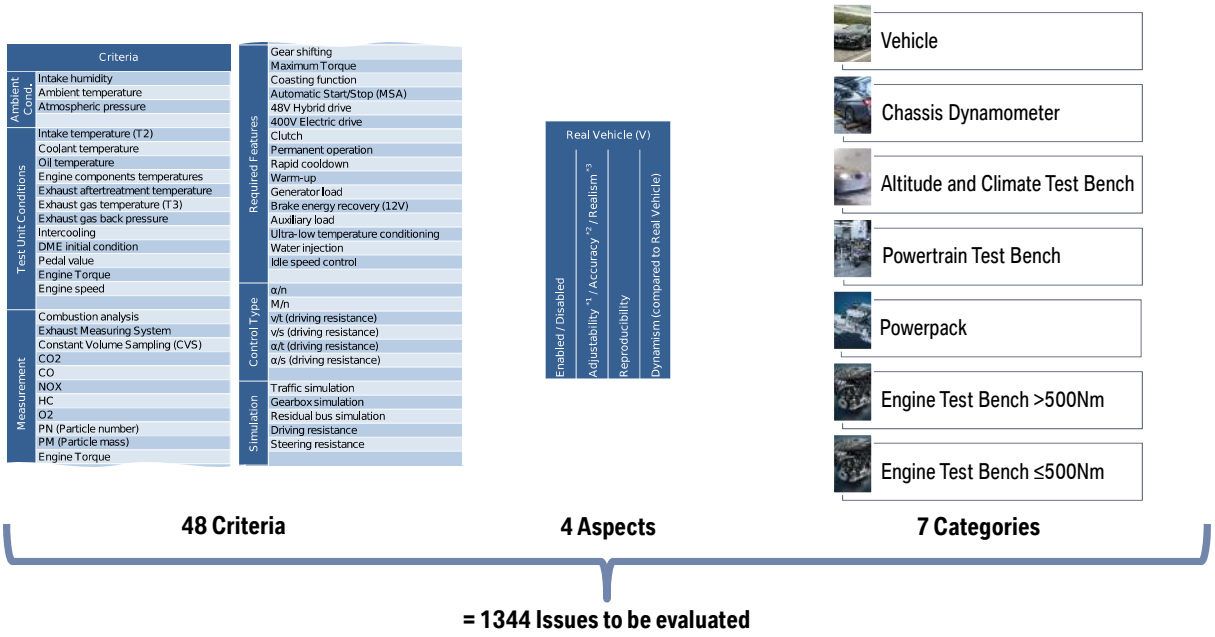

Figure 3.3: Process of Evaluation of RDE relevant Criteria

Due to the high amount of work to be done to get results from the tool, an attempt to reduce the amount of issues was made. However, it turned out that a reduction to a single key indicator results in a loss of detail and does not significantly simplify the input. With the approach of a user input based on checkboxes, user-friendliness has been increased substantially. The need for numerical input has been largely eliminated. Only essential numerical inputs are required under the new treatment (Further detailed in 3.5) . Through several iteration loops involving

the previously determined use cases, a tool has been developed which, with the help of a manageable user input, delivers an accurate result on the performance of the test field.

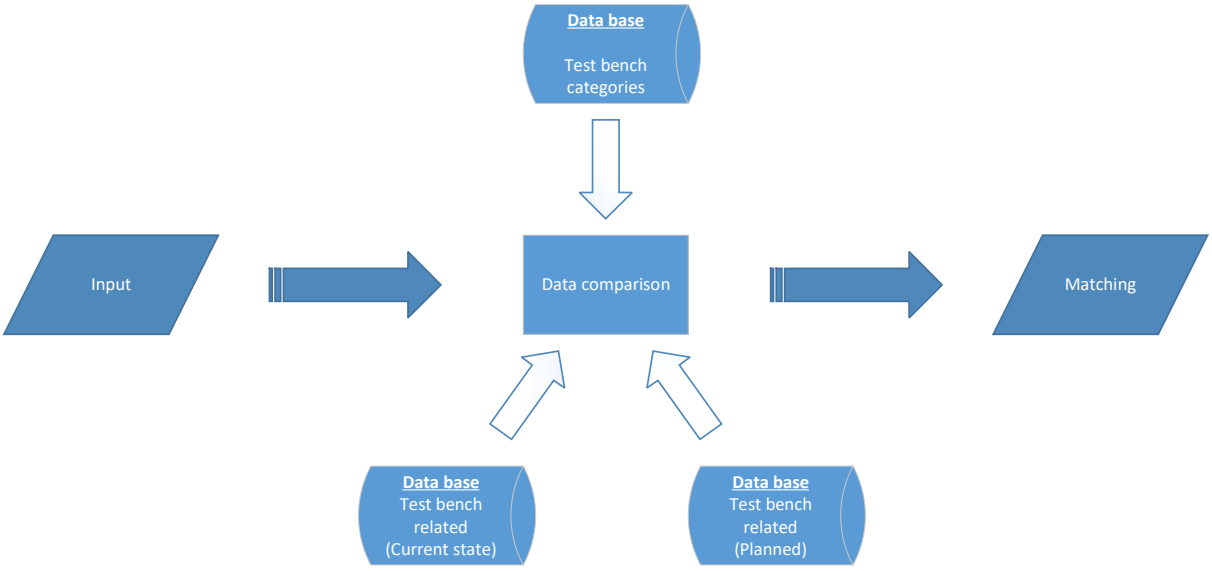

Figure 3.4: Functional principle of the evaluation tool

The schematic structure of the tool is presented in figure 3.4. The data input collected in the input form is compared with the data provided by three different data bases. One database is used to collect the specific characteristics of each test bench category. This includes, for instance, the supported control types, the conditioning and exhaust gas measurement instruments characteristics for the respective test bench category, as well as the specific features provided by the platforms. In order to allow a more detailed examination of the individual test platforms, two further databases are used. These databases, shown in the lower part of figure 3.4, are identically structured and represent the specific performance data of the individual test benches at the current time and the planned status for the short term. The knowledge provided is used to permit an evaluation of the proposed modification and extension activities within the test field based on the relevant use cases.

The selection tool itself is based on Microsoft Excel worksheets that have been enhanced with Visual Basic for Applications (VBA) macros to compute the evaluation and ActiveX controls to enable the data input and output. Figure 3.5 shows the overall input form used by the tool.

The input is divided into four parts. In the upper part, the determination of the control type takes place. Furthermore, optional enhancements can be added to the selected types. An input type to control the engine and an output type to respectively control the electrical machine are to be selected for the test execution. The tool also only allows the selection of valid combinations.

Figure 3.5: Input form of the evaluation tool

The implemented additions relate to the combination of road load as output and vehicle speed as input. The road load simulates the driving resistance forces during the test to be performed. Additions are the simulation of tire slip resulting from acceleration and deceleration and a possible cornering resistance. The target speed can be further enhanced by the use of a realistic driver controller acting like a human driver.

Another addition based on the driver controller is the execution of a test run in which the target speed cannot be reached due to external influences, traffic lights, the tolerated lateral acceleration of the vehicle or traffic. A related challenging task is to reproduce a performed free ride with external influences with a modified engine control unit (ECU) dataset. Even the slightest latencies cause deviation from the trip to be reproduced. An assumable case would be a traffic light switching to red which is only passed in time during one experiment due to latencies.

In the second part, the type of the required exhaust gas measurement system is determined. The current status of the tool evaluates the measurement systems that have to be differentiated fundamentally. A further distinction was not made, since the performance characteristics of the exhaust gas measurement technology required for the respective use case cannot be defined in general terms. Cross influences based on the characteristics of the test require an individual analysis of the possibilities given by the measurement technique. The tool is prepared to include special measuring technology into the selection. This feature has not been considered in the current version because mobile special measuring technology is only partially assigned to an individual platform.

The third part containing the conditioning systems of the different test platforms was reduced to basic demands towards the temperature ranges of the main operation media coolant, charge air, intake air and ambient air. Oil temperature is not considered in the tool because of its indirect coupling to the coolant temperature. The use cases of RDE emission control does not require a special differentiation of these two media. Charge air, intake air and ambient air are considered separately because of the different test bench designs.
While, for example, chassis dynamometers only temper the ambient air, the three temperatures specified can be individually controlled, for instance on altitude and climate test benches. The test bench design of the chassis dynamometer thus couples the ambient temperature with the intake air temperature. The resulting charge air temperature depends on the charge air cooling system of the vehicle and therefore cannot be conditioned. This is inherent to a real vehicle and is therefore implemented as additional input. The characteristics of the medium temperatures of coolant and the charge air are divided into a stationary behaviour and a vehicle realistic behaviour. In addition, this option can be selected for the exhaust gas. A demanded stationary behaviour of the exhaust would result in an exhaust gas conditioning system which is not state of the art, but is listed due to completeness.

To conclude the input, various additional functions and specific test requirements can be defined. An important information for engine test benches which operate without a installed transmission system are the required gear shift operations. Due to the availability of different models for gear shift operation simulation on the engine test benches with varying precision grades on the one hand and varying implementation grades on the other, a distinction is made between four

shift operations: Up and down shiftings are both split into shifting operations under load and coasting. In addition, a realistic torque intervention can be required. The correct and complete reproduction of shifting operations is not a trivial task.
The TCU of the currently used automatic transmission system differs between three shift speed levels [10]. The speed level is chosen depending on the selected driving program and the load actuator gradient. The levels indicate comfortable, fast and comfortable or sports gear shifts. In addition to the correct implementation of the different shift speed levels, the determination of the speed level which would be chosen in the vehicle's shifting operation as well as the correct shifting points is another challenging task.

Referring to the electrical machine, the power output of the engine in different operation modes can be given as an input to evaluate the torque compatibility. Due to the basically two different test bench configurations with and without transmission system, two different engine torque levels are to be evaluated. First, the engine torque during acceleration from standstill has to be considered. In case of an engine test bench, this means that the dyno torque is the same as the engine output torque, while in the case of a powertrain test bench configuration, the dyno torque is up to an order of a magnitude higher than the engine torque due to torque converting components like the transmission and differentials and is therefore a limiting factor when utilizing a powertrain test bench.

To evaluate the engine torque at higher speeds, there is a second input. This value is necessary to determine the required torque to perform a shift operation at the engine test bench and to calculate the required dynamometer torque at higher speeds when utilizing a powertrain test bench configuration. The required transmission ratios are predetermined but can be changed in the input form. The evaluation of the values is further analysed in section 5.5.

In addition to the input of the engine torque, there is the possibility to determine a dynamic demand of two cases of relevance: The first important case is a shifting operation which is relevant for the engine test bench configuration. Modern automatic transmission systems allow engine speed gradients up to 6000 1/min/s. The electric machine must be able to provide these gradients. The second possible input is particularly relevant for test bench configurations with vehicle transmission systems. A possible case is an acceleration from creep speed up to the speed limiter of the first gear. Depending on the vehicles power to weight ratio, speed gradients up to 640 1/min/s can be expected. The evaluation process of the dynamic demands is further detailed in section 5.5 as well.

Using the input fields of the scope of experiments, the tool is able to determine the most cost-efficient platform for the specific use case. The required period of time and the number of different test carriers together with the cost data of the respective test bench categories in an

estimation of the costs incurred. In addition and because it must be differed for the specific cases, an input for the test carriers to be mounted, assembled on a pallet system or commissioned is necessary. These data are required for the estimation of costs on platforms without real vehicles. The commissioning of a test carrier on a powertrain test bench can take about two weeks, while the commissioning of a real vehicle on a chassis dynamometer takes place in only about half an hour. Thus, it is necessary to determine whether commissioning is necessary or not.

Three more features are currently integrated into the tool. Due to the high data transfer between ECU and TCU and the dependency of some engine functions on the functionalities a gearbox provides, a vehicle transmission can be a requirement for test operation. In some cases it is also necessary to apply the transmission datasets for purposes of emission development. An existing vehicle gearbox can be demanded with a checkbox. Another point worth mentioning is the ability of permanent operation of the test facilities. A second additional checkbox can be used to include it in the evaluation process.

The last point included in the input form is the regulation of air pressure. The existing positive altitude gain limit for RDE trip validity is set to 1300 m which results in an air pressure of approximately 865 hPa. The lower air pressure affects the vehicle's performance, fuel consumption and emissions formation as studies of FIAT Automobile SA in Brazil [96] and the University Malaysia Pahang [1] show. Modern engine configurations are able to compensate for the lower air pressure by setting a given charge air pressure, but due to ideal gas laws the compression end temperature changes because the necessary pressure adjustment is higher due to the lower initial pressure. The regulating systems of the altitude and climate test benches are able to regulate the air pressure down to 600 hPa which is equivalent to an altitude of about 4200 m.

The current status of the evaluated input represents some relevant points resulting from the investigations. The necessary input can vary due to upcoming new demands regarding to RDE and therefore has to be reevaluated from time to time. The current status provides a list of possible enhancements which can be implemented if necessary. The fan control of the test bench setup, a revision of the data sets to calculate the economic efficiency and the implementation of the additional driving resistances resulting from inclination are extensions worth mentioning at this point.
Figure 3.6 illustrates the output resulting from the evaluation tool in its initial state. It is divided into seven columns to refer to the different test bench categories. They are arranged from left to right according to the degree of modeling required and the deviations from the RDE relevant setups, respectively. The rows are related to the different input sections and provide further detailed data about the evaluation of each category. Signs on the left side of the text boxes indicate the degree of fulfillment of each point. A green indicator means a total fulfillment of the required input data or respectively a fulfillment of the given criteria of at least 90 % of the

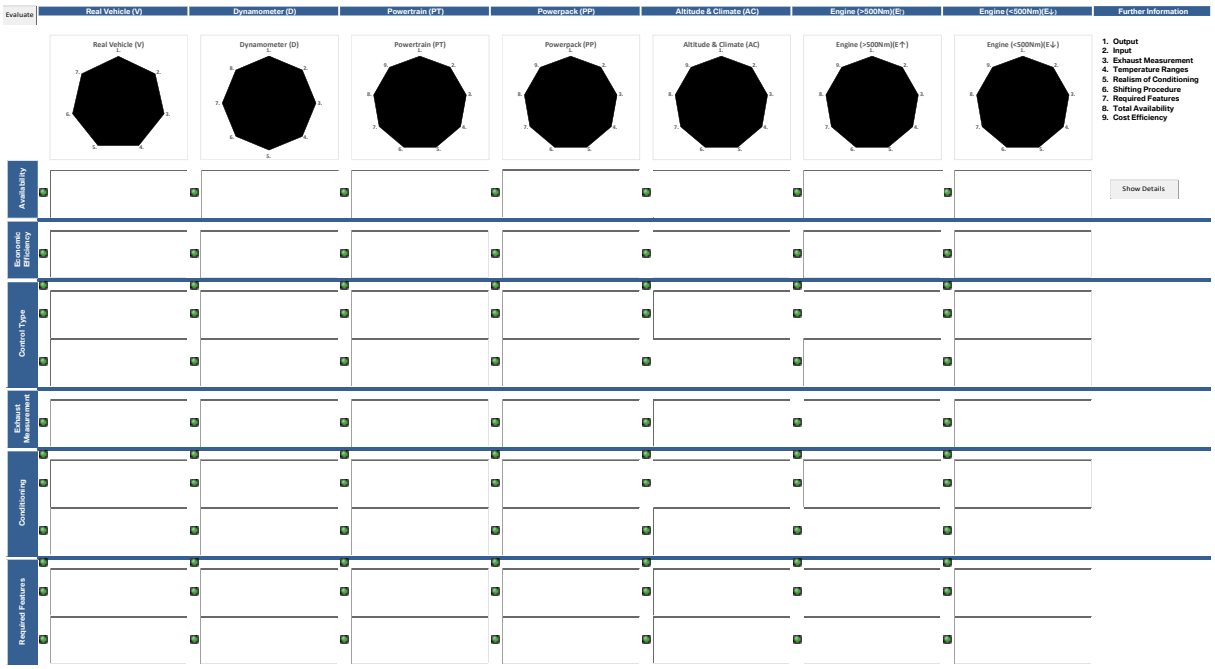

Figure 3.6: Output of the evaluation tool

specific platforms. A yellow indicator light implies a fulfillment of the input with restrictions, which are shown in the text boxes. A red indicator points to the non-fulfillment of the required performance obligation.

The radar charts in the upper part of figure 3.6 provide an easily graspable visualization of the degree of fulfillment, divided into the evaluated criteria as a whole and are aligned to the indicators. Each section of the diagram can be set to a value between 0 and 3, whereby 0 represents a missing input and 1 - 3 stand for the colors red, yellow and green.
Figure 3.7 shows the resulting diagram of an exemplary evaluated use case for the category of engine test benches with a high output torque. The main limiting requirement in this case are the temperature ranges. The input requires an initial coolant and intake air temperature of -7 °C which represents valid RDE test conditions. Section 4 of the diagram indicates, that not all the platforms are able to fulfill the requirements. Section 8 represents the total availability of platforms and is linked to the values given in the text box below.
In this case, the use case is supported by approximately 14 % of the platforms in the current state and in the planned status as well, but with a different total quantity. Section 8 visualizes the combination of all other requirements and is therefore the indication for a performable test. A partial availability in multiple other sections can also result in a non-availability of the test bench category for the specific use case.
Figure 3.8 provides an overview over the functionality of the tool. In total, the tool consists of the three databases with a total amount of more than 8000 values and a VBA code to match the requirements with the performance data of the test field. The flowchart shows that the

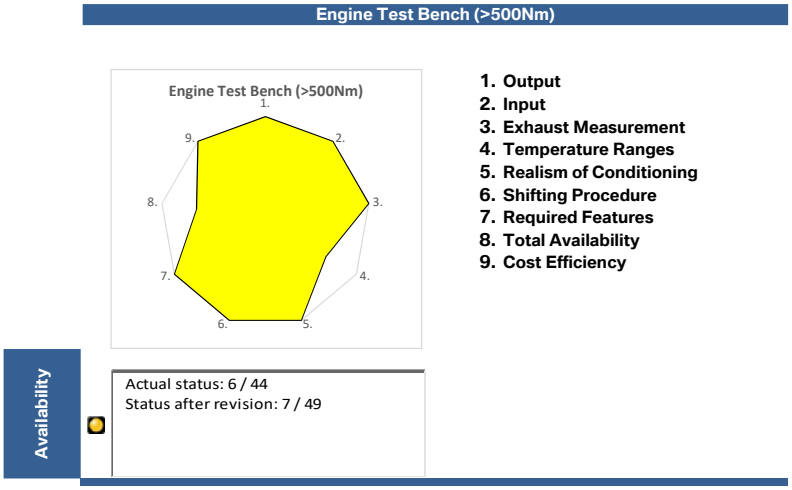

Figure 3.7: Detail of an exemplary output of the evaluation tool for a related use case

program systematically analyses the different sections of the evaluation. In the first part, the default values are set, the databases are imported and the areas to be assessed are defined. In the following sections, the input values of cost effectiveness, output and input control type, the exhaust measurement system, ranges and characteristics of the medium temperatures, the gear shifting demands as an independent part and the features to be complied with, are evaluated. Afterwards, the total availability is evaluated and the results are displayed in the text box.

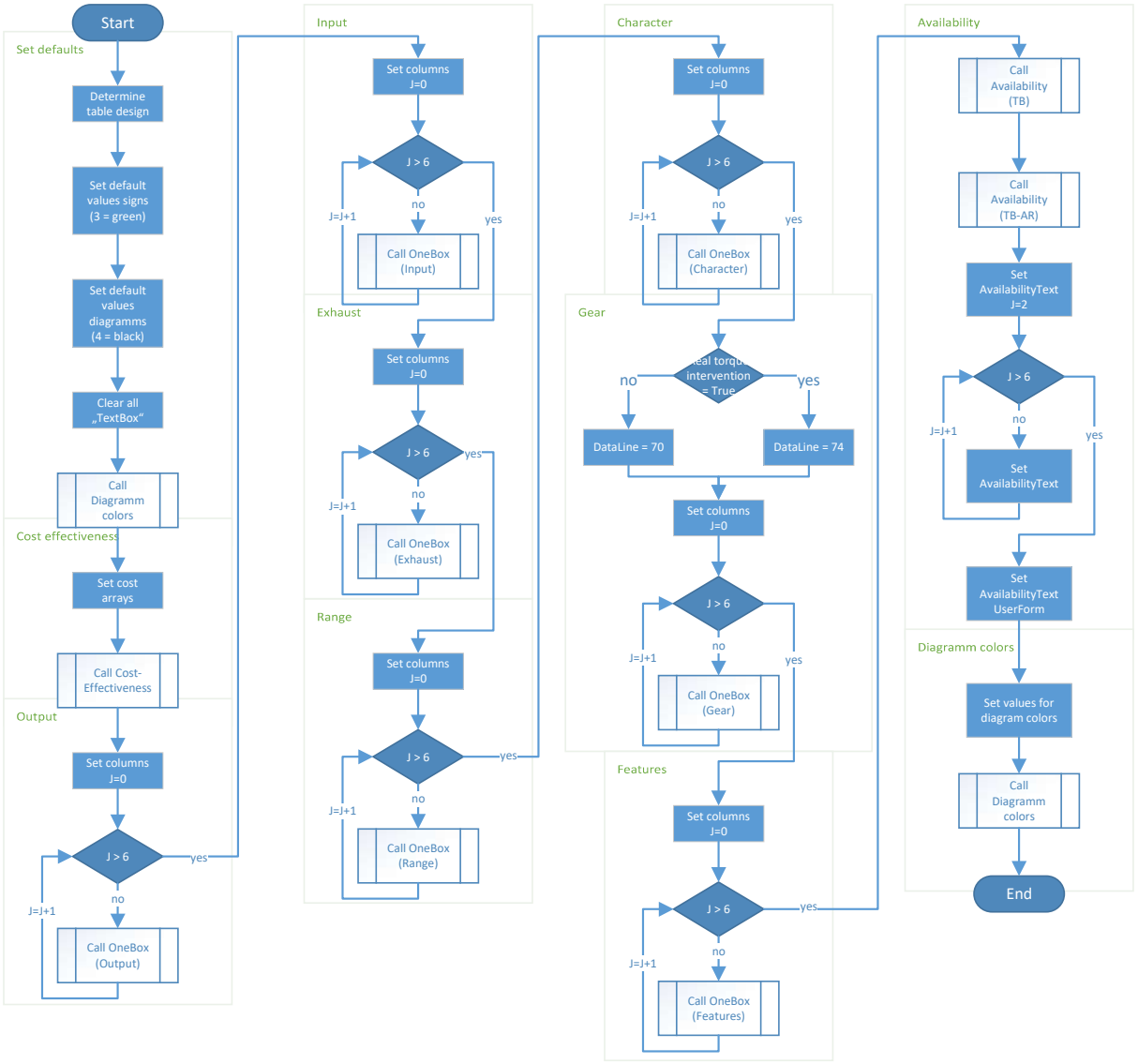

Figure 3.8: Program flow chart of the main part of the evaluation tool

4 Test Units, Facilities and Experiments

To further analyse the knowledge gained from the tool, to test its implementability and to validate developed systems, various test platforms are available for the department of trial and simulation. In the following, the main test unit and its test stand related to this work will be presented. Furthermore, the performed experiments are described.

4.1 Test Units and Facilities

Most of the measurements related to this work were carried out on a test bench that belongs to the powerpack category. Figure 4.1 illustrates a representative test bench configuration at the BMW Group Research and Innovation Center. In case of the used test bench, the engine is coupled to a vehicle's transmission, connected to a drive shaft as it is used in a vehicle setup. The shaft is directly coupled with the electrical machine. In this case, the rear axle drive is simulated by the automation system.

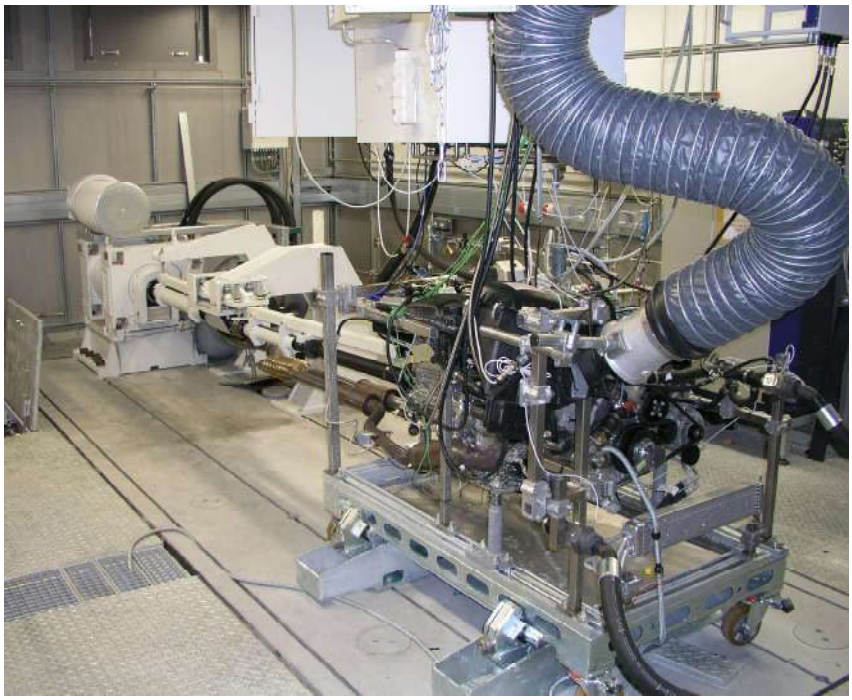

Figure 4.1: Exemplary test bench configuration of the BMW Group Research and Innovation Center [53]

The raised floor allows access to the wiring underneath it and the test bench's conditioning system which is connected at the engine control site. The engines are mounted on a pallet system and are connected to a gallows positioned above the engine. Access to the test bench is not possible during test operation. However, the test bench can be monitored at any time via cameras and microphones. Test operation is possible around the clock through modern security technology. The test configuration used for the measurements uses the blown air with ambient temperature as intake air.

The technical details of the test carrier and the test bench configuration are summed up in table 4.1 and 4.2. The engine is a turbocharged four-cylinder in-line engine with direct injection, as used in the current BMW 5 Series. The exhaust aftertreatment complies with the current Euro 6d-temp emissions limits and is equipped with a near-engine catalytic converter and an GPF.
Due to the high output torque at the gear shaft, the electric machine has a correspondingly high maximum torque of 2500 Nm. The maximum speed of 8500 1/min is suitable for every conceivable case. The high inertia of 2.7 kgm^2 results of the high torque and does not cause any problems because of the use as a powertrain test bench, as the speed gradients at the gearbox output are low compared to the crankshaft. Due to their temperature range, the test bench conditioning systems are suitable for cold-start applications at moderate temperatures.

Table 4.1: Technical details of the test carrier

Engine / Transmission

Power output	in kW at rpm	141 5000
Torque	in Nm at rpm	280 1350 - 4600
Design / Number of cylinders		Row 4
Displacement	in cm^3	1998
Bore / Stroke	in mm	82 / 94.6
Compression ratio		11:1
Valves per cylinder		4
Exhaust aftertreatment		3-way catalyst GPF
Transmission		8-speed AT 8HP51

In addition to the measurement of the gaseous exhaust components, the test bench is equipped with two particle counters which use the condensation particle counter (CPC) measuring principle and can be positioned individually in the exhaust system depending on the test procedure. Furthermore, the engine is equipped with cylinder pressure indication of all cylinders and a fuel consumption measurement system, which is sufficiently precise to measure even minor variations.

Table 4.2: Technical details of the test bed systems and exhaust measurement system

Electrical machine

Power output	in kW	450
Torque	in Nm	2500
Speed	in 1/min	8500
Inertia	in kgm^2	2.7

Test bench conditioning

Coolant temperature	in °C	12 - 120
Charge air temperature	in °C	12 - 60
Ambient temperature	in °C	20 - 40 [a]

Measurement equipment

Exhaust gas measurement system [b]	HC, CO, CO_2, O_2, NO_x, CO_2EGR HORIBA MEXA-7100HEGR
Particle measurement system [b]	2 x PN HORIBA MEXA-2100SPCS
Cylinder pressure indication	Cylinder 1 - 4
Fuel consumption measurement system	AVL FuelExact^{TM} Mass Flow & PLU

[a] Possible temperature range depends on outdoor temperature
[b] The measuring point can vary depending on the experiment

4.2 Experiments

In order to get an overview of the possibilities of the test field, various experiments were analysed during this work. The first analysed experiment is a valid PEMS measurement, which could occur at type approval in this way and represents the real trip to be simulated on the EiL test bench. The speed profile is given in figure 4.2.

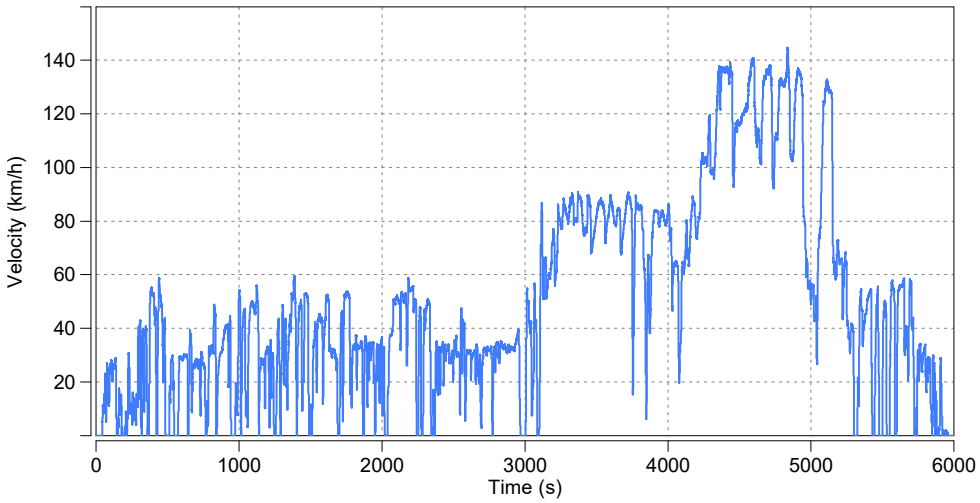

Figure 4.2: Valid PEMS measurement as basis for the analyses

The total duration of the test performed is 98 minutes and 30 seconds. The maximum driving speed is 144 km/h and the total distance covered during the test is about 83.5 km. The test was performed at an ambient temperature of about 9 °C at an altitude between 445 m and 505 m. The highest acceleration amounts to 5.13 m/s^2.
In addition to the measurement quantities for type approval, which also contain the GPS data, the measurement data also include other important measurement quantities that are relevant for assessment regarding the reproduction of a real trip.

Furthermore, various sections of real world based data which serve as a reference for the investigations in chapter 5 were analysed in more detail. An exemplary profile containing several acceleration and deceleration phases combined with a longer driving phase without high dynamic is given in figure 4.3. It consists of a 520 s test with a maximum speed of 97 km/h. The maximum acceleration is 2.60 m/s^2 and thus only half the value of the complete RDE measurement. The alternating acceleration and deceleration phases are very well suited for investigating the performance of a driver controller, but also for investigating the torque build-up and shifting operations.

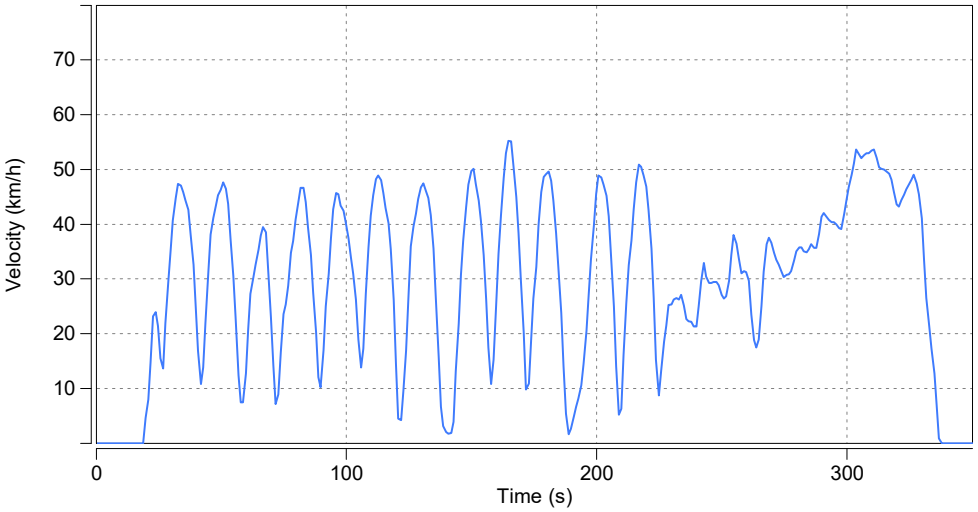

Figure 4.3: Section of a real data based cycle set as a reference for the analysis

The third analysed experiment was a short manoeuvre of an acceleration from standstill to 60 km/h continued with a phase of constant speed. This critical manoeuvre can be used, for example, to investigate cold start emission behaviour or to represent a standing start at traffic lights. A corresponding speed profile is represented by figure 4.4 and equals an acceleration of 4.0 m/s^2. This value corresponds to an RDE relevant acceleration and depending on the power-to-weight ratio of the vehicle describes a full load acceleration. In any case, however, this use case represents a combination of creep torque, low-end torque and high load at high engine speed.

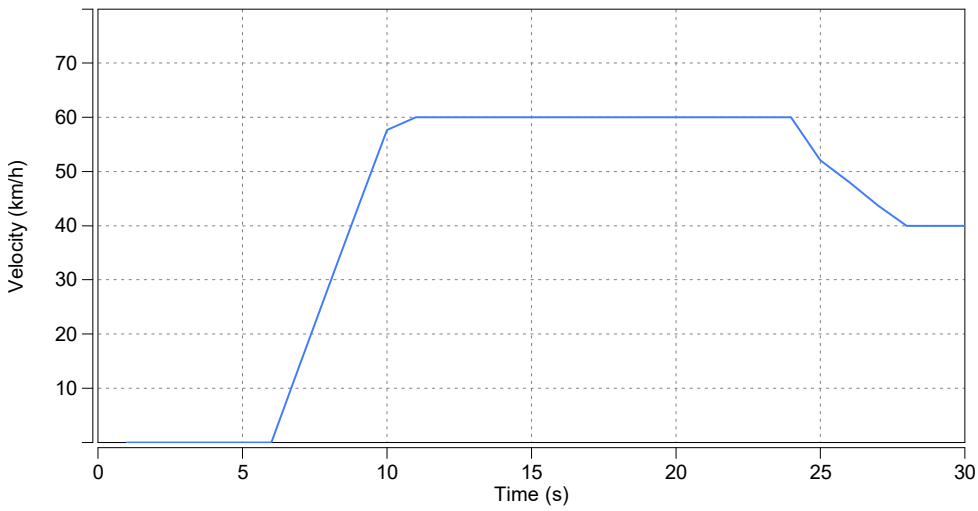

Figure 4.4: RDE-relevant driving manoeuvre

To compare the coasting behaviour of a real vehicle with the provided data and to confirm the validity of those, on-track coasting experiments were performed and compared with the results observed on the test bench. The speed profile of the performed test is given in figure 4.5. Two measurements each in opposite directions were carried out. The graphs show two averaged filtered speed profiles each. The measurement was started at a velocity of 90 km/h. The slight difference between the two speed profiles which results in a divergence of more than 6 km/h after 120 seconds is caused by an inclination of the road the test was performed on, or the influences of different wind speeds and varying environmental conditions.

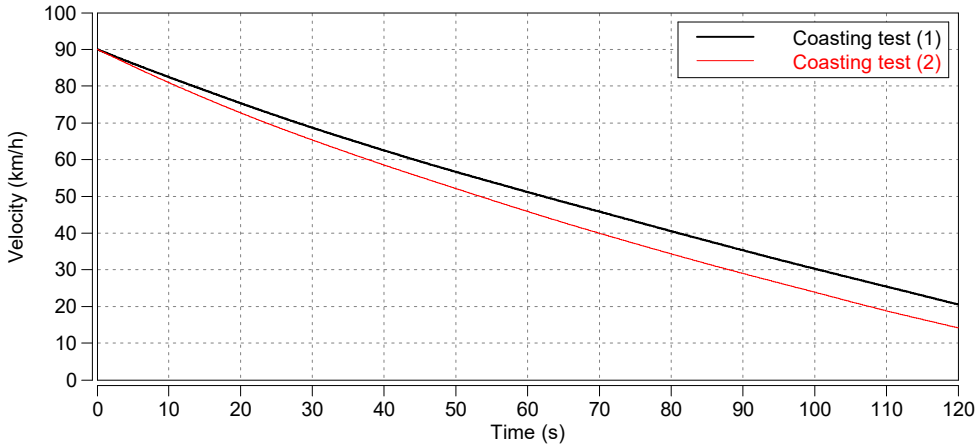

Figure 4.5: Coasting experiment to determine coast down parameters

5 Results and Derived Recommendations

Based on the previous results and the experiments described in chapter 4, the following outcomes have been obtained. In order to thematically assign the results and put them into context, sections 5.1 - 5.5 discuss the driver controller and the engine operating conditions, the road load and its potential extensions, the test bench conditioning and the performance of the load unit in more detail.
Different aspects of the problems and potential solutions are presented for selected topics. The results may provide an estimation of future development demand and the expected workload.

5.1 Evaluation of Driver Controller

This section is dedicated to both realistic and reproducible test execution under test bench conditions. Different driver controllers are compared with each other and with a human driver and their individual behaviour characteristics are analyzed. As the driver has a major emission influence [70] [38] in addition to technical aspects and the new legislation aims to cover exactly this aspect, great attention is paid to realistic driver behaviour simulation of an automated driver controller in test bench operation.

Figure 5.1 depicts the repeated load build-up after coasting under slightly different initial conditions and increasing vehicle speed and absolute acceleration. All three experiments are based on the same target speed curve. The black line represents the human driver. It can be noticed that the course of the load actuator (middle part) is very smooth and is characterized by a certain experience value.

The driver is a qualified chassis dynamometer driver. His behaviour is characterised by a high reproduction quality and small deviations from the target speed. The main features of his behaviour are similar to those of a customer. However, as the driver only receives input from a speed profile and external influences from traffic and the environment are fully excluded, this driver must not be regarded as representative of a customer. In some cases, the driver's behaviour can deviate significantly from that of the client. Also there are no different driver types represented by a trained chassis dynamometer driver, since a high degree of reproducibility is the main target of the training those drivers go through.

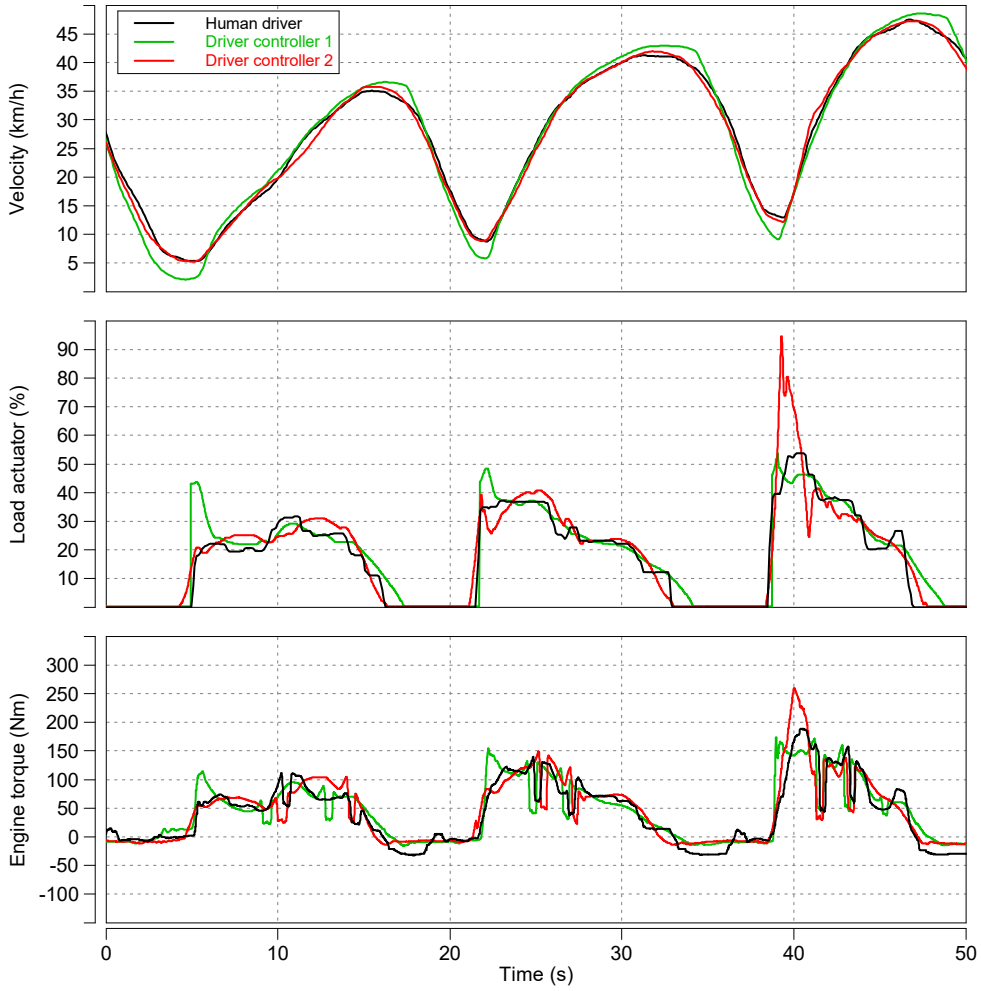

Figure 5.1: Comparison of a human driver recorded on a chassis dynamometer with two different driver controllers recorded on a powertrain test bench

In practical terms, a distinction is often made between a defensive, an aggressive and a normal driving style. [56] [58] [57] A series of studies reveals the following driving styles as a result of their investigations: aggressive driving style, inattentive driving style, drunk driving style and "normal" or safe driving style [3] [100] [77].

When considering a driver controller, basically a distinction can be made between two different objectives in the development is made. On the one hand, the driver can serve as a substitute for a trained chassis dynamometer driver, but on the other hand he can also imitate customer behaviour with all its varying characteristics. The former is a simpler task due to the recurring patterns of behaviour. Also in this case, a better comparability between different manoeuvres and vehicle derivatives is possible. However, it should not be forgotten that real customer behaviour is the actual objective and should therefore be investigated most intensively.

Another point worth mentioning regarding driving style, is the impact of external influences during a trip. The driver's behaviour can change drastically due to traffic hecticness or environmental influences. Taking into account historical effects with regard to emission formation, it can be assumed that such behavioural changes can lead to additional emission relevant events such as high dynamics and full load accelerations.
If a vehicle with automatic transmission is considered, the driver's possible degrees of freedom are limited to the accelerator and brake pedals and the steering angle. Looking at a vehicle with a manual transmission, a further degree of freedom has to be considered. The driver now has a direct influence on the shifting behaviour and the speed level, which multiplies the workload of the developers.
Although the driving behaviour of a driver controller has an influence on the shifting behaviour even when an automatic transmission is used, it can be seen as reproducible and deterministic. An adaptive transmission control uses standard operating elements such as: accelerator pedal, brake and steering, as it is the case with the adaptive Shifting strategy (ASIS) developed by ZF. [23] [10] [91]

When taking a closer look at the first tip-in in figure 5.1, it can be seen that driver controller 1, which is realized by a proportional–integral–derivative (PID) controller, has a very high accelerator pedal gradient of up to 2250 %/s. This high gradient cannot be achieved in practical terms and should therefore be regarded as unrepresentative. An overshoot can also be noticed. Overall, such a behaviour leads to a deviating gear selection when considering a reproduction of a trip and has a negative effect on the emission formation due to the deviating engine conditions. If the required engine power is increased as in the succeeding tip-ins, the overshoot behaviour of driver controller 1 is reduced.
If, on the other hand, driver controller 2 is taken into consideration, it can be seen that the accelerator pedal value gradients are generally lower and comparable with those of the trained chassis dynamometer driver. On the other hand, increasing the necessary engine load leads to high overshoots. The lower part of figure 5.1 shows the engine torque. The curve of the engine torque clearly corresponds to the overshoot behaviour of the accelerator pedal value. In addition to the gear shift behaviour, the torque build-up also has a large influence on the emission formation [84] and is therefore an important criteria for the analysis of driver controllers.

Figure 5.3 shows both the reproducibility of driver controllers and their inhuman behaviour patterns which can result from incorrect parametrization. In the upper part of the figure the speed profile of all three tests is shown. The tests are based on the same speed profile target curve as in Figure 5.1.
The response behaviour of the two driver controllers is very well reproducible as figure 5.2 shows. The load actuator behaviour and the torque curve are very well comparable. The prerequisite for exact reproduction under varying boundary conditions is thus created. The trained chassis

dynamometer driver, on the other hand, is characterised by stochastic deviations from his normal behaviour. A delayed load increase in the second acceleration increases the load level in the first part of the acceleration to a higher level to compensate the delay. As expected, the response times of driver controllers with the exception of negligible latencies are the exact same. This ensures very good reproducibility when repeating test drives. However, it does not reflect the behaviour patterns of real drivers. The stochastic behaviour of the trained chassis dynamometer driver would be reflected in an even stronger form when looking at customer driving behaviour.

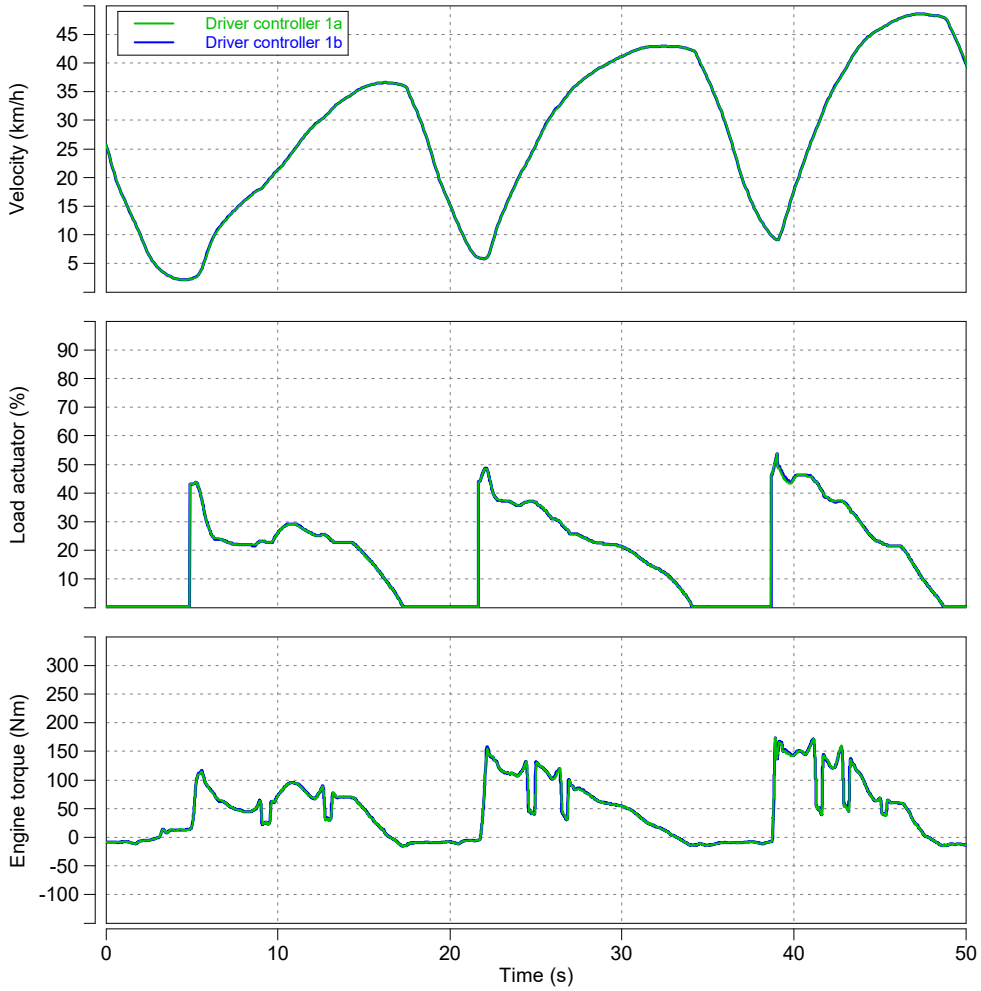

Figure 5.2: Comparison of two consecutive cycles performed with driver controller 1

Figure 5.3 also shows the different control characteristics of different driver controllers. In this example, driver controller 2 is characterized by load actuator gradients comparable to those of the human driver and high overshoots of low frequency. These can occur if the reset time of a selected PID controller is too low. Driver controller 1, as seen in figure 5.1, is characterized by very high load actuator gradients. As already shown in figure 5.1, the overshoot behaviour varies with load. In this case, the load is high enough to prevent overshoot. In addition, the absolute value of the accelerator pedal of driver controller 1 is superimposed by a harmonic of

0.5 Hz. A detail section (figure 5.3 right) shows that this harmonic is superimposed by another one with 133 Hz. These two harmonics have an effect on the engine torque and should therefore be avoided.

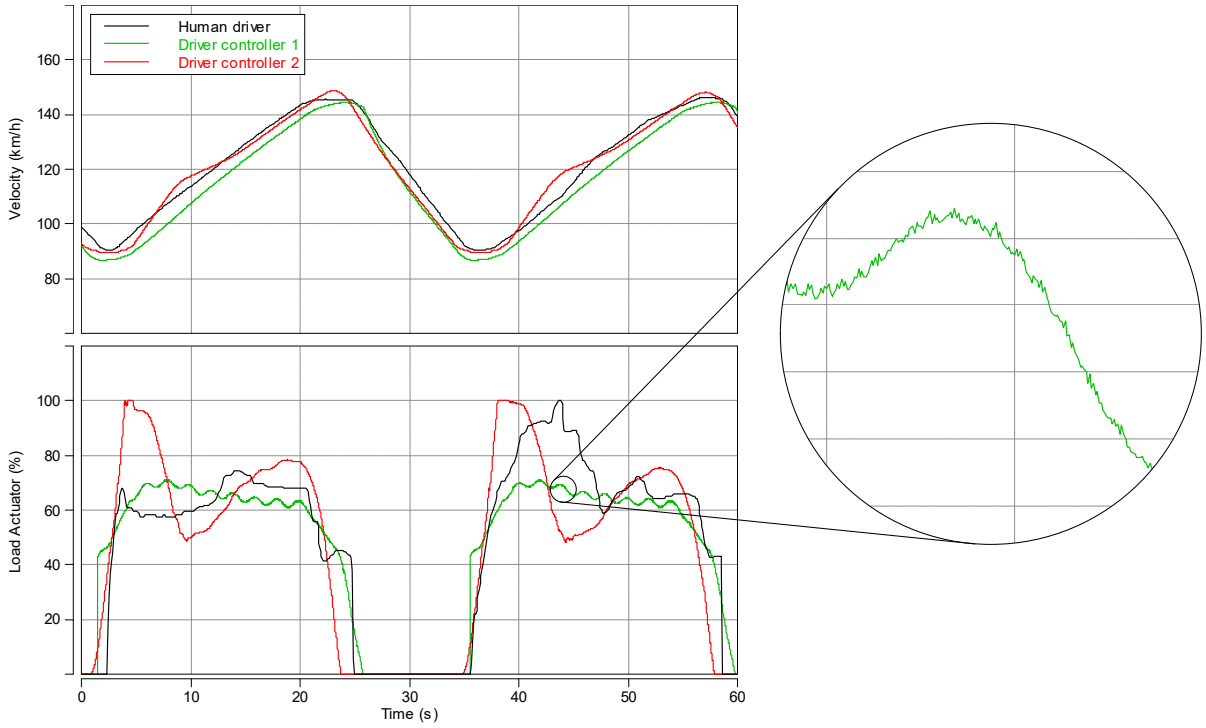

Figure 5.3: Comparison of two different driver controllers with a human driver with regard to the response behaviour to setpoint changes

Another characteristic of driver controls worth mentioning is the tolerance range. Figure 5.4 shows an exemplary comparison of an acceleration followed by a section of constant braking. The lower part of the figure shows the load actuator and the brake torque, respectively. The aforementioned overshoot of the driver controller's target speed change response can also be noticed in this example. This results in a positive deviation from the setpoint during the acceleration phase. In the deceleration phase, the driver controller adjusts to the lower tolerance limit. When the tolerance range is exceeded, an undesirable effect may occur, which must be prevented when designing the controller: The driver controller not only reacts to exceeding the tolerated range by releasing the brake pedal, but also actively counteracts it with a tip-in during the deceleration phase, where a partial release of the brake pedal would be sufficient. Once the target speed has been reached, the driver controller regulates again with its normal behaviour and is approaching to the lower tolerance limit.
The idle phases, which are visible in the speed curve of the driver controller are caused by the residual bus simulation and do not correspond with reality. In the actual speed curve, which also represents the controlled variable, there are no standstill phases.

There are two different objectives with regard to this issue: Reproducing a real trip and replacing a real trip based on a HiL concept. The reproduction of a real trip represents a much more complex problem. On the one hand, the tolerances must be kept very low in order not to lose any important details of the speed curve, on the other hand, however, the behaviour of the driver controller must not be influenced negatively. In the case of the distance-based speed profile of a virtual RDE trip, the tolerance range may be much wider in order to give the driver controller a certain degree of freedom. In any case, however, special attention should be paid to effectively preventing unwanted behaviour by leaving the tolerated range of speed. An additional uncertainty can be caused by an inaccurate road load, which is necessary for a specified velocity and is described in more detail in Section 5.3.

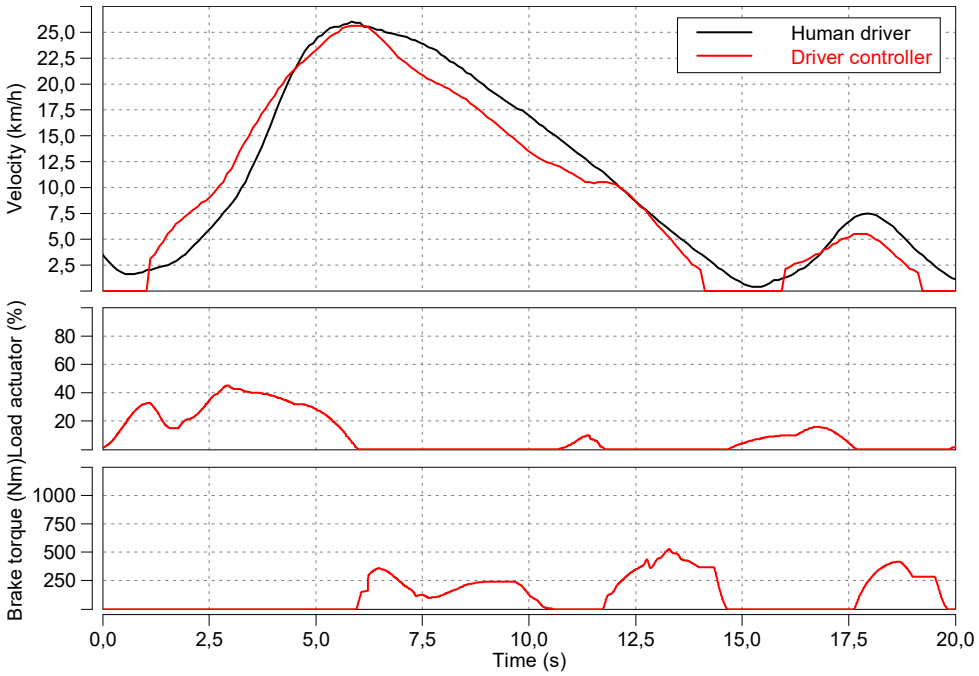

Figure 5.4: Example of the tolerance range of a virtual driver's speed and the driver's reaction if the tolerance range is exceeded

5.2 Engine Operating Condition

In the further course, the reproduction of emission-influencing engine conditions and engine internal measures will be analyzed with a focus on the reproduction of a real driving trip.
In order to keep the emission pattern as realistic as possible, care must be taken to ensure that both the driver and the engine behave realistically. Figure 5.5 shows the cumulative NO_x emission result of a fractional experiment. In order to achieve comparability, the emissions at time t = 100 s were set to equal to exclude the deviating emissions of the first acceleration of the day. The two emission curves of the measurement on the chassis dynamometer (black) and the

measurement on the powertrain test bench (green) tend to match very well, although constant volume sampling (CVS) is used for chassis dynamometer measurement and exhaust measurement system (AMA) for engine test bench measurement. During regular engine operation, the injectors are always activated at an engine speed of greater than 0, except for coasting cutout, engine speed at speed limiter, ignition faults, and by diagnosis cut-out for the actuator diagnosis. Furthermore, there are several digital motor electronics (DME) functions that prevent the overrun cut-off. Reasons for prevention can be time or temperature conditions, for example. After the overrun cut-off, increased NO_x emissions are to be expected due to the unfavourable conversion rate of the catalytic converter with increasing air-fuel ratio when a Turbocharging Valvetronic Direct Injection (TVID) combustion method is used. Some plane areas can be seen in the course, which can be associated with the overrun fuel cutoff shown in the bottom part.

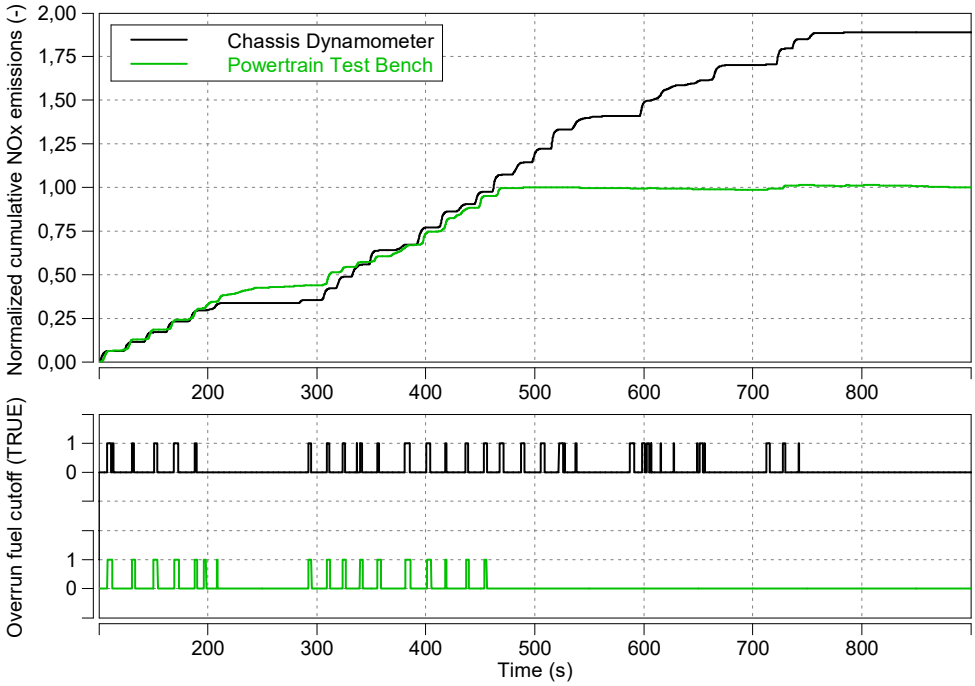

Figure 5.5: Comparison of NO_x emissions related to overrun fuel cutoff

In this case, again, a distinction must be made between the two different objectives of reproducing a real trip and replacing a real trip, for example using an EiL test bench. When reproducing a real trip, two different approaches can be followed to exactly reproduce these emission-critical events. The systematic reproduction of the engine conditions can be seen as very useful in this context, as it reproduces a certain behaviour. A much more accurate way is to enforce the events specifically by interacting with the DME. This ensures that these events occur and take place at the right time. However, as the triggering of these events was possibly based on a certain history during the real trip, it must be assumed that a targeted stimulation of the desired event may not result in the same outcome.

In the case of the measurement depicted in figure 5.5, the suspension of the overrun cutoff was caused by a temperature limit that was reached about five minutes later during the real trip. Even before that, deviations from the real drive can be observed within the range of 200 s, which are noticeable in an increased NO_x level in the area that follows. This exact reproduction of the engine conditions requires special attention.

It becomes more difficult if an attempt is made to precisely adjust the engine states at the beginning of a measurement. As aforementioned, the NO_x emission levels in figure 5.5 are set to equal in order to achieve comparability. Figure 5.6 shows the first standing start of the day of two consecutive measurements with a duration of each measurement of about 30 min.
In fact, this represents the second and third measurement of a measurement series of three measurements to ensure the same history of events and thus the same initial temperature conditions. The long duration of the individual measurements ensures that initial conditions remain consistent. Although all temperature deviations were reduced to a minimum, the engine was at normal operating temperature and the measurements are very well comparable regarding to the relevant engine parameters, the second measurement (red) shows a 45 % increase in NO_x emissions during the first five seconds. The outcome of highly deviating emission results of the first driving menoeuvre of the day was confirmed by numerous measurement results and continues to strongly increase with deviating parameters.

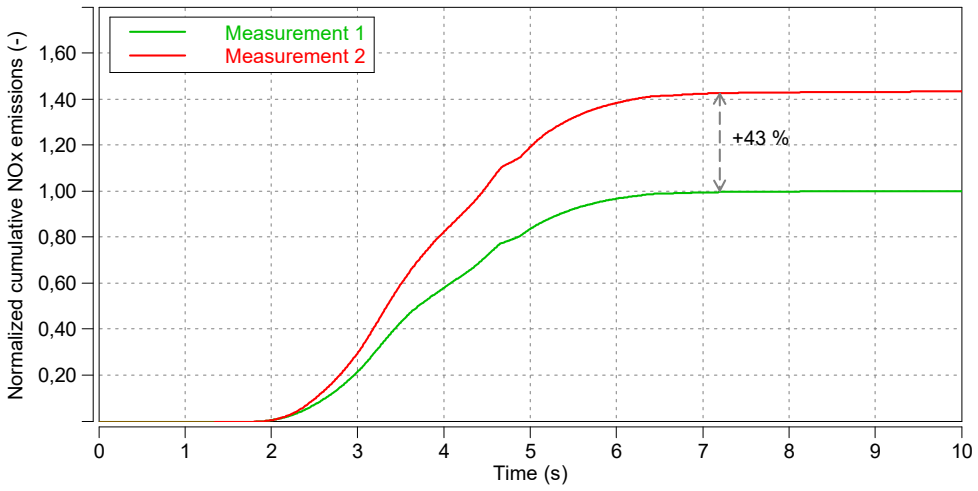

Figure 5.6: Comparison of NO_x emissions related to the engine's initial conditions of the test run

Although the equalization of emissions used in figure 5.5 ensures that measurement results of longer measurements are better comparable, it only excludes the deviations of the first manoeuvre of a day instead of correcting them. The emissions shown in figure 5.6 are tailpipe emissions, so the measurement results contain one more interfering variable: The deviation associated with the measurement results is certainly closely related to the exhaust aftertreatment, so that it can be assumed that the engine out NO_x emissions show a smaller deviation. Measurements of cold

start emissions show even higher deviations at this point. Here, the initial conditions of the engine and the exhaust aftertreatment are even more difficult to match.

In addition to the different driving styles mentioned before, the engine conditions play an important role as factors influencing emissions. Both emission-critical functions of the DME and engine conditions are of great importance in RDE relevant development use cases. In some cases it may be useful to enforce the desired engine behaviour, but in most cases it is more advisable to bring the test carrier into exactly the same state through the same sequence of events, so that the desired behaviour is initiated by the test carrier itself.

5.3 Evaluation of Road Load Parameters and Potential Enhancements

A key element of the transfer of experiments into the test environment is to correctly reflect the road load. In the conventional definition, the driving resistance consists of the three essential components of rolling, aerodynamic and acceleration resistance, as it is shown in the equations 5.1 and 5.2.
A distinction shall be made between two ways of determining driving resistances: The calculation using standard parameters or coast down parameters as it described in the equations 5.1 and 5.2, respectively. If the standard parameters are used, the individual determining variables are used for the calculation. The advantage is that individual values can be adjusted without influencing other values. It is possible, for example, to replace the wheel and therefore the rolling resistance of the virtual test carrier. The second variant is more accurate because the coast down parameters are determined by road tests. Therefore, they represent the driving resistance of a specific vehicle. Changes of individual components are not possible when using this method. [16] [73] [68]

Equation to determine the driving resistance using standard parameters:

$$\begin{aligned} F_{\text{road load}} &= F_{\text{rolling}} + F_{\text{aerodynamic drag}} + F_{\text{acceleration}} \\ F_{\text{road load}} &= f_{\text{rolling}} * m * g + \frac{1}{2} * \rho * A * c_{\text{w}} * v^2 + \frac{dv}{dt} * m \end{aligned} \tag{5.1}$$

Equation to determine the driving resistance using coast down parameters:

$$\begin{aligned} F_{\text{road load}} &= F_{\text{rolling}} + F_{\text{aerodynamic drag}} + F_{\text{acceleration}} \\ F_{\text{road load}} &= F_0 + F_1 * v + F_2 * v^2 + \frac{dv}{dt} * m \end{aligned} \tag{5.2}$$

The differences between these two options are the determination of rolling and aerodynamic resistances. These are combined in the calculation using coast down parameters. F_0 thereby

predominantly represents the effects of rolling resistance, F_1 includes the dependence of rolling resistance on velocity and drivetrain losses and F_2 includes the aerodynamic drag, which is represented by the air density (ρ), cross section area (A) and the drag coefficient (c_w). [2] The discussed driving resistance is a simplified way to represent the driving resistance on a plain road without other influences. With the aim of extending the considered driving resistances, further components must be considered and their feasibility must be tested. Additional driving resistances have to be considered, especially for the reproduction of real driving trips and virtual driving as a replacement for real driving trips.

Equation to determine an extended driving resistance approach:

$$\begin{aligned} F_{\text{road load}} &= F_{\text{rolling}} + F_{\text{swell}} + F_{\text{bearing}} + F_{\text{residual brake}} + F_{\text{toe-in angle}} + F_{\text{aerodynamic drag}} \\ &\quad + F_{\text{inclination}} + F_{\text{cornering}} + F_{\text{rotational}} + F_{\text{acceleration}} \end{aligned} \tag{5.3}$$

The equations 5.3 show an approach that extends the conventional components of the driving resistance by additional components. In addition to the rolling resistance, the swelling and the bearing resistance are also taken into account in this calculation. A residual brake resistance and a toe-in resistance are also listed. According to Bernhardt et al. [15], the bearing, residual brake and toe-in angle resistances are negligible. Therefore, and due to the fact that those resistances can be partially taken into account by using the coast down parameters, they are excluded from the further course. Since the swell resistance is only relevant when the road is wet, no further consideration is made in this thesis. The mentioned rotational proportion of the acceleration resistance has to be determined as a function of the gear. Mitschke [73] describes the exact determination and a generally valid simplification towards a rotational mass factor, which will not be considered further. The remaining additional driving resistances considered in more detail in this thesis are therefore the inclination and cornering resistance. Equation 5.4 indicates the driving resistance equation to be considered.

Equation of the considered driving resistances in the context of this work:

$$F_{\text{road load}} = F_{\text{rolling}} + F_{\text{aerodynamic drag}} + F_{\text{inclination}} + F_{\text{cornering}} + F_{\text{acceleration}} \tag{5.4}$$

Within the scope of the work, coast down experiments were carried out to verify the validity of the coast down coefficients determined for the WLTC type approval and to specify possible deviations. In order to obtain a valuable result, four tests were carried out, two of them in each driving direction.
Figure 5.7 shows the velocity and the resulting acceleration curves of the two measurements over the time in the upper part, and the calculated coast down forces due to the test mass over the velocity of the vehicle in the bottom part. The measurements were not carried out until standstill, but were aborted at low speeds. A deviation due to the test conditions is to be

recognized. This deviation is caused either by an inclination in the course of the road or by the influence of wind.

In order to obtain a usable curve of the vehicle acceleration, the speed data were filtered. The two velocity curves of the same direction are averaged and smoothed by a low-pass filter. A finite impulse response filter (FIR) with a cut-off frequency of 0.5 Hz is used. This filter is characterized by an effective damping of 6 dB at the cut-off frequency. In a further step, the velocity signal is smoothed by a moving average trend curve which operates over 1000 unweighed measuring points. With a resolution of 100 Hz, this equals a period of 10 s. The coast down force calculated based on the acceleration curve is plotted in the lower part of the figure.

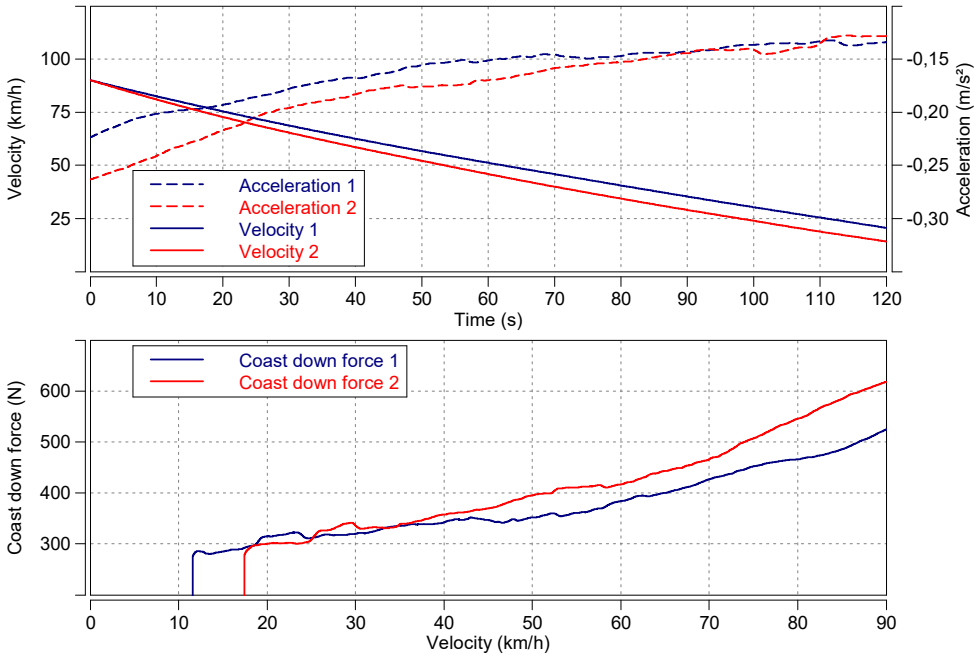

Figure 5.7: Results of a coast down test to validate the reference values

For a comparison with the data provided by the type approval, the two force curves shall be processed using the least squares method as it shall be done for type approval. Figure 5.8 shows a comparison of both measured curves (blue) processed with the least squares method and the curve provided by the WLTC type approval (red).

The course of the curves shows that the results of the experiments tend to show a lower driving resistance than expected. Without knowledge of the actual road conditions, only assumptions about the underlying reasons can be made at this point. Additionally, the driving tests were only carried out up to a speed of 100 km/h. Therefore, the high speed range is only an extrapolation of the given measurement data and must therefore be considered accordingly. As the two opposite routes do not represent the same roadway, but are adjacent to each other, a falsification of the

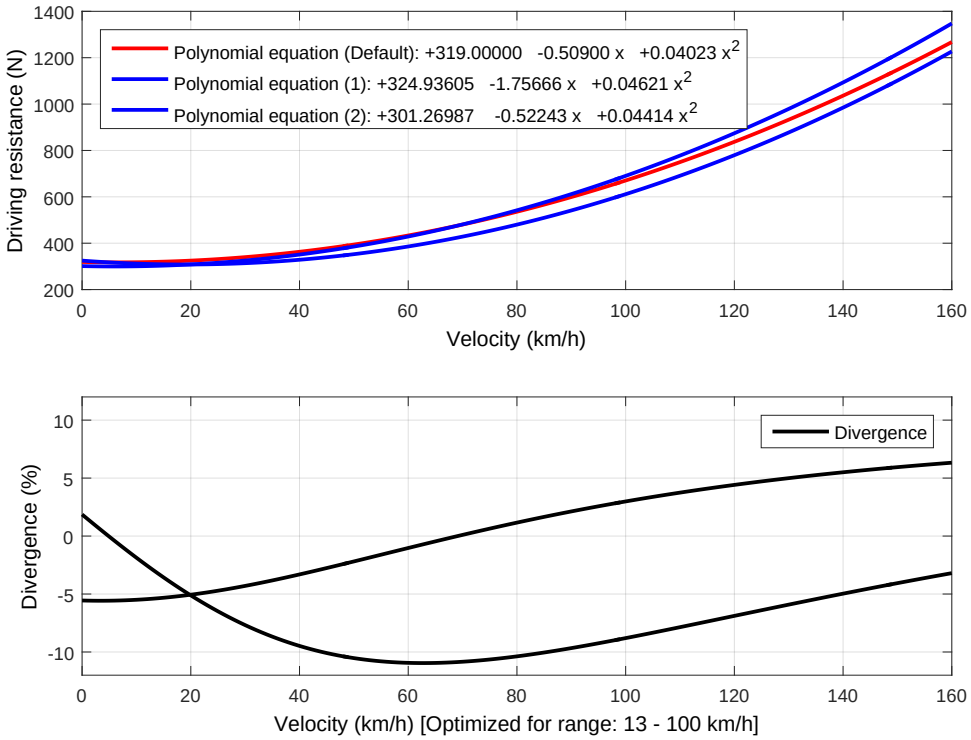

Figure 5.8: Evaluation of the results of the coast down experiment and comparison with parameters to be used during WLTC type approval

expected results due to inclination influences cannot be excluded. Another factor to consider when evaluating coast down experiments is the influence of wind. A steady and locally not changing wind influence should also have a similarly steady effect on the resistance curves. Opposed driving experiments should therefore be characterized by a more or less constant offset. The ambient structure of the area can have a significant influence on local wind speeds and directions [88].
Due to the fact that the average deviations in the speed range covered by the coast down tests are mostly negative, a constantly lower driving resistance can be assumed. This can be caused, for example, by increased tyre pressure. This influence becomes less significant with increasing speed, because the proportion of the air resistance is included with the square of velocity in the aerodynamic driving resistance. This possible deviation correlates positively with what results from the measurements and is therefore a probable explanation for the deviations.

In some cases it may be necessary to adapt the given coast down coefficients. Some vehicle models may not cover certain value ranges. Specific vehicle characteristics, for example, result in the speed-dependent coefficient of the parameters becoming negative. An example of the described problem is the handling of the coast down parameters by CarMaker by IPG. This software is used for the entire virtualization of a vehicle and is used in EiL test bench environments. CarMaker internally exclusively uses standard parameter settings. CarMaker also provides a tool to convert coast down parameter settings due to virtual coast down experiments

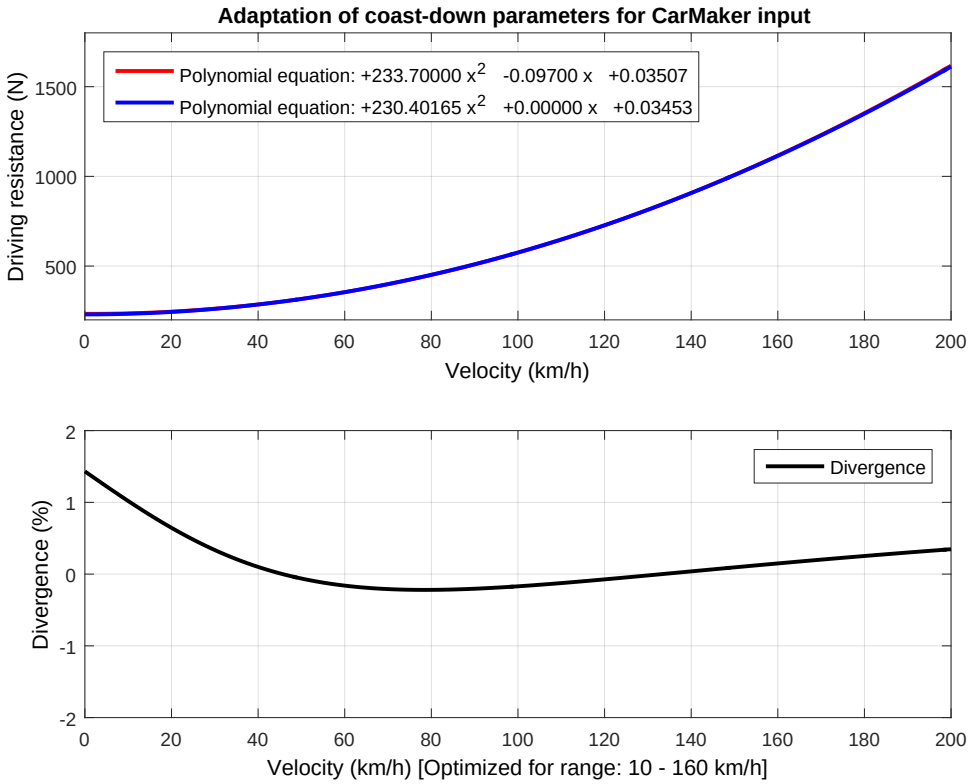

Figure 5.9: Polynomial function for CarMaker input resulting from coast-down adaptation

into standard parameter settings. The tool does not tolerate negative coefficients because the tire model cannot handle them. It is therefore necessary to convert the parameters beforehand. Figure 5.9 shows the conversion of the coefficients based on the least squares method, which was developed as a Matlab script in the context of this work.

It is possible to set certain requirements for the equation to be calculated when using the tool. The input of the tool consists of coast down coefficients that are translated to a resistance curve over the velocity. Due to the expected deviations of the calculated curve from the input, the tool can optimize the calculation for a predefined speed range to improve the result. For the presented example, the deviation in the optimized range is consistently less than 1 %. This deviation does not pose a major problem for a good reproduction, but is additionally added to the possible deviations associated with 5.8.

In conjunction with equation 5.4, possible deviations due to imprecise reflection of parameter sets for determining rolling and aerodynamic drag resistance are thus identified. In the following, the inclination and cornering resistances will be discussed in more detail. These factors effectively turn a straight and plane course into a real route for both during the reproduction of a real trip and during the virtualization of a possible type approval trip.
To give an example of the importance, the inclination resistance of a 10 % grade of a current BMW 5 Series is approximately equal to the driving resistance of a constant speed driving of

220 km/h. As the inclination resistance has a very large influence on the total driving resistance which leads to a high load increase in certain situations, the implementability of an inclination input for test bench measurements based on measured data is examined in more detail below. Figure 5.10 gives an example of the possible deviations of the total driving resistance due to an inclination.

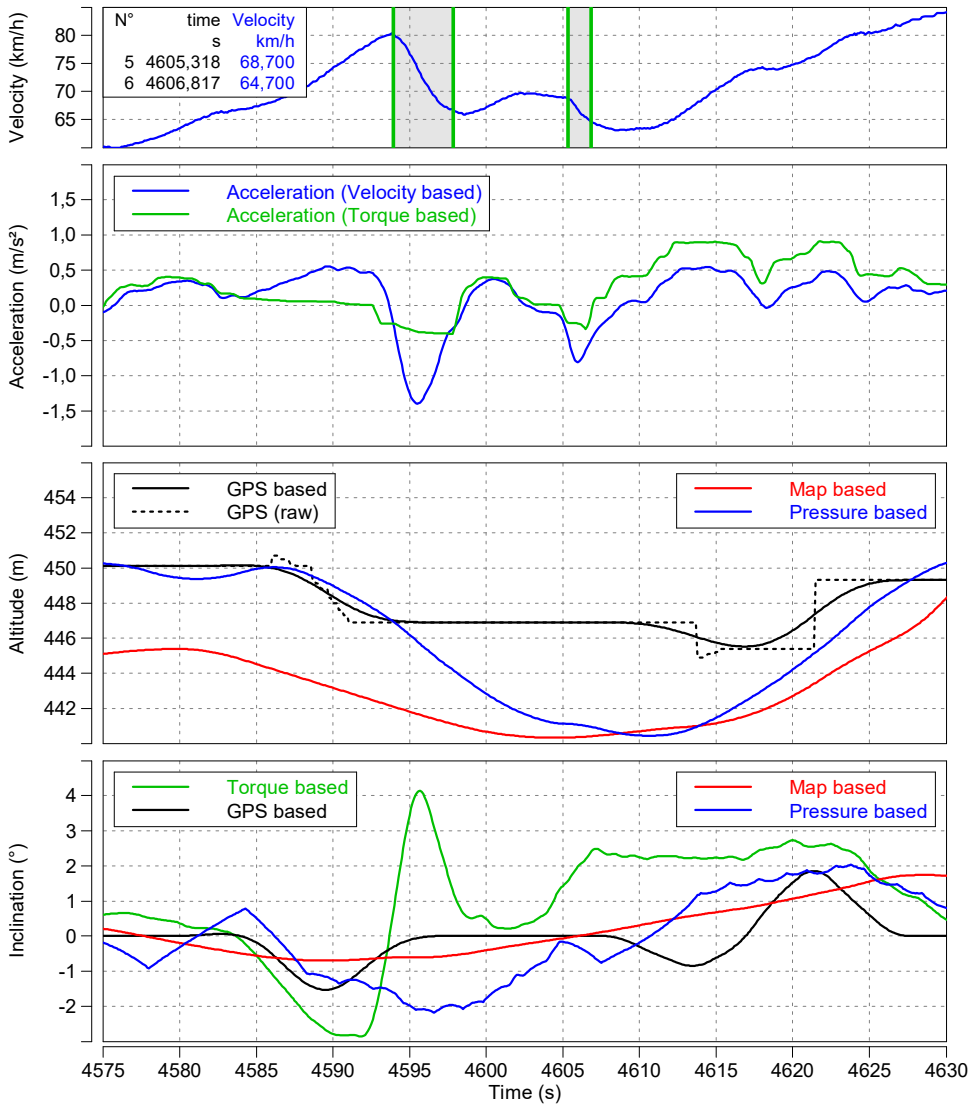

Figure 5.10: Comparison and plausibility check of different altitude data for the implementation of inclination data

In the upper part of figure 5.10, there is the measured speed profile of a section of an on-road trip. The section of the graph below the speed profile depicts the real vehicle acceleration as a derivative of the vehicle speed (blue) and, in addition, the theoretical acceleration calculated on the basis of the wheel torque on a plane track (green). In the speed profile, the sections where the vehicle decelerates using the brake are marked using band-cursor. Within the marked areas, the wheel torque cannot be used to determine the theoretical acceleration due to the fact that

the braking forces are not taken into account there. However, during acceleration phases of low dynamics, this calculated acceleration delivers a very precise result with deviations less than 0.1 m/s^2.

Before the first deceleration, the calculated acceleration is significantly lower the actual vehicle acceleration. After the second deceleration, however, the calculated acceleration is significantly higher over a long period than the actual vehicle acceleration. Considering the three altitude profiles arranged below, each one from a different source, this correlates with the acceleration deviations depicted above. During this section, a negative inclination followed by a positive inclination is to be expected. However, if one compares the three different altitude profiles, it is noticeable that they result in differently strong inclinations, and also have a time shift to each other.

Since the inclination resistance changes tremendously over time, it is very important for the reproducibility to map this correctly with regard to time. Looking at the altitude profile resulting from the GPS measurement (black dotted line), it can be clearly seen that this is characterized by a discontinuous change. It is therefore necessary to filter the signal as it is the case with the black line. It can also be assumed that these discontinuous changes may have a variable offset to each other and thus no unequivocal allocation of such a discontinuous change to an exact location is possible. As described in section 2.2.2, the GPS altitude signal is used in type approval as the basis for determining the cumulated elevation curve. The necessary filtering of the raw signal can be used as a basis for a filter for the inclination calculation.

Looking at the map based elevation signal obtained from topographic altitude data (that is freely available) using the recorded route, a much smoother height profile can be obtained. Due to its characteristics, this signal only needs to be filtered in certain areas.

Another way to directly generate the elevation profile from a vehicle's measurement data is to calculate it based on the ambient pressure. The pressure sensor installed in the vehicle for injection quantity adaptation has a sufficiently high accuracy to determine an altitude difference of less than 1 m. Moreover, at first glance there is no significant dependence on other variables such as speed. The concern that speed-dependent dynamic pressure will have a major impact on the quality of the signal remains unsubstantiated. The reliability of these signals is also demonstrated by the study of their use for indoor positioning in high-rise buildings as studied by Retscher [86].

To determine the height difference and thus the inclination data, the barometric altitude calculation formula can be applied. According to ISA [81], the terrestrial atmosphere can be divided into layers with linear temperature distribution. Through various approaches for simplification,

Grigorie et al. [48] achieve a purely pressure-based formula for evaluating the pressure based altitude data (equation 5.5). Due to the simplifications, this formula is not suitable for determining the absolute altitude without any doubt. This requires the inclusion of the temperature and the day-dependent deviation from the atmospheric normal pressure. The offset of the calculation from figure 5.10 was compensated by eliminating the offset.

Calculation to determine the barometric altitude (H) based on the absolute pressure (p):

$$H = 44330.76923 * (1 - \frac{p}{760}^{0.190263}) \tag{5.5}$$

The bottom part of figure 5.10 represents the inclination values of the different altitude sources in addition to the calculated inclination based on the deviation between the wheel torque based acceleration and the speed derivative acceleration. The data show that the inclination data correlate very well in certain situations, but on the other hand sometimes show very large deviations from each other. Within the scope of the present work, the various height data were examined for plausibility and in some cases large deviations were detected. The inclusion of the map based data can be omitted under the condition that a combination of the data measured during the vehicle measurement (GPS altitude and ambient pressure) provides an equally accurate result.
In addition, the wheel torque can partly be used to verify the plausibility of the outcomes. Figure 5.11 shows another possibility to improve the inclination data using the measured data.

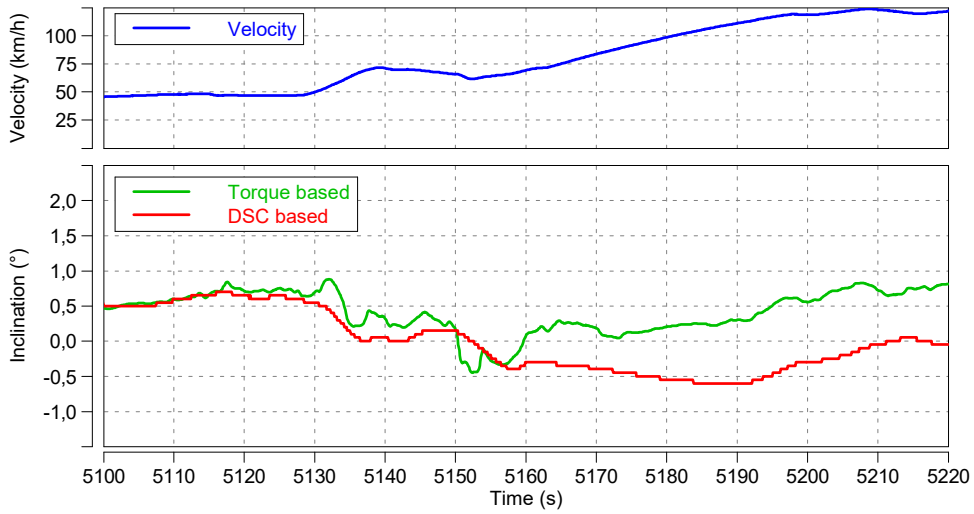

Figure 5.11: Comparison torque based and dynamic stability control (DSC) based inclination data

The upper part of figure 5.11 shows the velocity profile which the torque based inclination data (green) of the bottom part is based on. The additional signal (red) is DSC based and determines an inclination signal based on the combination of different sensor signals and calculated quantities based on the combination of an acceleration sensor with a corresponding evaluation unit

for arithmetically determining the slope of a signal of the acceleration sensor [52]. A comparison of the two signals shows a good matching in the first part. After the short more dynamic part, the two signals drift apart so that the DSC signal indicates a negative inclination and the torque-based signal indicates a positive inclination.

As it is important to avoid exactly these errors when implementing an inclination signal into the reproduction of real trips on the EiL test bench, the data must be plausibilised so that it is guaranteed that no opposing load correction is made. A solution approach can be to include only the plausibilised proportions in order to keep the imprinted error as low as possible and thereby achieve an improvement in the representation of load maxima. In addition to the three different altitude signals, there are thus at least two measured variables of the DME available which enable the plausibility check of the respective signals.

Based on the aforementioned considerations for the implementation of the inclination data, the knowledge gained can be applied to the implementation of the cornering resistance, as well. In this case, it is also suitable to use acceleration data from the DSC sensors. Current versions of the DSC are equipped with a combined sensor to determine the longitudinal and lateral acceleration and the yaw rate in the centre of gravity of the vehicle [87]. If these signals are not available, it is also possible to determine the data from the vehicle speed and from the steering angle. Figure 5.12 shows the comparison of the torque based longitudinal acceleration of the vehicle with the actual acceleration determined by the vehicle's speed. The bottom part of the figure indicates the lateral acceleration provided by the sensor data.

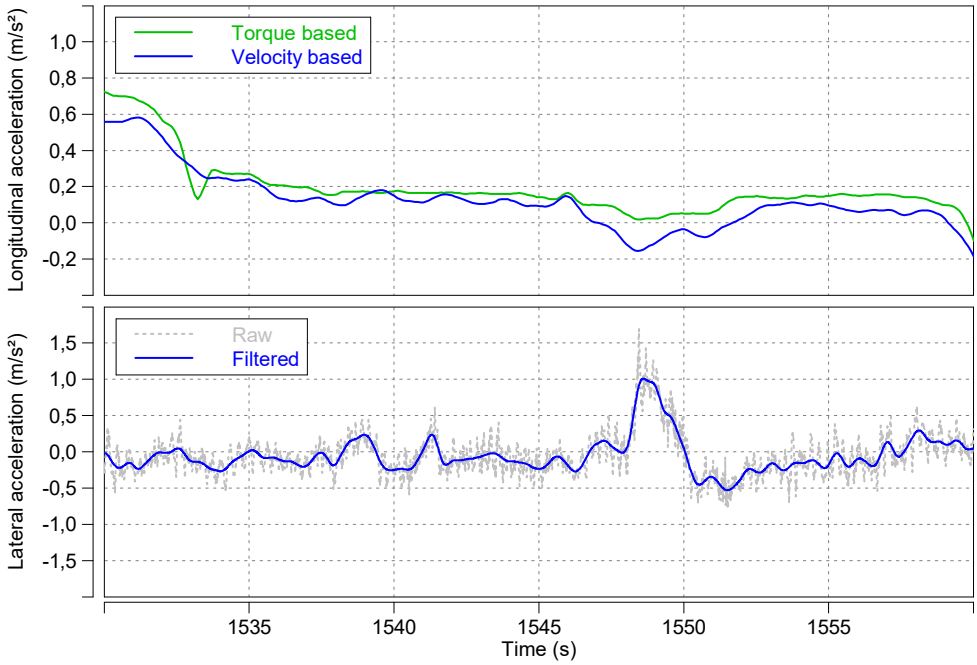

Figure 5.12: Longitudinal acceleration divergence caused by a lateral acceleration

From these signals a clear interrelation of these two quantities can be seen. Although the deviation caused by the lateral acceleration is comparatively small, its determination and thus its implementability is much easier than that of the inclination resistance. A consideration of the resulting driving resistance is to be contemplated if the lateral acceleration is 0.4 g or higher [15]. By simulating cornering with a lateral acceleration of 0.4 g at 30 km/h, Hirano et al. [51] show that the driving resistance approximately doubles. In fact, a value significantly smaller than 0.4 g is detectable by a deviating power demand. By some simplifications, assumptions and the use of geometric relations of the vehicle, a formula for the determination of the curve resistance can be established.

Simplified equation for determining the cornering resistance [73]:

$$F_{\text{cornering}} = m * \frac{v^2}{r} * sin(\alpha_{\text{f}}) \tag{5.6}$$

Equation 5.6 shows the simplified calculation of the cornering resistance dependent on the lateral acceleration and the slip angle. To simplify, it is assumed here that the distance of the front axle and the distance of the rear axle to the centre of gravity of the vehicle are identical. The vehicle thus has an optimum weight distribution. Otherwise, the slip angles (α) of both axles must be taken into account to calculate the additional resistance. The slip angle can be determined on the basis of a characteristic map or modelled using a tyre simulation model. Additional dependencies are given by mass (m), vehicle speed (v) and circular radius (r).

In summary, it can be stated that the implementation of additional driving resistances is associated with hurdles, but a precise implementation provides a quality improvement for the simulation of real driving resistances. Especially with regard to RDE emissions, a realistic road load is an important factor for the representation of realistic thermal conditions. These in turn bring improvements with regard to the specific reproduction of the previously discussed engine conditions and the associated emission events they cause.
With reference to the test bench selection tool developed as part of this work, which was presented in section 3.4, the results discussed in the present section can be considered as possible input for the tool. In case of necessity, this can provide a clear overview of the current possibilities in the test environment.

5.4 Test Bench Conditioning

The various test bench categories presented in section 3.3 are equipped with complex conditioning units, some of which differ considerably from each other. This section outlines the differences between the individual systems as well as the gap between the real vehicle and the test bench environment.

Depending on the development objective, the requirements of the experiments with regard to test bench conditioning vary greatly. While, for example, heat balance tests aim to achieve temperatures that are as constant as possible with deviations of less than 0.3 K, it is recommended in terms of RDE to reflect changing vehicle temperatures as closely as possible. In order to be able to transfer the RDE development tasks to the test environment, it must therefore be possible both to map realistic temperature curves in the test field and to reproduce them specifically from vehicle measurements.

The focus of this work is placed both on charge air temperature and on coolant temperature, which, depending on the conditioning system and operating mode, can deviate significantly from the actual vehicle characteristics. Based on the measurements described in section 4.2, supplemented by further measurements, the following conclusions were obtained.

With regard to charge air cooling, the real vehicle differs from a typical test bed structure in that the test bed is equipped with a very large and sluggish conditioning system. The vehicle system can differ, depending on the conceptual design of the specific engine. The first and significantly more simple variant is the direct cooling of charge air via an air-to-air intercooler before routing the charge air via the throttle valve into the intake manifold. A more complex but significantly more powerful system is indirect charge air cooling. Heat is taken from the charge air by means of an air-to-coolant heat exchanger. This heat is then given off via a second coolant-to-air heat exchanger into the ambient air. It is characterized by a more stable charge air temperature caused by the extended heat capacity of the system.

A comparable system is also used in the conventional test bench setup. Within certain limits, the charge air can thus be regulated to a constant value during test operation. Due to the high-performance capability of these systems, they have a very high heat capacity and are therefore significantly more sluggish than comparable systems in the vehicle. Although it is possible to set a target value for dynamic operation, the occurring temperature curves differ considerably from the vehicle temperature curves. In most cases, these systems are therefore operated at a constant temperature. Figure 5.13 compares an identical speed profile reproduced on a chassis dynamometer and a powertrain test bench.

Both measurements start at comparable temperature levels. While the averaged curve of the measurement performed on the powertrain test bench is rather constant, the chassis dynamometer measurement shows a constant temperature drift during the test operation depending on the combination of heat input and heat dissipation. The vehicles system is characterized by a more or less constant heat dissipation. More precisely, the heat dissipation is strongly dependent on the temperature difference between the cooling air flow and the flowed-on heat exchanger and the speed of the cooling air flow. The system would stabilize at a load-specific temperature level

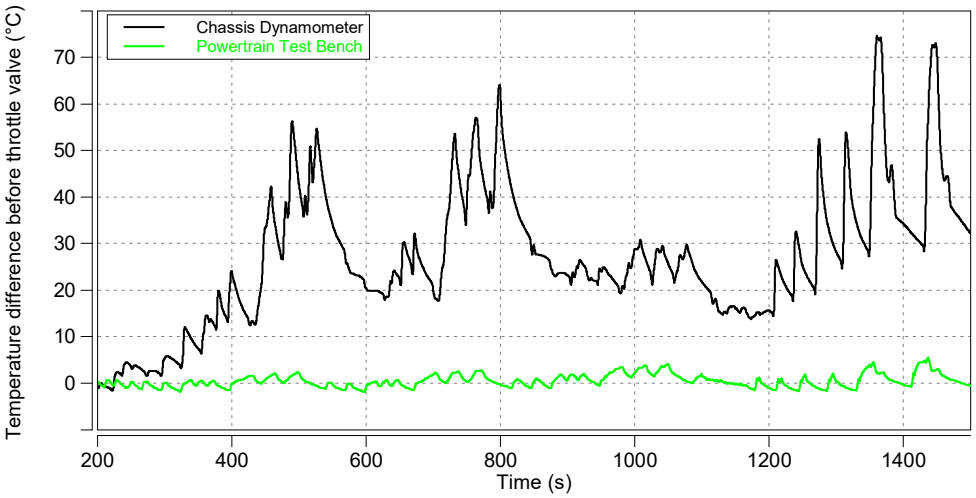

Figure 5.13: Comparison of charge air temperature of a vehicle and a test bench intercooling system

over a longer period of time. In case of the test bench system the heat dissipation is higher by orders of magnitude. The high heat capacity of the system and the high flow rate of the cooling medium ensure an almost constant temperature level. Even the high temperature peaks of the vehicle measurement are actively compensated by the test bench system.
The test bench control also allows a temperature target to be set, but since this is characterized by high latencies, it should not be used for dynamic measurements, as this control could further falsify the results or complicate the assignment of emission-relevant states.

In order to face this problem, the TU Darmstadt is carrying out tests on the use of the real charge air cooler in the test environment. [50] In this configuration, the intercooler is blown on by the test bench fan and can be extended by additional spots and water spraying systems. The enthalpy of the evaporation of the water ensures the high-performance capability of this system through specific reduction of the temperature. The identified differences represent an important issue for RDE emission development. Due to the ongoing investigations, a more in-depth analysis within the framework of this work is refrained from.

The temperature differences between the test bed and the vehicle with respect to the coolant temperature are within a comparable range. The test carrier used to perform the measurements is equipped with an advanced cooling concept. By means of an electrical valve a split cooling is realized to enable on-demand decoupling of the crankcase from the coolant flow both in the warm-up phase and in partial load operation. [12]. The engine operating temperature is reached more quickly and in partial load, the emissions are reduced significantly. The coolant supply for the cylinder head and the crankcase is controlled individually by the DME.

The control of the coolant flow and the temperature level is performed by the heat management module (HMM). The opening cross-sections of various coolant ducts can be opened or closed

individually. Figure 5.14 gives an overview of the possible operating strategies of the HMM. Table 5.1 gives the explanation of the highlighted areas. Basically, a distinction is made between the five operating modes: Cold start, warm-up phase, operating temperature, transition from normal operation to maximum cooling requirement and maximum cooling requirement. The diagram also seperates the three circuits of the cylinder head flow (3), the crankcase flow (2) and the heater circuit (1).

As in the case of charge air cooling, the test bench conditioning system has a much higher thermal mass compared to the vehicle. The system has a total capacity of approximately 20 - 25 liters of coolant and an additional total mass of over 100 kg of steel. In comparison, the vehicle configuration has a lower coolant volume and a high proportion of non-metallic parts with a lower heat capacity.

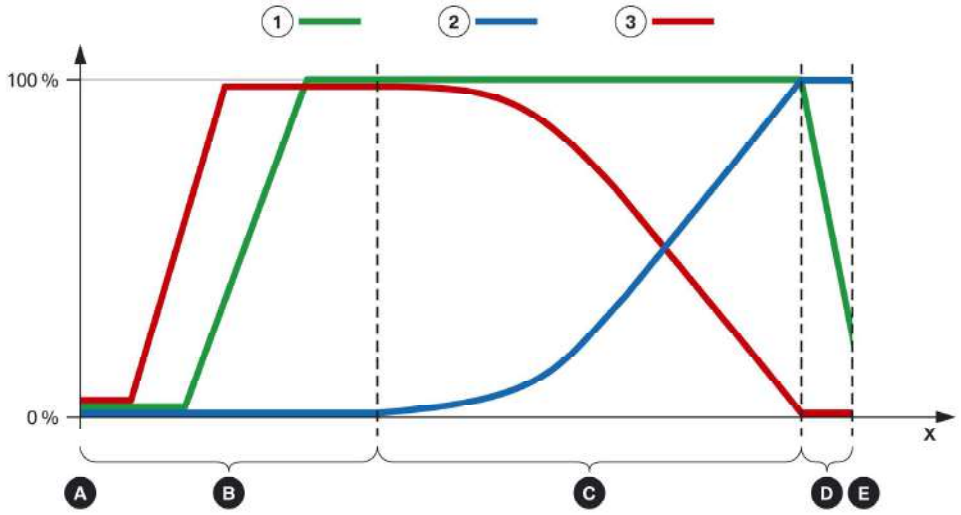

Figure 5.14: Switching diagram of the heat management module of a B38 TU engine [12]

Table 5.1: Index explanation of figure 5.14

Index	Explanation
0%	Rotary valve closed
100%	Rotary valve open
A	Cold start
B	Warm-up phase
C	Operating temperature
D	Transition from normal operation to maximum cooling requirement
E	Maximum cooling requirement
X	Rotational angle in angular degrees
1	Heater circuit
2	Main coolant circuit
3	Minor coolant circuit

The test bench conditioning system can be operated in four different ways. The easiest and most reproducible is to maintain a constant temperature. The high thermal mass of the system helps to reduce deviations to the target temperature.

Another way to regulate the coolant temperature is to use a data-map thermostat based target value of the conditioning system. This can be based on a real characteristics map as it is used in vehicle systems. An example is BMW's recognized map-controlled thermostat. In addition to the non-electrically operation with coolant temperatures between 105 °C and 120 °C, an electric heater in the thermostat is used to make the thermostat open already at a lower coolant temperature. [11] This system is capable of reproducing real vehicle temperatures. Due to the unchanged thermal mass of the total system, it is only in a limited way able to simulate the dynamics occurring in the vehicle.

A significant improvement of the system behaviour is achieved by using the temperature control used on the vehicle side. By controlling the coolant flow, a more realistic dynamic can be achieved.
In this case, the main deviation from the real vehicle is the heat exchanger outlet temperature. The system boundaries of the minor circuit are set correctly, but the main coolant circuit still deviates from the vehicle configuration. Due to the temperature deviations, an identical regulatory intervention results in a differing temperature change. A further improvement to minimize the dynamic volatility can be made by adjusting the heat exchanger outlet temperature to the maximum value possible.
This can be achieved by determining the maximum heat transfer of the engine into the coolant circuit. The resulting increase in temperature of the coolant when the engine is passed through is applied with a safety margin and results in the value to be adjusted.

Figure 5.15 illustrates the resulting temperatures when an identical speed profile is reproduced twice on the chassis dynamometer using the HMM and twice on the powertrain test bench using a constant target temperature. Both temperature curves of the respective measurements are well comparable with each other.
The temperature curves of the powertrain test bench show only the slightest deviations, due to the use of a driver controller that has a high reproducibility in its behaviour. The chassis dynamometer measurements were performed on different days by the same driver. Most of the temperature deviation is a result from differing load actuator position. The overall heat balance of the cooling system is therefore very well reproducible.

Figure 5.16 shows the same speed profile as it is used in figure 5.15, but reproduced with other test carriers. The measurements are performed on the chassis dynamometer and an engine test bench. For reproduction on the engine test bench, the torque-speed profile resulting from the

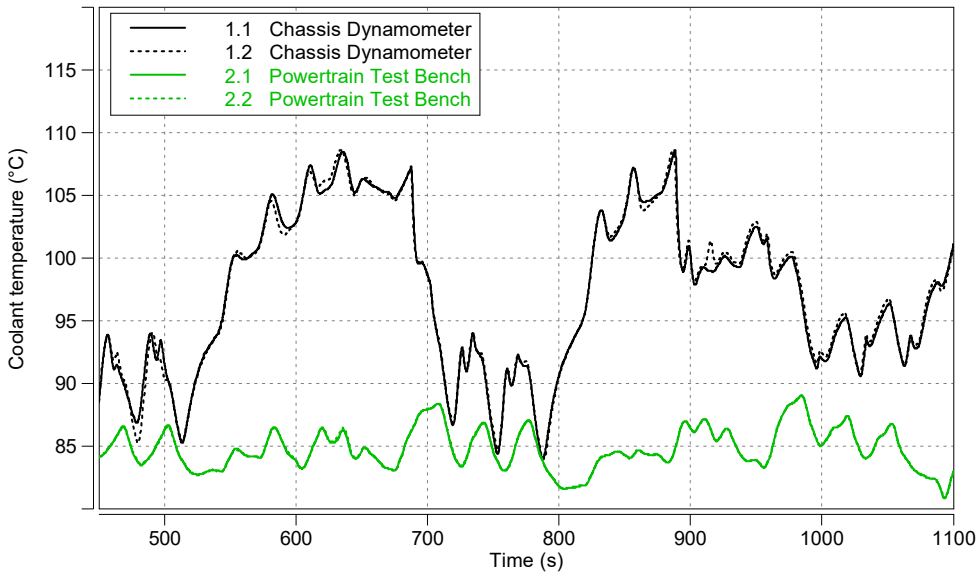

Figure 5.15: Comparison of coolant temperature of a vehicle on the chassis dynamometer and an engine test bench using a constant set-point temperature of the cooling system

chassis dynamometer measurement is used. Both measurements are performed using the vehicle's HMM.

In contrast to measurements 1.1 and 1.2, the two temperature curves are less comparable. The general temperature levels tend to be matched well, but the dynamic behaviour of the coolant temperature occurring on the engine test bench differs greatly from that of the real vehicle.

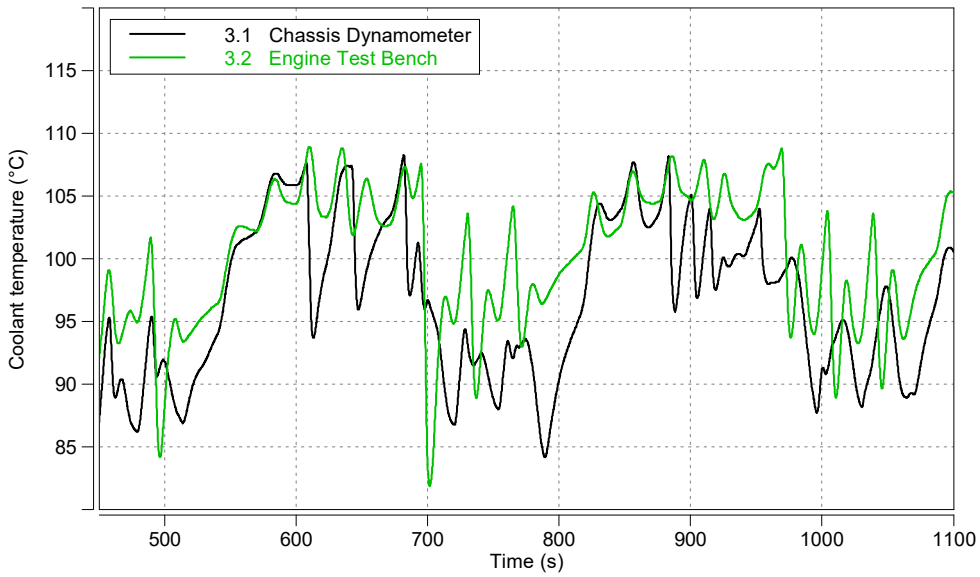

Figure 5.16: Comparison of coolant temperature of a vehicle on the chassis dynamometer and an engine test bench using the vehicle's heat management

To further improve the occurring temperature behaviour using test bench conditioning systems, the heat exchanger output temperature has to match with the vehicles temperature. Due to the test bench design, it is not possible to replicate the thermal mass and heat exchange with the environment of the vehicle system. At this point, a model approach that simulates both the thermal mass and the heat dissipation can contribute to a more accurate representation of a real vehicle behaviour.

In the case of a vehicle measurement run to be reproduced, the additional data obtained from the vehicle measurement, such as ambient pressure and temperature, weather conditions and vehicle speed, can be used to calculate the heat dissipation.

5.5 Performance of the Load Unit

Regarding the cases of section 3.4 describing the relevant driving manoeuvres for engine and powertrain test benches, the requirements to be considered for the electric machine are examined in more detail in the following. Figure 5.17 illustrates the platform types to be differentiated.

Configuration (a) of figure 5.17 refers to the conventional engine test bench and is classified by its direct coupling of the crankshaft with the electrical machine. The configuration of figure 5.17 (b) represents a powertrain test bench which is characterized by the interconnected gearbox. The following equations refer to an automatic transmission system. The mass moment of inertia of the gearbox refers to the test bench side and includes the torque converter.

The equations 5.7 describe the most important influencing factors to determine the maximum speed gradient that can be achieved during a shifting process. The static torque of the electrical machine corresponds with the engine torque in this configuration. The momentum of inertia is summed up to a total value. The effective torque, which causes a negative speed gradient, is therefore the electrical machine torque which is reduced by the engine torque.

Due to the torque intervention during the shifting process, the engine torque is reduced by up to 90% of the nominal torque. The major influencing factors are therefore the total mass moment of inertia and the dynamometer torque.

Calculation to determine the maximum speed gradient of an engine test bench setup:

$$\begin{aligned} M_{\text{dyno,stat}} &= M_{\text{engine}} \\ J_{\text{total}} &= J_{\text{test carrier}} + J_{\text{flanges}} + J_{\text{shaft}} + J_{\text{dyno}} \\ \frac{dn}{dt}^{\text{dynomax}} &= \frac{M_{\text{dyno}} - M_{\text{engine,shifting}}}{\frac{\pi}{30} * J_{\text{total}}} \end{aligned} \tag{5.7}$$

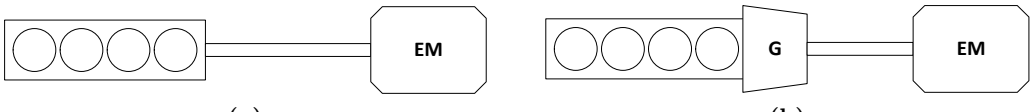

EM: Electrical machine; G: Gearbox

Figure 5.17: Comparison of the basic structure of an engine test bench and a powertrain test bench

The other case of relevance according to section 3.4 is related to the occurring drive shaft torque during acceleration from standstill. Due to the highest speed ratio of the first gear in combination with the moment superelevation of the torque converter, the highest torque can be expected during this use case.

The main equations are described in 5.8. The first main difference between the two configurations is the static dynamometer torque which is calculated by multiplying the engine torque with the effective speed ratio (i_{total}). Compared to the engine test bench configuration, a gear efficiency factor must also be included. Due to mechanical laws, the resulting mass moment of inertia related to the test bench side of the test carrier is orders of magnitude higher than in the engine test bench configuration. Furthermore, the mass moment of inertia of the electrical machine is expected to be higher to support the drive shaft torque. The mass moment of the gearbox (J_{gearbox}), the flanges (J_{flanges}) and the shaft (J_{shaft}) are summed up with the high mass moment of inertia of the dynamometer (J_{dyno}).

The occurring dynamometer torque is calculated by subtracting the momentum needed to accelerate the rotating masses from the static dynamometer torque. To calculate this moment, the speed gradient of the dynamometer, representing the road load, is necessary. Depending on the power-to-weight ratio and the speed ratio of the first gear, the speed gradient ($\frac{dn}{dt}$) is expected to be below 640 1/min/s. A precise calculation of the speed gradient requires a complex model of the whole vehicle and the resulting driving resistance.

Another factor that increases the complexity of the system is the timing of the highest expected torque. In most cases, it is the phase where the torque converter lockup clutch is to be engaged. Due to the undefined motor speed gradient condition, a reliable calculation of the expected torque is not possible. Therefore it is recommendable to determine the speed gradient experimentally or to simplify the calculation through assumptions. Equation 5.9 represents an already partially simplified calculation of moments to illustrate the complexity.

Calculation to determine the maximum dynamometer torque of a powertrain test bench setup when the torque converter speed ratio is a static value:

$$\begin{aligned} i_{\text{total}} &= i_{\text{engine}} * i_{\text{torque converter}} \\ M_{\text{dyno,stat}} &= M_{\text{engine}} * i_{\text{total}} \\ J_{\text{total}} &= J_{\text{test carrier}} * {i_{\text{total}}}^2 + J_{\text{gearbox}} + J_{\text{flanges}} + J_{\text{shaft}} + J_{\text{dyno}} \\ M_{\text{dyno,max}} &= M_{\text{engine}} * i_{\text{total}} * \eta_{\text{gearbox}} - \frac{\pi}{30} * J_{\text{total}} * \frac{dn}{dt}_{\text{dyno}} \end{aligned} \tag{5.8}$$

Partially simplified calculation to determine the maximum dynamometer torque of a powertrain test bench setup:

$$\begin{aligned} M_{\text{dyno,max}} = \quad & M_{\text{engine}} * i_{\text{total}} * \eta_{\text{gearbox}} - (\frac{\pi}{30} * J_{\text{mot,I}} * \frac{dn}{dt}_{\text{enginge}}) * i_{\text{total}} * \eta_{\text{gearbox}} \\ & - (\frac{\pi}{30} * (J_{\text{dyno}} + J_{\text{drive shaft}} + J_{\text{gearbox}}) * \frac{dn}{dt}_{\text{dyno}}) \end{aligned} \tag{5.9}$$

To represent a worst case scenario of the vehicle, the engine speed gradient can be set to 0. In this case, only the output-side fraction of the mass moment of inertia of the torque converter is to be taken into account and is summarized with the output-side mass moment of inertia of the gearbox. The dynamometer speed gradient is to be determined using vehicle data. Simplified, the speed ratio of the first gear could be used. When determining the maximum torque, the case of misuse [17] as well as an unfinished application must be taken into account in addition to the regular use case. In relation to the worst case scenario, a speed ratio of the torque converter has to be considered as well, because the highest dyno torque is to be expected when the torque converter clutch is not yet engaged. Within the scope of the work, a value of 1.30 is used to determine the maximum torque.

A representative case that does not occur in a completely applicated vehicle, but reflects the calculation issues in a very accurate form anyway, is shown in figure 5.18. The variables relevant for the calculation of the standstill acceleration process are plotted. The red lines refer to engine values, the black lines to test bench values. The lower part of the graph shows the total gear ratio, calculated on the basis of the speed ratio (blue). The torque curve shows two relevant peaks that should be taken into account during the calculation. These result from the fast speed adjustment of the torque converter at about 1.4 s as well as from the engagement of the lock-up clutch at about 1.9 s.

Due to the system interrelationships, engine inertia is considered quadratically in the calculation of the total mass moment of inertia. As the cursor at 1.4 s shows, the engine speed gradient is negative at the point of highest torque. According to the second term of equation 5.9, the dynamometer must apply higher torque in this case to accurately reproduce the road load.

A sufficiently accurate calculation can only be achieved by the assumption of the engine speed gradient, the torque multiplication of the torque converter, the resulting efficiency and in addition the input of the expected speed gradient of the electrical machine as a function of the power to mass ratio and the driving resistance of the vehicle. The easiest way to determine the highest speed gradient of the electrical machine is to perform a road test on the real vehicle.

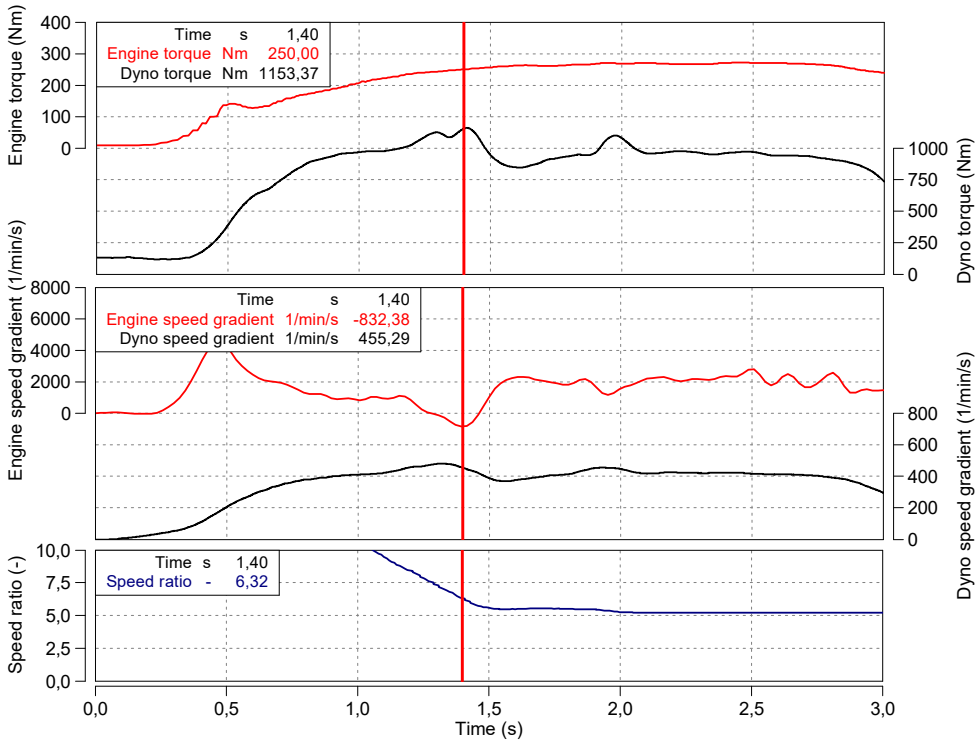

Figure 5.18: Acceleration torque at the powertrain test bench under RDE conditions

The second case of relevance for the dimensioning of electrical machines in the context of the tool development is shown in figure 5.19. Due to the direct connection, the calculation of the maximum speed gradient of the gear shift simulation is much easier and more accurate. The total mass moment of inertia is the simple summation of the mass inertia. Gear efficiencies do not have to be taken into account. The given example describes a case in which the maximum torque of the electrical machine is not sufficient to produce the necessary speed gradient.

The measurement shown in Figure 5.18 (red) represents an exact reproduction of a vehicle measurement (black) by following the speed/load profile. Due to the dynamics being limited by the maximum torque, the shifting process of the reproduction is extended by approximately 75%. Walter et al. identify a direct correlation between an increase in particle emissions and the parametrization of the shifting duration [108]. By varying the shifting duration, it becomes clear that small differences in the shifting duration parametrization lead to significant emission pattern changes due to interactions of the engine components.

Another point worth mentioning in relation to the reproduction of a speed-load profile is the torque intervention. In the case of an extended shifting duration due to insufficient speed gradients, the duration and also the level of torque intervention do not change. This leads to a load point displacement and thus to a clearly noticeable deviation of the emission results.

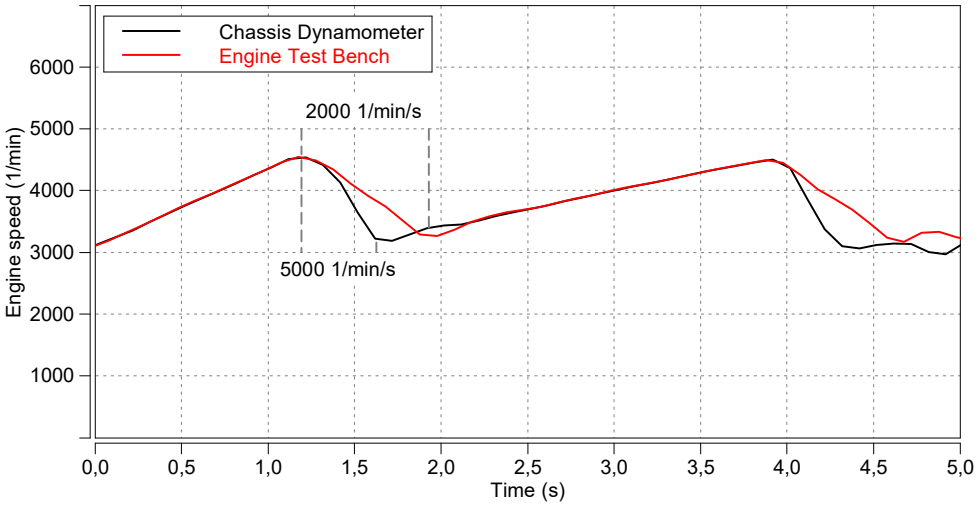

Figure 5.19: Comparison of the speed gradient of a gearbox shifting process and a reproduction on a small scaled engine test bench

A consistently correct and largely realistic representation of RDE relevant driving manoeuvres claims high demands on the performance of the electric machine and is therefore an important aspect for the selection of the test platform. The high dynamic requirements often lead to major restrictions in the selection of the platform. Due to the new requirements, lower mass moments of inertia, such as those of synchronous machines, are becoming increasingly important.

6 Conclusion and Outlook

In the context of this work on the optimal test platform selection for methodical RDE emission development, a tool has been developed which provides an overview of the current and future implementation possibilities for test scopes based on the development tasks of the emission developers and the test bench performance.
Based on the current legislation, a method was developed that establishes requirements for the test environment by means of selected use cases.

By means of the tool, a matching between the requirements of the respective experiment and the performance of the respective platform can be accomplished. On the one hand, this makes it possible to select the optimal test platform, but on the other hand, it also enables an estimation of the performance of the entire test environment with regard to the completion of the development tasks. By taking into account various different aspects required to perform the respective development task, the tool provides a valuable result in being able to evaluate the various combinations of requirements and thus evaluate the use case implementability as a whole by creating a big picture.

Some important topics for RDE emission development were examined in more detail. It has been shown that virtualizing, i.e. reproducing a real trip or using an EiL test bench to replace a real trip, is an important step towards efficient treatment of RDE related issues. It is therefore preferable to shift many development tasks from PEMS based road tests to the test environment. In this way a cost-effective and reproducible development can be ensured.

The development of a realistic and automated driver controller is indispensable for the transfer of development tasks into the test environment. The investigations have shown that the already available controllers still have deficits. The realistic mapping of human driving behaviour varies depending on the driving situation. In addition, driver types can still be reproduced only with a certain degree of difficulty.
Furthermore, it has been discovered that an exact reproduction of the engine actuation is not sufficient. Depending on the experiment, it may be necessary to ensure that the initial engine conditions are set correctly, to either consciously control emission-influencing events, or to have them triggered by the DME itself. The latter represents a major challenge due to its complexity.

To use a driver controller for RDE development, a road load simulation is required. Depending on the development goal, it may be appropriate to extend the conventional driving resistances of rolling, air and acceleration resistance by suitable components such as inclination or cornering resistance for mapping a three-dimensional environment.

In addition and supplementary to the previous sections, the test bench systems and their characteristics were also analyzed. Differences between the test bench conditioning systems and the vehicles' cooling systems were discussed. This revealed that there is still potential for improvement, particularly with regard to dynamic behaviour, but also in terms of stationary temperature levels. On the one hand, those deficits can be improved by hardware adaptations or the approximation to real vehicle hardware, but also by model approaches that simulate the heat balance of the cooling systems.
Furthermore, investigations of the electrical machines have revealed interesting conclusions regarding the required performance. For consideration purposes, a basic distinction can be made here between the setups as engine test bench and powertrain test bench. Due to the direct coupling of an engine test bench, the engine speed gradient for the simulation of a shifting process is mostly the limiting factor. However, the dynamic demands on the powertrain test bench are significantly lower, but the electrical machine has to support a much higher torque due to the transmission ratio. Although the highest torque to be expected is only required for a short period of time, it is a case relevant to the dimensioning.

In the course of the thesis, the tool was used to gain important insights into RDE-relevant test bench hardware and software and important simulation approaches. The tool can be used in conjunction with relevant use cases to estimate future demand. It can be stated that a successful refinement of existing systems and methods for RDE emission development cannot be achieved by means of individual components alone, but rather by continuous improvement of all components involved. A key role in this context is played by HiL solutions, which are available with varying degrees of virtualization and require further intensive development efforts.

En el contexto de este trabajo sobre la selección de la plataforma de pruebas ideal para el desarrollo metódico de las emisiones, se ha desarrollado una herramienta que proporciona una visión general de las posibilidades actuales y futuras de implementación de los alcances de las pruebas, basada en las tareas de desarrollo de los desarrolladores de las emisiones y en el rendimiento del banco de pruebas.
Basado en la legislación actual, se desarrolló un método que establece requisitos para el entorno de prueba mediante casos de uso seleccionados.

Mediante la herramienta, se puede lograr una correspondencia entre los requisitos del experimento y el rendimiento de la plataforma respectiva. Por un lado, esto permite seleccionar la plataforma de pruebas ideal, pero por otro lado, también permite estimar el rendimiento de todo el entorno de pruebas con respecto a la realización de las tareas de desarrollo. Al tener en cuenta los diferentes aspectos necesarios para llevar a cabo la tarea de desarrollo correspondiente, la herramienta proporciona un resultado valioso al poder evaluar las diversas combinaciones de requisitos y, de este modo, evaluar si el caso de uso es implementable en su conjunto mediante la creación de un panorama general.

Se examinaron con más profundidad algunos temas importantes para el desarrollo de las emisiones. Se ha demostrado que la virtualización, es decir, la reproducción de un viaje real o el uso de un banco de pruebas EiL para reemplazar un viaje real, es un paso importante hacia el tratamiento eficiente de los problemas relacionados con RDE. Por lo tanto, es preferible trasladar muchas tareas de desarrollo de las pruebas en carretera basadas en PEMS al entorno de pruebas. De esta manera se puede garantizar un desarrollo rentable y reproducible.

El desarrollo de un control de conductor realista y automatizado es indispensable para la transferencia de tareas de desarrollo al entorno de pruebas. Las investigaciones han demostrado que los controladores ya disponibles siguen siendo deficientes. La cartografía realista del comportamiento humano al volante varía en función de la situación de conducción. Además, los tipos de conductores sólo pueden reproducirse con cierto grado de dificultad.
Además, se ha descubierto que una reproducción exacta del accionamiento del motor no es suficiente. Dependiendo del experimento, puede ser necesario asegurarse de que las condiciones iniciales del motor estén ajustadas correctamente, ya sea para controlar conscientemente los eventos que influyen en las emisiones, o para que sean activados por el DME si mismo. Este último representa un gran desafío debido a su complejidad.
Para utilizar un controlador de conductor para el desarrollo de RDE, se requiere una simulación de carga en carretera. Dependiendo del objetivo de desarrollo, puede ser apropiado extender las resistencias de conducción convencionales de resistencia a la rodadura, al aire y a la aceleración

a través de componentes adecuados, tales como la resistencia a la inclinación o a las curvas, para cartografiar un entorno tridimensional.

Además de las secciones anteriores, se analizaron los sistemas de los bancos de pruebas y sus características. Se discutieron las diferencias entre los sistemas de acondicionamiento del banco de pruebas y los sistemas de refrigeración de los vehículos. Esto reveló que todavía hay potencial para mejorar, especialmente en lo que se refiere al comportamiento dinámico, pero también en términos de niveles de temperatura estacionarios. Por un lado, estos déficits pueden mejorarse mediante adaptaciones de hardware o la aproximación al hardware real del vehículo, pero también mediante modelos que simulan el balance térmico de los sistemas de refrigeración.
Además, las investigaciones de las máquinas eléctricas han revelado conclusiones interesantes con respecto al rendimiento requerido. A efectos de consideración, se puede hacer una distinción básica entre las configuraciones como banco de pruebas de motores y banco de pruebas de la transmisión. Debido al enganche directo de un banco de pruebas de motores, el gradiente de revoluciones del motor para la simulación de un proceso de cambio es, en su mayoría, el factor limitante. Sin embargo, las exigencias dinámicas en el banco de pruebas de la transmisión son significativamente menores, pero la máquina eléctrica tiene que soportar un momento de torsión mucho mayor debido a la relación de transmisión. Aunque el momento de torsión más alto que se puede esperar sólo se requiere por un corto período de tiempo, es un caso relevante para el dimensionamiento.

En el transcurso de la tesis, la herramienta se utilizó para obtener importantes conocimientos sobre el hardware y el software de los bancos de pruebas relevantes y sobre importantes enfoques de simulación. La herramienta puede utilizarse junto con casos de uso relevantes para estimar la demanda futura. Puede afirmarse que no se puede lograr un refinamiento satisfactorio de los sistemas y métodos existentes para el desarrollo de las emisiones de RDE únicamente mediante componentes individuales, sino más bien a través de la mejora continua de todos los componentes implicados. Un papel clave en este contexto lo juegan las soluciones HiL, que están disponibles con diferentes grados de virtualización y que requieren esfuerzos de desarrollo más intensos.

List of Symbols

Notation	Description	Unit
ASM	Additional safety margin which may be applied at the request of the manufacturer. ASM is limited to 50 %	
A	Cross sectional area	m^2
F_0	Coast down coefficient	N
F_1	Coast down coefficient dependent on velocity	N/(km/h)
F_2	Coast down coefficient dependent on the square of velocity	$N/(km/h)^2$
F	Force; component of driving resistance	N
H	Barometric altitude	m
J	Momentum of Inertia	kgm^2
$M_{CO_2,RDE,k}$	Distance-specific mass of CO_2, emitted over the RDE trip	g/km
$M_{CO_2,WLTC,k}$	Distance-specific mass of CO_2, emitted over the WLTC trip	g/km
$M_{CO_2,d,cc}$	Distance-specific mass of CO_2, emitted over one sample	g/km
M	Torque	Nm
N_k	Total sample number for urban, rural and motorway shares	
N	Quantity	
$P_{available,i,j}$	Available power in gear i at second j	kW
$P_{required,j}$	Required power at second j	kW
P_{wot}	Available power at $n_{i,j}$ at full load condition from the full load power curve	kW
RF_{L1}	First parameter of the function used to calculate the result evaluation factor	
RF_{L2}	Second parameter of the function used to calculate the result evaluation factor	
RF_k	Result evaluation factor calculated for the RDE trip	

Notation	Description	Unit
SM	Safety margin accounting for the difference between the stationary full load condition power curve and the power available during transition conditions. SM is set to 10 %	
TM	Test mass of the vehicle	kg
α	Slip angle (front or rear wheels	∘
$\bar{v}_{\mathrm{k}}$	Average vehicles speed for each speed bin	m/s
η	Energy conversion efficiency	
$\frac{dn}{dt}$	Speed gradient	$\frac{1/\mathrm{min}}{\mathrm{s}}$
λ	Air-fuel ratio, stoichiometric ratio = 1.00	
ρ	Air density	$\mathrm{kg/m^3}$
a_1	Coefficient used to determine characteristic curve	
a_{j}	Vehicle acceleration at second j	$\mathrm{m/s^2}$
$a_{\mathrm{pos,k}}$	Average positive acceleration at sample k	$\mathrm{m/s^2}$
b_1	Coefficient used to determine characteristic curve	
c_{w}	Drag coefficient	
f	Rolling resistance coefficient	
g	Gravitational constant	$\mathrm{m/s^2}$
i_{actual}	Actual gear	
i_{max}	Highest final possible gear	
i_{min}	Lowest final possible gear	
i	Gear ratio	
j	Index for each time step j	s
kr	Factor taking into account the inertial resistances of the powertrain during acceleration	
m	Mass	kg
n_{95_high}	Engine speed where 95 % of rated power is reached	$\mathrm{min^{-1}/(km/h)}$
$n_{\mathrm{i,j}}$	Engine speed	1/min
n_{idle}	Idling speed	1/min
$n_{\mathrm{min\_drive}}$	Minimum engine speed when the vehicle is in motion	1/min
n_{rated}	Rated engine speed declared by the manufacturer as the engine speed at which the engine develops its maximum power	1/min
ndv_{i}	Ratio of engine speed for gear i	1/min
p	Absolute ambient pressure	m
r_{k}	The RDE result evaluation factor for vehicles with ICE	
r	Circular radius	m

Notation	**Description**	**Unit**
t	Time	s
v_{i}	Vehicles speed at step i, i = 0 to N_{k}	m/s
v_{j}	Vehicle speed at second j	m/s
v_{k}	Vehicles speed at sample k	m/s
v	Vehicle speed	$\mathrm{m/s}^2$

List of Abbreviations

Notation	Description
-NCO	Isocyanate
AMA	Exhaust measurement system
ASIS	Adaptive Shifting strategy
AT	Automatic transmission
BMW	Bayerische Motoren Werke
C.F.R.	Code of Federal Regulations
CATC	China Automotive Testing Cycle
$CF_{pollutant}$	Conformity factor
CH	Methylidyne
CH4	Methane
CL3	Class 3 vehicle
CN	Cyanide
CO	Carbon monoxide
CO_2	Carbon dioxide
CPC	Condensation particle counter
CVS	Constant volume sampling
DHC	A WLTP Sub-group on the Development of the Harmonized driving Cycle
DME	Digital motor electronics
DoE	Design of Experiments
DSC	Dynamic stability control
ECU	Engine control unit
EEC	European Economic Community
EGR	Exhaust gas recirculation
EiL	Engine in the Loop
EMROAD	Microsoft Excel add-in for analyzing vehicle emissions data recorded with PEMS

Notation	Description
EPA	Environmental Protection Agency
EU	European Union
EUDC	Extra Urban Driving Cycle
FIR	Finite impulse response filter
FTP	Federal Test Procedure
GDI	Gasoline direct injection
GPF	Gasoline particulate filter
GPS	Global Positioning System
HC	Hydrocarbon
HCN^-	Hydrogen cyanide
HiL	Hardware in the Loop
HMM	Heat management module
HWFET	Highway Fuel Economy Test
ICE	Internal combustion engine
ISC	In-service conformity
IWG	Informal working group
JRC	Joint Research Centre
MAW	Moving average window
MIIT	Ministry of Industry and Information Technology
MiL	Model in the Loop
N_2	Molecular nitrogen
N_2O	Nitrous oxide
N_2O_4	Nitrogen tetroxide
NCN	Cyanonitrene
NEDC	New European Driving Cycle
NGO	Non governmental organization
NH_3	Ammonia
NMVOC	Non-methane volatile organic compounds
NO	Nitrogen monoxide
NO_2	Nitrogen dioxide
NO_x	Nitrogen oxide

Notation	**Description**
NTE	Not-to-exceed
OEM	Original Equipment Manufacturer
P	Reference points (1-3) of the vehicle CO_2 characteristic curve
PEMS	Portable emissions measurement system
PID	Proportional–integral–derivative
PM	Particulate matter (a number attached to the back refers to the aerodynamic diameter in µm)
PN	Particle number
RDE	Real Driving Emissions
RPA	Relative positive acceleration
SC03	Speed correction driving schedule
SFTP	Supplemental Federal Test Procedure
SO_2	Sulfur dioxide
TCU	Transmission control unit
THC	Total hydrocarbons
TU	Technical University
TVID	Turbocharging Valvetronic Direct Injection
UC	Use case
UDC	Urban driving cycle
UNECE	United Nations Economic Commission for Europe
US	United States
US06	Supplemental FTP Driving Schedule
USA	United States of America
VBA	Visual Basic for Applications
ViL	Vehicle in the Loop
VKM	Institute for Internal Combustion Engines and Powertrain Systems
VOC	Volatile organic compounds
WHDC	Worldwide Harmonized Heavy Duty Cycle

Notation	Description
WLTC	Worldwide Harmonized Light Vehicles Test Cycle
WLTP	Worldwide Harmonized Light Vehicles Test Procedure
WP.29	World Forum for Harmonization of Vehicle Regulations

List of Figures

List of Tables

Bibliography

[1] N. R. Abdullah, N. S. Shahruddin, R. Mamat, A. M. I. Mamat, and A. Zulkifli. Effects of Air Intake Pressure on the Engine Performance, Fuel Economy and Exhaust Emissions of A Small Gasoline Engine. *Journal of Mechanical Engineering and Sciences*, 6:949–958, June 2014.

[2] R. Ahlawat, J. Bredenbeck, and T. Ichige. Estimation of Road Load Parameters via On-road Vehicle Testing. In *Tire Technology Expo 2013*, Feb. 2013.

[3] G. Albertus Marthinus Meiring and H. Myburgh. A Review of Intelligent Driving Style Analysis Systems and Related Artificial Intelligence Algorithms. *Sensors*, 15:30653–30682, Dec. 2015.

[4] J. O. Anderson, J. G. Thundiyil, and A. Stolbach. Clearing the Air: A Review of the Effects of Particulate Matter Air Pollution on Human Health. *Journal of Medical Toxicology*, 8(2):166–175, Dec. 2011.

[5] AVL List GmbH. Emissions Legislation Update from WLTP/RDE to EU7. In M. Schöggl, editor, *AVL Powertrain Engineering Techday 4*, Apr. 2017.

[6] AVL List GmbH. Real Driving Emissions (RDE). In M. Schöggl, editor, *AVL Emission TechDay 2018*, Apr. 2018.

[7] M. Baghbeheshti, M. Zolfaghari, and R. Rueckerl. Fine Particulate Matter (PM2.5) and Health Effects: An Unbridle Problem in Iran. *Galen Medical Journal*, 6(2), June 2017.

[8] D. S. Barth. Federal Motor Vehicle Emission Goals for CO, HC and NOx-based on Desired Air Quality Levels. *Journal of the Air Pollution Control Association*, 20(8):519–523, Aug. 1970.

[9] S. Bauer, C. Beidl, and T. Düser. Methodik zur Erzeugung RDE-relevanter Szenarien im Prüfstandsumfeld. In *Proceedings*, pages 95–113. Springer Fachmedien Wiesbaden, 2018.

[10] G. Bayerische Motorenwerke Aktiengesellschaft Händlerqualifizierung und Training Röntgenstraße 7, 85716 Unterschleißheim. *Technical Qualification - Product Information - GA8HP Automatic Transmission*, Aug. 2009.

[11] G. Bayerische Motorenwerke Aktiengesellschaft Händlerqualifizierung und Training Röntgenstraße 7, 85716 Unterschleißheim. *Technical Qualification - Product Information - N74TU Engine*, June 2016.

[12] G. Bayerische Motorenwerke Aktiengesellschaft Händlerqualifizierung und Training Röntgenstraße 7, 85716 Unterschleißheim. *Technical Qualification - Product Information - B38/B48 TU Engine*, Apr. 2017.

[13] M. L. Bell and D. L. Davis. Reassessment of the Lethal London Fog of 1952: Novel Indicators of Acute and Chronic Consequences of Acute Exposure to Air Pollution. *Environmental Health Perspectives*, 109:389, June 2001.

[14] C. Berggren and T. Magnusson. Reducing Automotive Emissions - The Potentials of Combustion Engine Technologies and the Power of Policy. *Energy Policy*, 41:636–643, Feb. 2012.

[15] P. Bernhardt, C. Sauer, and M. Hendrix. Ermittlung des Energiebedarfs zur Bewegung von Fahrzeugen in mikroskopischen Verkehrssimulationen. *Wissenschaftliche Beiträge 2015*, 19:29–37, 2015.

[16] H.-H. Braess, U. Seiffert, H.-H. Braess, and U. Seiffert. *Vieweg Handbuch Kraftfahrzeugtechnik*. Springer-Verlag, Berlin Heidelberg New York, 7. aufl. edition, 2013.

[17] H. Brandhoff, W. Pfau, and F.-J. Tögel. Extrembelastungen im Pkw-Antriebsstrang durch Missbrauch. *ATZ - Automobiltechnische Zeitschrift*, 101(12):1006–1015, Dec. 1999.

[18] R. D. Brook, S. Rajagopalan, C. A. Pope, J. R. Brook, A. Bhatnagar, A. V. Diez-Roux, F. Holguin, Y. Hong, R. V. Luepker, M. A. Mittleman, A. Peters, D. Siscovick, S. C. Smith, L. Whitsel, and J. D. Kaufman. Particulate Matter Air Pollution and Cardiovascular Disease. *Circulation*, 121(21):2331–2378, June 2010.

[19] Comisión Europea. Recopilación de la Jurisprudencia. Official Journal of the European Union, Dec. 2018.

[20] Comisión Europea. Sentencia Del Tribunal General - ECLI:EU:T:2018:927 - T-290/16. Diario Oficial de la Unión Europea, Dec. 2018.

[21] Delphi Technologies. Worldwide Emissions Standards - Passenger Sars and Light Duty Vehicles - 2018 | 2019, Apr. 2018.

[22] P. Dilara. RDE GTR: Scope of U.S. Work to Inform Development of GTR. RDE IWG 4th meeting, Apr. 2019.

[23] P. Dong, editor. *Optimized Shift Control in Automatic Transmissions with Respect to Spontaneity, Comfort, and Shift Loads*, number Heft 15.2 in Schriftenreihe. Fakultät Für Maschinenbau - Institut: Product and Service Engineering, 2015.

[24] Environmental Protection Agency. Dynamometer Drive Schedules.

[25] Environmental Protection Agency. Part 1065 - Engine-testing Procedures, 2011.

[26] Environmental Protection Agency. Part 86 - Control of Emissions from New and In-use Highway Vehicles and Engines (continued), 2011.

[27] Environmental Protection Agency. Light-Duty Vehicles and Light-Duty Trucks: Tier 0, Tier 1, National Low Emission Vehicle (NLEV), and Clean Fuel Vehicle (CFV) Exhaust Emission Standards. Technical Report EPA-420-B-16-010, EPA - United States Environmental Protection Agency, Mar. 2016.

[28] European Commission. Commission Regulation (EU) 2016/427 of 10 March 2016. Official Journal of the European Union, Mar. 2016.

[29] European Commission. Commission Regulation (EU) 2016/646 of 20 April 2016. Official Journal of the European Union, Apr. 2016.

[30] European Parliament and the Council of the European Union. Commission Regulation (EC) 333/2014 of 11 March 2014. Official Journal of the European Union, Apr. 2014.

[31] European Parliament and the Council on type-approval of motor vehicles. Directive 2007/46/ec of the European Parliament and of the Council of 5 September 2007. Official Journal of the European Union, June 2007.

[32] European Parliament and the Council on type-approval of motor vehicles. Regulation (EC) No 715/2007 of the European Parliament and of the Council of 20 June 2007. Official Journal of the European Union, June 2007.

[33] European Parliament and the Council on type-approval of motor vehicles. Commission Regulation (EC) No 692/2008 of 18 July 2008. Official Journal of the European Union, July 2008.

[34] European Parliament and the Council on type-approval of motor vehicles. Commission Regulation (EU) 2017/1151 of 1 June 2017. Official Journal of the European Union, June 2017.

[35] European Parliament and the Council on type-approval of motor vehicles. Commission Regulation (EU) 2017/1154 of 7 June 2017. Official Journal of the European Union, June 2017.

[36] L. Faubel, C. Lensch-Franzen, A. Schuhardt, and C. Krohn. Übertrag von RDE-Anforderungen in eine modellbasierte Prüfstandsumgebung. *MTZextra*, 21(S2):44–49, Sept. 2016.

[37] C. P. Fenimore. Formation of Nitric Oxide in Premixed Hydrocarbon Flames. *Symposium (International) on Combustion*, 13(1):373–380, Jan. 1971.

[38] G. Fontaras, B. Ciuffo, N. Zacharof, S. Tsiakmakis, A. Marotta, J. Pavlovic, and K. Anagnostopoulos. The Difference Between Reported and Real-World CO2 Emissions: How Much Improvement Can ce Expected by WLTP Introduction? *Transportation Research Procedia*, 25:3933–3943, 2017.

[39] G. Fontaras, N.-G. Zacharof, and B. Ciuffo. Fuel Consumption and CO2 Emissions from Passenger Cars in Europe - Laboratory Versus Real-World Emissions. *Progress in Energy and Combustion Science*, 60:97–131, 2017.

[40] M. Friedmann, C. Lensch-Franzen, M. Gohl, and M. Kronstedt. Methodik zum Übertrag von RDE-Entwicklungsansätzen auf Antriebsstrangprüfstände unter Nutzung eines Emissions-Prädiktions-Modells. In *Proceedings*, pages 81–94. Springer Fachmedien Wiesbaden, 2018.

[41] General Court of the European Union. Press Release No 198/18, Dec. 2018.

[42] J. Gerstenberg, H. Hartlief, and S. Tafel. RDE-Entwicklungsumgebung am hochdynamischen Motorprüfstand. *ATZextra*, 20(S8):36–41, Sept. 2015.

[43] J. Gerstenberg, H. Hartlief, and S. Tafel. Introducing a Method to Evaluate RDE Demands at the Engine Test Bench. In *Proceedings*, pages 549–563. Springer Fachmedien Wiesbaden, 2016.

[44] J. Gerstenberg, C. Schyr, S. Sterzing-Oppel, and D. Trenkle. RDE Engineering via Engine-in-the-loop Test-Bench. *MTZ worldwide*, 78(6):16–23, may 2017.

[45] P. Gniffke. National Trend Tables for the German Atmospheric Emission Reporting - Final version 14.02.2018 (v1.0). Technical report, Umweltbundesamt, Feb. 2018.

[46] E. Goos, C. Sickfeld, F. Mauß, L. Seidel, B. Ruscic, A. Burcat, and T. Zeuch. Prompt NO Formation in Flames: The Influence of NCN Thermochemistry. *Proceedings of the Combustion Institute*, 34(1):657–666, Jan. 2013.

[47] D. A. Grantz, J. H. B. Garner, and D. W. Johnson. Ecological Effects of Particulate Matter. *Environment International*, 29(2-3):213–239, June 2003.

[48] T. Grigorie, L. Dinca, J. Corcau, and O. Grigorie. Aircrafts' Altitude Measurement Using Pressure Information: Barometric Altitude and Density Altitude. *WSEAS Transactions on Circuits and Systems*, 9:503–512, 07 2010.

[49] E. Gutt. Chemische Prozesse bei der Entstehung von Stickoxiden (NOx) in Diesel- und Benzinmotoren. *atene KOM Schriftenreihe / Verkehr und Umwelt 1*, page 3, Feb. 2018.

[50] J. Hipp, D. Schmidt, S. Bauer, T. Steinhaus, and C. Beidl. Methodikbaukasten zur Effizienten, Zielgerichteten RDE-Entwicklung – Potenziale und Perspektiven. In *Proceedings*, pages 127–146. Springer Fachmedien Wiesbaden, 2019.

[51] Y. Hirano, S. Inoue, and J. Ota. Model-based Development of Future Small EVs using Modelica. In *Proceedings of the 10th International Modelica Conference, March 10-12, 2014, Lund, Sweden*. Linkoeping University Electronic Press, Mar. 2014.

[52] S. Härdtl. Control Unit and Method for Preventing an Unintended Vehicle Motion. Technical Report DE102015202093A1, Bayerische Motoren Werke AG, https://patents.google.com/patent/DE102015202093A1/en, Feb. 2015.

[53] M. Härtl. BMW Schulung zur Einführung von Prüfstandstechnikern - Antriebsprüffeld FIZ.

[54] ICCT. China's Stage 6 Emission Standard for New Light-duty Vehicles (Final Rule). Technical report, International Council on Clean Transportation, Mar. 2017.

[55] ICCT. Changes to the Motor Vehicle Type-Approval System in the European Union. Technical report, International Council on Clean Transportation, May 2018.

[56] IPG Automotive GmbH, editor. *Powertrain Entwicklung mit CarMaker*, Tech Day BMW München, 21.11.18, 2018.

[57] IPG Automotive GmbH. *User Manual Version 7.1.1 - IPGDriver*, 2018.

[58] IPG Automotvie GmbH. *Carmaker, Truckmaker, Motorcyclemaker - the Open Integration and Test Platforms for Virtual Test Driving.*

[59] I. Jacobson. *USE-CASE 2.0 The Definitive Guide.* Ivar Jacobson International, 2011.

[60] F. Karagulian, C. A. Belis, C. F. C. Dora, A. M. Pruess-Ustuen, S. Bonjour, H. Adair-Rohani, and M. Amann. Contributions to Cities' Ambient Particulate Matter (PM): A Systematic Review of Local Source Contributions at Global Level. *Atmospheric Environment*, 120:475–483, Nov. 2015.

[61] H. W. Kennedy and M. E. Weekes. Control of Automobile Emissions. California Experience and the Federal Legislation. *Law and Contemporary Problems*, 33(2):297, 1968.

[62] S. Kirschke et al. Three Decades of Global Methane Sources and Sinks. *Nature Geoscience*, 6:813, Sept. 2013.

[63] M. J. Kleeman, J. J. Schauer, and G. R. Cass. Size and Composition Distribution of Fine Particulate Matter Emitted from Motor Vehicles. *Environmental Science & Technology*, 34(7):1132–1142, Apr. 2000.

[64] Z. Kregar, V. Franco, and P. Dilara. Real-Driving Emissions Regulation Update. ERMES plenary meeting, Nov. 2017.

[65] G. A. Lavoie, J. B. Heywood, and J. C. Keck. Experimental and Theoretical Study of Nitric Oxide Formation in Internal Combustion Engines. *Combustion Science and Technology*, 1(4):313–326, Feb. 1970.

[66] A. Marotta, J. Pavlovic, B. Ciuffo, S. Serra, and G. Fontaras. Gaseous Emissions from Light-Duty Vehicles: Moving from NEDC to the New WLTP Test Procedure. *Environmental Science & Technology*, 49(14):8315–8322, July 2015.

[67] H. Maschmeyer, C. Beidl, T. Düser, and B. Schick. RDE-Homologation – Herausforderungen, Lösungen und Chancen. *MTZ - Motortechnische Zeitschrift*, 77(10):84–91, Sept. 2016.

[68] W. Mayer, J. Wiedemann, and J. Neubeck. Road Load Determination in Real Road Tests. *ATZ worldwide*, 104(5):18–21, May 2002.

[69] G. P. Merker and R. Teichmann, editors. *Grundlagen Verbrennungsmotoren.* Springer Fachmedien Wiesbaden, 2019.

[70] J. V. Mierlo, G. Maggetto, E. V. de Burgwal, and R. Gense. Driving Style and Traffic Measures-influence on Vehicle Emissions and Fuel Consumption. *Proceedings of the Institution of Mechanical Engineers, Part D: Journal of Automobile Engineering*, 218(1):43–50, 2004.

[71] Ministry of Ecology and Environment of the People's Republic of China. Limits and Measurement Methods for Emission from Light-Duty Vehicles (CHINA 6), 2016. GB18352.6-2016.

[72] T. Mink, C. Lensch-Franzen, M. Schäfer, and A. Ebel. Development Methods for RDE-compliant Powertrains. In *Proceedings*, pages 117–126. Springer Fachmedien Wiesbaden, 2018.

[73] M. Mitschke and H. Wallentowitz. *Dynamik der Kraftfahrzeuge.* Springer-Verlag, Berlin Heidelberg New York, 5. aufl. edition, 2014.

[74] MLIT - Ministry of Land, Infrastructure, Transport and Tourism. Development of the Japan's RDE (Real Driving Emission) Procedure. Technical Report GRPE-76-18, United Nations Economic Commission for Europe, Jan. 2018.

[75] P. Mock, J. German, A. Bandivadekar, and I. Riemersma. Discrepancies Between Type-approval and "Real-world" Fuel-consumption and CO. *The International Council on Clean Transportation*, 13, 2012.

[76] A. Mukherjee and M. Agrawal. World Air Particulate Matter: Sources, Distribution and Health Effects. *Environmental Chemistry Letters*, 15(2):283–309, Feb. 2017.

[77] Y. L. Murphey, R. Milton, and L. Kiliaris. Driver's Style Classification Using Jerk Analysis. In *2009 IEEE Workshop on Computational Intelligence in Vehicles and Vehicular Systems*, pages 23–28, March 2009.

[78] K. M. Nichols, L. M. Thompson, and H. L. Empie Jr. A Review of NOx Formation Mechanisms in Recovery Furnaces. *IPST Technical Paper Series*, 1991.

[79] R. Nicolas. The Different Driving Cycles, 2013.

[80] Office of Transportation and Air Quality. Fuel Economy Labeling of Motor Vehicle Revisions to Improve Calculation of Fuel Economy Estimates. Final Technical Support Document EPA420-R-06-017, United States Environmental Protection Agency, Dec. 2006.

[81] I. C. A. Organization. Manual of the Icao Standard Atmosphere - Extended to 80 Kilometres (262 500 Feet), 1993.

[82] S. N. Pandis, R. A. Harley, G. R. Cass, and J. H. Seinfeld. Secondary Organic Aerosol Formation and Transport. *Atmospheric Environment. Part A. General Topics*, 26(13):2269–2282, Sept. 1992.

[83] A. Peters, R. Rueckerl, and J. Cyrys. Lessons From Air Pollution Epidemiology for Studies of Engineered Nanomaterials. *Journal of Occupational and Environmental Medicine*, 53:S8–S13, June 2011.

[84] C. Rakopoulos, A. Dimaratos, E. Giakoumis, and M. Peckham. Experimental Assessment of Turbocharged Diesel Engine Transient Emissions during Acceleration, Load Change and Starting. In *SAE Technical Paper*. SAE International, 04 2010.

[85] K. Reif, editor. *Abgastechnik für Verbrennungsmotoren*. Springer Fachmedien Wiesbaden, 2015.

[86] G. Retscher. Augmentation of Indoor Positioning Systems with a Barometric Pressure Sensor for Direct Altitude Determination in a Multi-storey Building. *Cartography and Geographic Information Science*, 34(4):305–310, 2007.

[87] D. B. Robert D. Mitchell. Dynamic Stability Control: Now Standard on Virtually the Full Range of 2000 Model BMW. *BMW Group PressClub*, 2000.

[88] R. Royles. Wind Effects on Buildings and Structures - Proceedings of the Fourth International Conference, London. Edited by K. J. Eaton. Cambridge University Press, 1977. Pp. 845. £25. *Quarterly Journal of the Royal Meteorological Society*, 103(437):530–530, Sept. 1975.

[89] R. Rueckerl, A. Schneider, S. Breitner, J. Cyrys, and A. Peters. Health Effects of Particulate Air Pollution: A Review of Epidemiological Evidence. *Inhalation Toxicology*, 23(10):555–592, Aug. 2011.

[90] SAE International. Drive Quality Evaluation for Chassis Dynamometer Testing. Technical report, SAE International, 2017.

[91] H. Scherer, M. Bek, and S. Kilian. ZF New 8-speed Automatic Transmission 8HP70 - Basic Design and Hybridization. *SAE International Journal of Engines*, 2(1):314–326, 2009.

[92] U. Schäffler, D. K. Stroh, and D. H. Ott. Umweltwissen - Schadstoffe - Bodennahes Ozon und Sommersmog. Technical report, Bayerisches Landesamt für Umwelt (LfU) Bürgermeister-Ulrich-Straße 160 86179 Augsburg, Aug. 2004 (revised: 2015).

[93] D. Schmidt, H. Maschmeyer, C. Beidl, and F. Raß. Neue Verfahren zur effizienten antriebsstrangspezifischen RDE-Entwicklung. In *Proceedings*, pages 1–18. Springer Fachmedien Wiesbaden, 2017.

[94] M. Shelef and R. W. McCabe. Twenty-five Years After Introduction of Automotive Catalysts: What Next? *Catalysis Today*, 62(1):35–50, Sept. 2000.

[95] A. Smith and H. Davies. A Review of the History of Emission Legislation, Urban and National Transport Trends and their Impact on Transport Emissions. *WIT Transactions on The Built Environment*, 26:10, 1996.

[96] S. M. C. Soares and J. R. Sodre. Effects of Atmospheric Temperature and Pressure on the Performance of a Vehicle. *Proceedings of the Institution of Mechanical Engineers, Part D: Journal of Automobile Engineering*, 216(6):473–477, June 2002.

[97] T. Stefanos. From NEDC to WLTP: Effect on the Type-approval CO2 Emissions of Light-duty Vehicles. *Publications Office of the European Union*, 2017.

[98] H. Steven. Development of a Worldwide Harmonized Heavy-duty Engine Emissions Test Cycle (WHDC). techreport 41st GRPE , 16-18 January 2001, agenda item 1.1., ECE-GRPE WHDC Working Group, Jan. 2001.

[99] J. Sutton, B. Williams, and J. FLEMING. Laser-induced Fluorescence Measurements of NCN in Low-pressure CH4/o2/n2 Flames and Its Role in Prompt NO Formation. *Combustion and Flame*, 153(3):465–478, May 2008.

[100] O. Taubman-Ben-Ari, M. Mikulincer, and O. Gillath. The Multidimensional Driving Style Inventory—scale Construct and Validation. *Accident Analysis & Prevention - V 36*, (3):323–332, 2004.

[101] The Council of the European Communities. Council Directive of 26. June 1991. Official Journal of the European Communities, June 1991.

[102] U. Tietge. A Comparison of Official and Real-world Fuel Consumption and Co2 Values for Passenger Cars in Europe, the United States, China, and Japan. *International Council on Clean Transportation Europe*, page 69, Nov. 2017.

[103] D. Tilman, K. G. Cassman, P. A. Matson, R. Naylor, and S. Polasky. Agricultural Sustainability and Intensive Production Practices. *Nature*, 418(6898):671–677, Aug. 2002.

[104] J. R. Torti. Sistemas de Energía a Partir de Residuos y Medio Ambiente. ITBA - Director de la Maestría en Gestión Ambiental, 2018.

[105] M. Tutuianu. Development of a Worldwide Harmonized Light Duty Driving Test Cycle (WLTC). techreport GRPE-68-03, WLTP DHC Chair, Dec. 2013.

[106] Verband der Automobilindustrie e.V. (VDA). Quo Vadis, Diesel? *Verband der Automobilindustrie e.V. (VDA)*, page 28, Nov. 2017.

[107] S. Wakamatsu, T. Morikawa, and A. Ito. Air Pollution Trends in Japan between 1970 and 2012 and Impact of Urban Air Pollution Countermeasures. *Asian Journal of Atmospheric Environment*, 7, 12 2013.

[108] S. Walter, N. Meyer, T. Schulze, J. Andert, S. Klein, and D. Guse. Durchgängig von der Straße auf den Prüfstand bis zur Simulation – eine qualitative Analyse am Beispiel RDE. In *Proceedings*, pages 125–144. Springer Fachmedien Wiesbaden, 2018.

[109] M. Williams. A Technical Summary of Euro 6/VI Vehicle Emission Standards. Technical report, The International Council of Clean Transportation, June 2016.

[110] World Forum for Harmonization of Vehicle Regulations. Informal Document - Overview of CATC Development. 172nd WP.29 session, Agenda item 6, 2017.

[111] Y. B. Zeldovich. *The Oxidation of Nitrogen in Combustion and Explosions*, chapter Band 21, pages 577–628. Acta Physicochimica U.S.S.R., 1946.